UNIVERSITY OF OKLAHOMA

GRADUATE COLLEGE

EXPERIMENTAL AND MODELING STUDIES ON AXIAL OSCILLATION-SUPPORTED DRILLSTRINGS

A DISSERTATION

SUBMITTED TO THE GRADUATE FACULTY

in partial fulfillment of the requirements for the

DOCTOR OF PHILOSOPHY

By

EMMANUEL OLUSEGUN OMOJUWA

Norman, Oklahoma

2019

EXPERIMENTAL AND MODELING STUDIES ON AXIAL OSCILLATION-SUPPORTED DRILLSTRINGS

A DISSERTATION APPROVED FOR THE

MEWBOURNE SCHOOL OF PETROLEUM AND GEOLOGICAL ENGINEERING

BY

Dr. Ramadan Ahmed

Dr. Harold Stalford

Dr. Catalin Teodoriu

Dr. Saeed Salehi

Dr. Bor-Jier (Ben) Shiau

Acknowledgments

I would like to extend profound appreciation to my advisor and committee chairman, Dr. Ramadan Ahmed for his mentorship, support, and guidance through this journey. Many thanks to the committee members (Dr. Catalin Teodoriu, Dr. Saeed Salehi, Dr. Bor-Jier (Ben) Shiau and Dr. Harold Stalford) for their contributions to the success of my research.

Special thanks to James Acquaye, the President of JA Oilfield Manufacturing Inc. and my boss for the support and allowing me to pursue my Ph.D. degree while working full-time.

I also appreciate the faculty and staff of the Mewbourne School of Petroleum Engineering (MPGE), the University of Oklahoma for their warmth, kindness, and support through my graduate study.

Thanks to my wife (Adebola Omojuwa), my daughter (Kanyinsola Omojuwa) and to family and friends for their support, well wishes, and words of encouragements.

To everyone that shared knowledge and solutions online and in books valuable to this research, you are highly appreciated. Keep sharing and making the world better.

Table of Contents

List of Tables

List of Figures

Abstract

Extending the reach of high-angle and extended-reach wells through slide drilling operations are hindered by high downhole friction (static and dynamic), which emanates to inefficiencies, such as poor weight transfer from surface to bit, limited rate of penetration (ROP), high mechanical specific energy, bit-wear, and erratic toolface control. Experimental and field studies have demonstrated that downhole vibrations induced by axial oscillation tools (AOTs) in the drillstring is one of the most efficient methods for friction reduction and improving axial force transfer while slide drilling with mud motors in high-angle and extended-reach wells.

Modeling the dynamic response (axial displacement and accelerations) of axial oscillation-supported drillstrings is of high importance and required to predict the performance and functionality of AOTs under the surface and downhole conditions. Even though, reliable predictions are needed during the performance evaluation of AOTs, an accurate drillstring dynamic model that is capable of predicting the dynamic response of axial oscillation-supported drillstrings is currently lacking. Hence, this study is aimed to perform mathematical analysis of axial oscillation-supported drillstrings to provide an accurate prediction of the dynamic response of these systems under the surface and downhole conditions.

This study includes experimental studies on axial oscillation tools and mathematical modeling of the dynamic response of axial oscillation-supported drillstrings operating at the surface and downhole conditions. To perform experimental studies, a flow loop has been developed to assess the dynamic response of the axial oscillation tool at the surface. During the test, the pressure drop across the tool and axial displacements of the tool were measured while varying flow rate and spring rate within the tool.

The axial oscillation-supported drillstring is modeled as an elastic continuous system subjected to viscous damping, Coulomb friction, and displacement (or support) excitation using the dynamic equilibrium approach. The introduction of the spring rate as an experimental variable in the test and the mathematical modeling approach used are unique to this study. The model developed in this investigation can predict natural frequencies, axial displacements, and acceleration of axial oscillation-supported drillstrings. The model is validated with experimental results and published measurements obtained from experiments conducted using field-scale drillstring models. Results show reasonable agreement (maximum discrepancy of approximately 14.5%) between model predictions and measurements at different excitation frequencies and pressure drops. In addition, results emphasize that flow rate is the most critical parameter in the operations of axial oscillation tools because it affects the magnitude of pressure drop, operating frequency of the tool and vibrating force. Furthermore, incorporating the spring rate in the model formulation improves the accuracy of the model.

Chapter 1: Introduction

1.1. Overview

Drillstring rotation is the most efficient method of reducing axial friction along the drillstring and highly beneficial for weight transfer and extending the reach of horizontal wells (Figure 1.1). However, in low-cost drilling markets, mud motors are chosen as the economic alternative over rotary steerable systems (RSS) in driving the bit. When slide drilling with mud motors, frictional forces significantly oppose drillstring motion, leading to poor weight transfer to the drill bit. Frictional forces are generated from forced contact between the borehole and drillstring. The forced contacts are prompted by buckling of drillstring (sinusoidal and helical), gravity acting on the pipe in the lateral section of deviated wellbores, or hydraulic loading against the drillstring and wellbore.

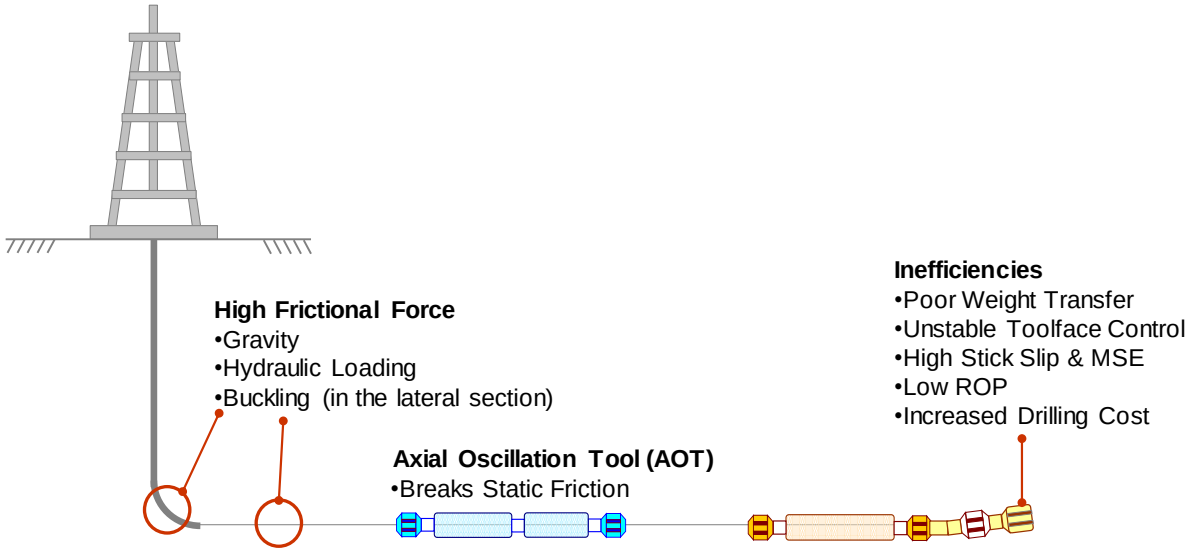

Figure 1. 1: Inefficiencies caused by high friction in extended reach wells

Friction reduction along drillstrings in high-angle and extended-reach wells suppresses drilling dynamic dysfunctions such as torque and drag, buckling, whirling, buckling and stick-slip, consequently leading to improvement of drilling efficiency and reduction of nonproductive time (NPT). Industrial methods of friction reduction used to extend the reach of a well or improve weight transfer include: drillstring rotation, hole cleaning, addition of lubricants to drilling fluid systems, non-rotating drillpipe protectors (NRDPPs) and application of downhole vibrating tools which dynamically excite the drillstring and reduces friction (Samuel, 2010; Newman et al., 2009).

Downhole vibrating tools have increasingly become a viable means of extending the reach of high-angle and extended-reach wells, improve the transfer of WOB and increase ROP (Newman et al., 2009). Lateral vibrating tools, flow interrupting tools and axial oscillation tools are types of downhole vibrating tools used for friction reduction. Flow interrupting tools or fluid hammer vibrating tools employs the change in flow resistance within the tool to induce oscillations due to pressure changes above the tool. Lateral vibrating tools utilize eccentric rotating masses set into motion by mud flow which generates oscillations in the lateral direction, perpendicular to the longitudinal axis of the tool (Gee et al, 2013). Axial oscillation tools utilize the flow of mud to generate pressure pulses which are converted into axial oscillating motion.

The application of downhole vibrating tools in friction reduction, specifically the axial oscillation tools have turned out to be one of the most efficient methods of improving weight transfer to the bit, increasing rate of penetration (ROP) and extending reach of the well (Newman et al., 2009; Barakat, 2007; McCarthy et al., 2009; Schultz, 2013; Gee et al., 2015). The axial oscillation tools reduce the frictional forces by providing axial oscillations, providing an increased friction reduction benefit than lateral vibration tools. The friction reduction benefit

provided by lateral vibrations tools is significantly localized when compared to axial oscillation tools. In addition, axial motions travel a greater distance uphole and downhole along the drillstring.

Axial oscillation-supported drillstrings consists of one or more axial oscillation tools in the assembly, and are in operation when circulating drilling fluid through the drillstring. Axial oscillation tools are also used in jarring stuck pipes and fishing operations (Voghell et al., 2013, NOV, 2016). In addition, axial oscillation tools have become common in coiled tubing drilling and intervention for milling bridge plugs and packers in completion applications (Robertson et al., 2004). The significant reduction in friction along the coil allows milling and conveyance of logging tools and perforating guns in extended reach applications. In fishing applications, the axial oscillation tool proves to be effective in assisting the retrieval of stuck BHAs, packers, sand screens and several downhole components, specifically when differentially or sand stuck (NOV, 2016).

The working mechanism of axial oscillation tools is based on using pressure fluctuations as the source of excitation, which generates axial oscillations as the response (Newman et al., 2009; Gee et al., 2015). The axial oscillation tool comprises of three (3) main sections: power, valve (or orifice) and oscillation sections. The power section is a positive displacement motor (PDM) powered by drilling fluid (or mud), creating an eccentric motion of the rotor. The rotor eccentric motion is transferred to the valve section located at the bottom of the power section. As the rotor moves eccentrically, the center of the flow exiting the power section also moves. Mudflow leaving the power section is directed towards the valve section, which contains orifices or valve plates. The varying position of the flow with respect to the inner output orifice creates

pressure pulses or pressure fluctuations. These pressure pulses are used as excitations of the pressure responsive device, such as a shock-sub or oscillation section.

The effectiveness of axial oscillation-supported drillstring can be measured using several key performance indicators, such as improvement in the rate of penetration (ROP), reduction in mechanical specific energy (MSE), stick-slip reduction, percent of weight transfer, percent of friction reduction, toolface control. Optimization of axial oscillation tools is key to the excellent performance of axial oscillation-supported drillstrings. The performance and efficiency of axial oscillation-supported drillstrings are affected by operating parameters and setup of axial oscillation tools, drilling parameters, friction, borehole geometry, drillstring characteristics. Some of the important operating parameters of AOTs that needs to be optimized are flow rate, operating frequency, the density of drilling fluid, valve/orifice sizing, pressure drop, spring rate or spring constant, pump open area (POA). Johnson (2016) provided recommendations for optimization of axial oscillation-supported drilling systems.

1.2 Statement of the Problem

Currently, manufacturers of axial oscillation tools (AOTs) and drilling engineers lack an accurate drillstring dynamic model that is capable of predicting axial displacement and acceleration of axial oscillation-supported drillstrings. Reliable predictions are needed during the performance evaluation of AOT at the surface and AOT-supported drillstring downhole. The evaluation is performed varying magnitude of pressure pulses, the frequency of pressure pulse (flow rate), elastic properties, AOT spring rate and damping mechanisms (viscous and Coulomb's damping). The dynamic model developed in this study is used to simulate the

response of the axial oscillation tool (AOT) during experimental testing on the surface and downhole response of the entire axial oscillation-supported drillstring.

1.3 Objectives and Scope of the Study

The dynamic analysis of axial oscillation-supported drillstrings provides a quantitative and qualitative prediction of the dynamic response (axial displacement and accelerations) of these systems under the surface and downhole conditions. Hence, the dynamic model can be used by manufacturers and operators for functional testing of axial oscillation tools at the surface and for performance evaluation while operating downhole. Specifically, the objectives of this study are:

- To develop a practical mathematical model for predicting the dynamic response of axial oscillation-supported drillstrings operating at surface and downhole conditions
- To verify the functionality of developed model and validate its predictions with available experimental and field measurements
- To use the new model for parametric study and placement analysis of axial oscillation tools within axial oscillation-supported drillstrings

1.4 Research Methodology

The experimental testing of axial an oscillation tool required the designed and development of an experimental flow loop to measure pressure variations and axial displacements at the axial oscillation tool (AOT) while changing flow rates and spring rates within the tool. The experimental study was carried out to validate the mathematical model developed in this study. In addition, experimental testing helps to establish the feasibility and

performance of using an axial oscillation tool for downhole applications. The drillstring is modeled as an elastic continuous system of the concentric cylindrical bar that can deform axially along the longitudinal axis. The equation of motion of a continuous cylindrical bar subjected to displacement excitation in a viscous medium with Coulomb friction is derived using the dynamic equilibrium approach. The resulting nonlinear equation of motion is linearized using the concept of equivalent viscous damping and an analytical solution is obtained using the Eigenfunction superposition method. The model is used to predict natural frequencies, axial displacements, and acceleration of the system. The results from the model predictions are validated with the data obtained by surface testing of an axial oscillation tool (AOT) and other published experimental measurements.

1.5 Organization of the Study

Chapter 2 covers literature review on fundamental concepts of downhole vibrating tools, design and working mechanisms of axial oscillation tools, factors affecting the performance of axial oscillation-supported drillstrings, methods used to evaluate the effectiveness of axial oscillation-supported drilling systems, experimental measurements and modeling of axial oscillation-supported drillstrings. The experimental study of an axial oscillation tool is presented in Chapter 3. Chapter 4 focuses on the mathematical modeling of axial oscillation-supported drillstrings. Chapter 5 presents numerical calculation procedures applied to obtain the solutions of the response equations and discussion of results. Chapter 6 covers conclusions and recommendations.

Chapter 2: Literature Review

2.1. Downhole Vibrating Tools

An invention patent (Roper and Dellinger 1983) was put forward, with the proposed objective: "A deviated borehole is drilled with a rotary drilling technique in which the drill string is vibrated at a suitable frequency and amplitude to reduce the friction of the drillstring against the lower side of the borehole and to promote the free movement of the drillstring therein". The patent proposes the use of hydraulically driven vibrating tool attached to the drillstring powered by circulating drilling mud. The use of downhole vibrating tools has become an accepted method of dynamically exciting the drillstring to increase weight transfer and extend the reach of jointed pipes and coiled tubing in high-angle and extended-reach wells (Newman et al, 2009). Experimental testing shows that energy created by dynamic oscillations significantly reduces the amount of friction. Several types of downhole vibration tools have been introduced to the industry ranging from lateral vibration tools, fluid hammer vibrating tools, and axial oscillation tools.

With the introduction of downhole vibrating tools, the static friction encountered while drilling can be greatly reduced by effectively converting it to a kinetic form of friction, which improves drilling efficiency (Skyles et al., 2012). Static frictional forces are significantly higher than kinetic friction and limits axial load transferred to the bit from surface and toolface control.

Lateral vibration tools (LVTs) depends on the fluid flow to create linear or rotational motion of mass components inside the tool to generate inertial vibrations. Typically, LVTs use a rotor and stator in a positive displacement motor (PDM) to drive an eccentric mass (Thorpen and Sanders, 2015). Hence, they employ hydraulic and/or mechanical mechanisms to create

oscillations in the lateral direction (i.e. perpendicular to the longitudinal axis of the tool) and generate motion between the tool and the wall of the borehole. The action of LVTs reduces downhole friction. An advantage of an LVT is that they do not create axial up-and-down hammering motion or cause signal interference with Measurement While Drilling (MWD) equipment (Thorpen and Sanders, 2015). The limitation of LVTs is that their friction reducing effect is localized within the drillstring near the location of the tool since lateral vibrations do not push the drillstring back and forth along its length (Gee et al., 2015). Propagation of oscillations along the drillstring significantly alters measured pressure pulse signals at the surface or standpipe (Lear and Dareing, 1990). High-frequency AOT oscillations significantly interfere with low-amplitude pressure pulse or axial vibrations (Lear and Dareing, 1990).

Fluid hammer vibrating tools (also called flow interrupting tools, **Figure 2.1**) have been significantly used in drilling and coiled tubing operations. Recently, these tools have been utilized in casing operations (McIntosh et al., 2016). This type of tool utilizes a cyclic flow resistance, acting as a valve without having moving parts. The hydraulic (alternating) valve functions are created by employing fluidic elements connected together to produce a self-generated oscillating pressure change above the tool, which is often known as the fluid hammer effect (Schultz, 2015). As a column of fluid flows through the drillstring, the periodic restriction of flow in an alternating valve creates a water hammer effect or pressure surge (Schultz, 2015). One of the drawbacks of fluid hammer vibrating tools is the high energy vibrations induced into the drillstring which can be detrimental to the drilling system.

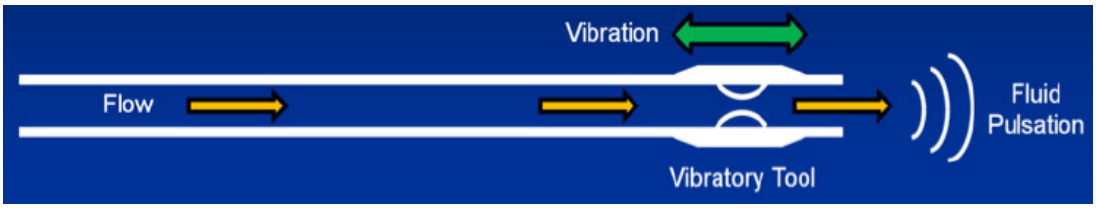

Figure 2. 1: Operating principle of fluid hammer vibrating tools (McIntosh et al., 2016)

Axial oscillation tool (AOT) utilizes a rotor/stator pair attached to a valve element to momentarily disrupt flow to create and release backpressure above the tool. The power section of the AOT consists of a rotor-stator configuration similar to a mud motor but instead of driving a bit box, the power section drives an oscillating valve in the tool (**Figure 2.2**). The axial oscillation generated by the AOT system oscillates the bottomhole assembly (BHA) in a gentle axial motion with low amplitude and frequency, reducing friction and improving weight transfer. Due to the action of the AOT, continuous weight is transferred without damage to the bit or any of the downhole tools (e.g. MWD, LWD or mud motor).

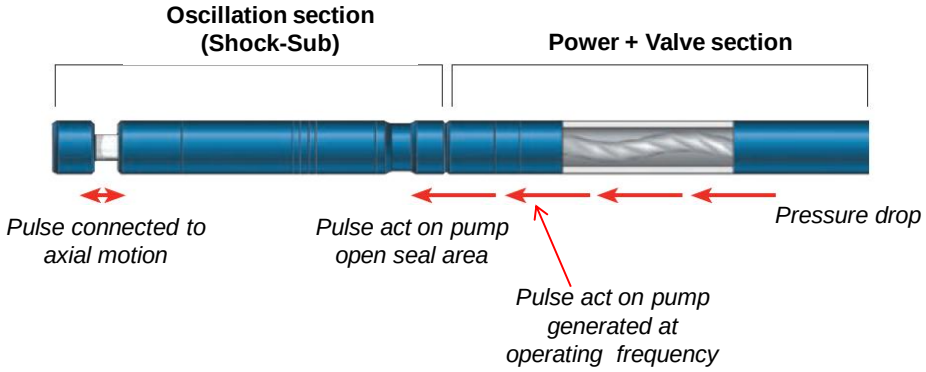

Figure 2. 2: Flow process in the axial oscillation tool (NOV, 2016)

Fishing through downhole vibrating tools can be difficult and almost impossible due to flow restriction of valves and stator-rotor configuration. Since downhole vibrating tools rarely have through-bore access for running fishing or retrieval tools, a safety joint is run below downhole vibrating tools. Safety joint is a two-piece sub containing a coarse thread between two sub-components, enabling back-off in case through-bore access is required. The safety joint is

positioned below the AOT, allowing it to be tripped out of the hole for access to the rest of the lower drillstring components (Gee et al., 2015).

2.2. Working Mechanisms of Axial Oscillation Tools

The concept behind the design of axial oscillation tool (AOT) is to use a fluid actuated positive displacement motor (PDM) and an associated valve assembly to provide pressure pulses to a shock-sub or oscillation section (Eddison and Hardie, 2001). The shock-sub or oscillation section extends or retracts in response to the oscillating drilling fluid pressure pulses created by varying the flow area. The extension or retraction of the oscillation section (shock-sub) creates the axial oscillation effect along the drillstring. The widely used AOT design (NOV Agitator System^{TM}) will be used as the base design layout in this current study. The commonly used axial oscillation tool (**Figure 2.3**) consists of three main sections: power section, valve section, and shock tool or oscillation section. The power section is the same as the one used in a positive displacement motor (PDM), operating at a certain range of revolutions per minutes (RPMs) for different flow rates. Different rotor and stator configurations (e.g., changing the number of lobes on the rotor) can be used to provide variations in speed and torque of the power section. Increasing the number of lobes on the stator/rotor configuration reduces the power section RPM while increasing the torque generated. The relationship between stator/rotor lobe configuration, RPM and torque are shown in **Figure 2.4**. As mud flows across the power section, the rotor is driven by the fluid between the sealed cavities of stator and rotor (Baez and Alali, 2011).

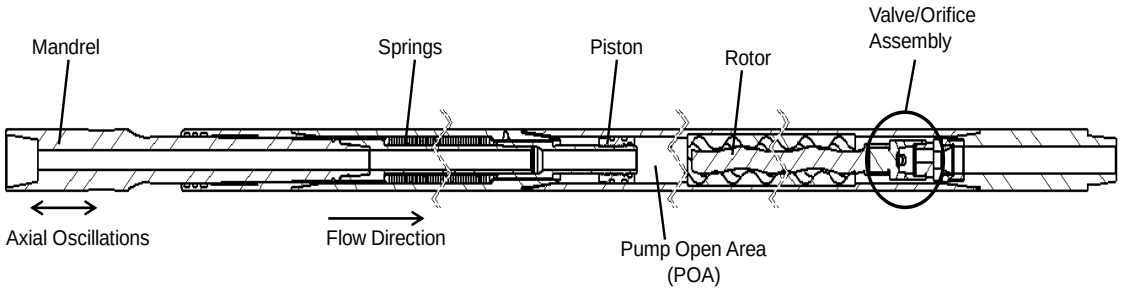

Figure 2. 3: Design layout of an axial oscillation tool

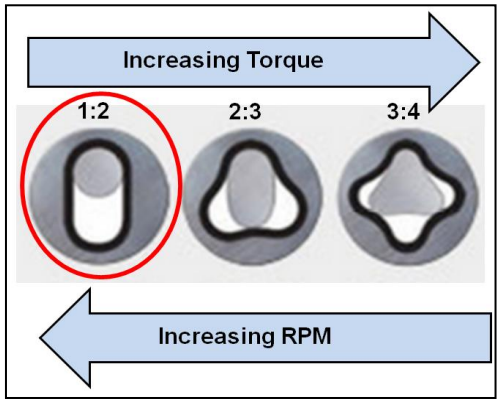

Figure 2. 4: Relationship between stator/rotor lobe configuration, RPM and torque

The valve section consists of an oscillating valve (or eccentric orifice) and a stationary plate (or concentric orifice) shown in **Figure 2.5**. The oscillating valve is coupled to the rotor and the stationary plate is attached in a fixed position to the bottom sub. As the rotor rotates within the stator, the oscillating valve moves in a close to linear motion called nutation, creating repeated or periodic restrictions in the flow path. The flow area between the stationary plate and the oscillating valve generates cyclic change in back pressure. The total flow area (TFA) alternates from minimum to maximum, creating pressure pulses inside the drillstring (Baez and Alali, 2011; Al Ali et al., 2011). This makes the valve section the heart of the axial oscillation tool (AOT).

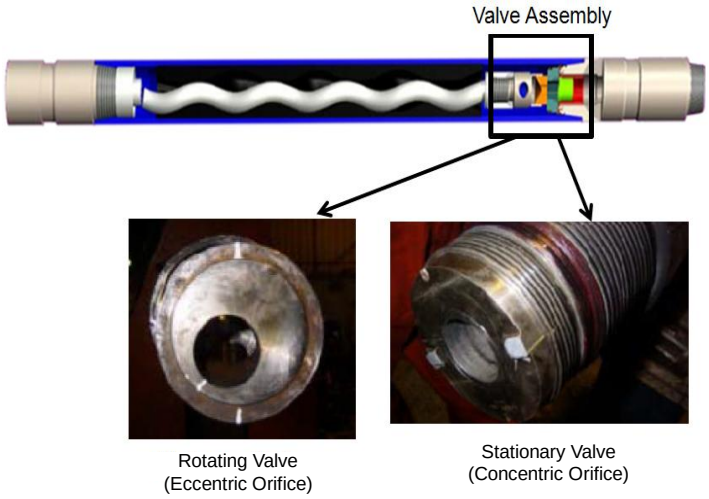

Figure 2. 5: Valve assembly of an AOT (Baez and Alali, 2011)

The pressure pulse inside the tool is high at minimum TFA, while it is low at maximum TFA. **Figure 2.6** shows the relative positions of the valve plates during operation. Due to the rotor-stator lobes configuration, the pressure pulses generated within the power and valve sections have frequencies in the range of 9 to 20 Hz, depending on the flow rate and the size of the tool. The pressure pulses are transmitted from the valve section through the viscous fluid inside the string to the shock tool or oscillation section. The pressure pulses exert a hydraulic force on the pump open area (POA) of the oscillation section (shock tool), producing axial vibrating force at a predetermined frequency which travels uphole and downhole, along the drillstring to reduce friction between borehole and drillstring. The oscillation section or shock tool is mostly used in jointed drillpipe applications, and it generates controlled axial oscillation of the drillstring to reduce downhole friction.

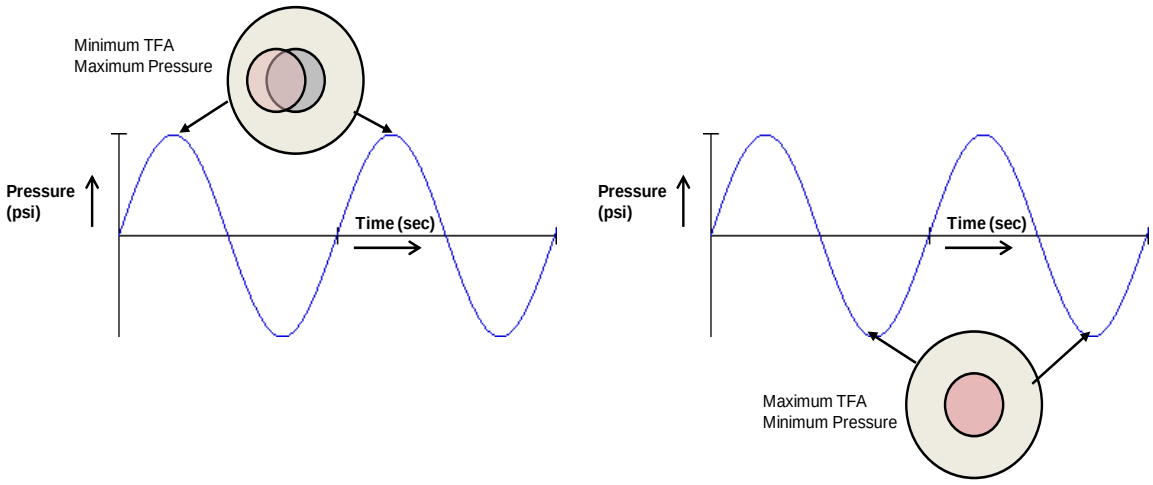

Figure 2. 6: Relative positions of the orifices and pressure pulses (adopted from NOV, 2006)

Belleville disc springs are loaded in the longitudinal direction on a mandrel located inside the shock tool. The spring stiffness or spring rate can be varied by stacking the convexly shaped disc in parallel in two sets (2×2) or three sets (3×3), where each parallel sets are then arranged in series, that is, with the convex side of each set facing the other set (**Figure 2.7**). The mandrel of the shock tool is sealed between the annulus pressure and internal drill pipe pressure, which creates a pump open area (POA) (Azike-Akubue et al., 2012). The mandrel extends when internal pressure exerts a hydraulic force on the pump open area and retracts to its initial position once the pressure is removed. In most applications, the shock tool or oscillation section is placed immediately above the power section and axially oscillates between 1/8" to 3/8" during operation (Baez and Alali, 2011). The axial vibrations generated by AOT can be measured several hundred or over a thousand feet away from the tool (Gee et al, 2015).

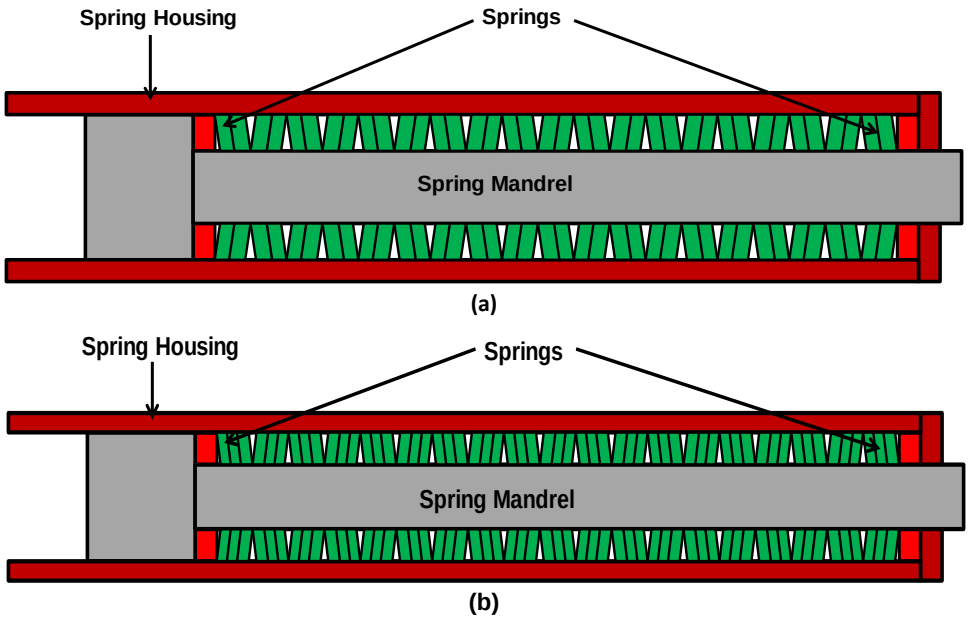

Figure 2. 7: Stacking configurations of the disc springs: (a) 2×2, and (b) 3×3

2.3. Factors Affecting Performance of Axial Oscillation Tools

The performance and efficiency of axial oscillation tools are affected by operating parameters and setup of the tool, drilling parameters, friction, borehole geometry, drillstring characteristics.

2.3.1. Effects of Operating Parameters

Some of the important operating parameters that contribute to the setup of axial oscillation tool (AOTs) are: flow rate, operating frequency, drilling fluid type and density, valve/orifice sizing, pressure drop across the AOT, AOT spring rate or spring constant, pump open area (POA), and downhole temperature.

Flow rate: Since AOTs are hydraulically operated, the flow rate is the most critical drilling parameter required for effective performance of AOTs and entire axial oscillation-supported drillstrings. Operators and drilling rigs should maintain flow rate within the recommended operating range of AOTs, as specified by manufacturers, for optimal performance.

The pressure drop across the AOT is strongly dependent on the operating flow rate. Experimental testing of AOTs shows an approximately linear relationship between flow rate and pressure drop (Martinez et al., 2013). Operating AOTs at higher flow rates increases the pressure pulses and create more aggressive and high energy axial oscillations.

Operating or excitation frequency: This is the number of cycles of pressure pulses generated and measured (or observed) in one second. The excitation frequency is directly proportional to the operating flow rate, which is directly related to the speed of the rotor in the power section. The relationship between excitation frequency and the flow rate is linear as shown in **Figure 2.8**, but the linear relationship varies by tool sizes and manufacturer's design. Therefore, operating frequency ω is defined as:

$\omega = f\{\text{Operating flow rate}\}$

Table 2.1 shows the linear relationship constant between frequency and flow rate for different tool sizes. The operating frequency of AOT needs to be compatible with the operating frequency of MWD equipment in order to avoid signal interference. The frequency of pressure pulses generated by the AOT can be controlled by increasing or decreasing the operating flow rate to avoid and prevent MWD signal interference. Most MWD companies have written standard operating procedures which prescribe actions taken to filter MWD signals to avoid interference (NOV, 2016).

Density of drilling fluid: The density of drilling fluid pumped through the AOT is one of the operating parameters of AOT that contributes significantly to the pressure drop generated within the AOT. Large pressure drops are generated at higher fluid density. Operators and drilling engineers should ensure the density of drilling fluid will not create a too high-pressure drop, beyond the operating range of the AOT. In the case where drilling fluid density is high, the

flow rate can be reduced to match the allowable pressured drop across the AOT. **Figure 2.9** shows the relationship between the pressure drop across an AOT and flow rate at different mud densities, for a specific valve size of 1.03 in.

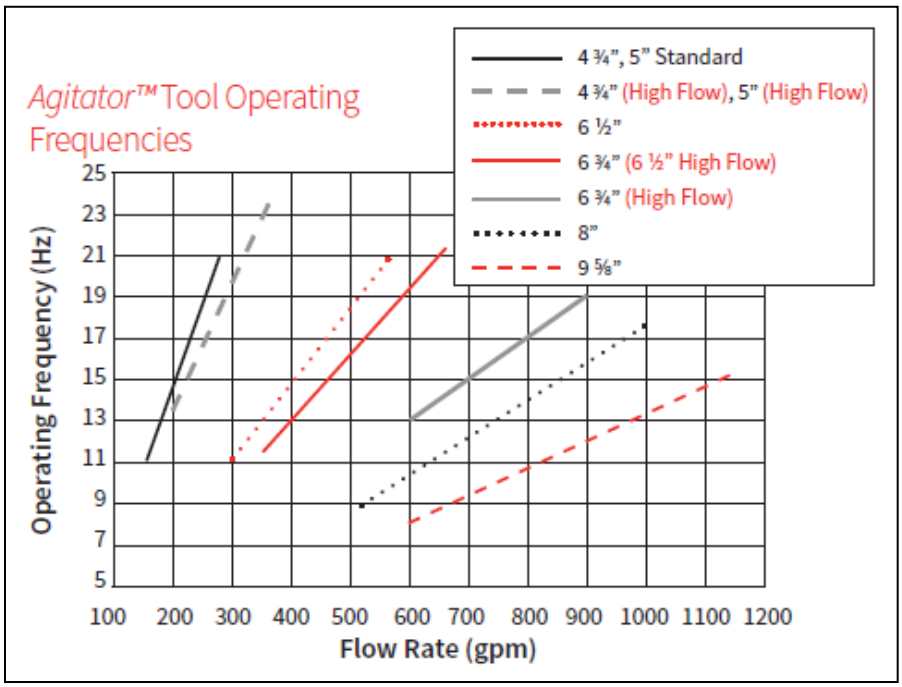

Figure 2. 8: AOT frequency at different flow rates (NOV, 2016)

As the mud density increases, the drillstring becomes lighter due to buoyancy and the normal contact force is reduced. Hence, axial oscillations generated by AOTs are lightly damped.

Table 2. 1: Linear relationship constant between frequency and flow rate (NOV, 2016)

Tool Size	Constant
1 11/16" (NEO)	0.215
3 1/8" (NEO)	0.043
3 1/2" (NEO)	0.037
2 1/8", 2 3/8"	0.225
2 7/8", 3 1/8", (High Flow)	0.125
3 3/4"	0.217
4 3/4", 5"	0.075
4 3/4" (High Flow), 5" (High Flow)	0.067
6 1/2"	0.038
6 3/4" (6 1/2" High Flow)	0.033
6 3/4" (High Flow)	0.020
8"	0.018
9 5/8"	0.013

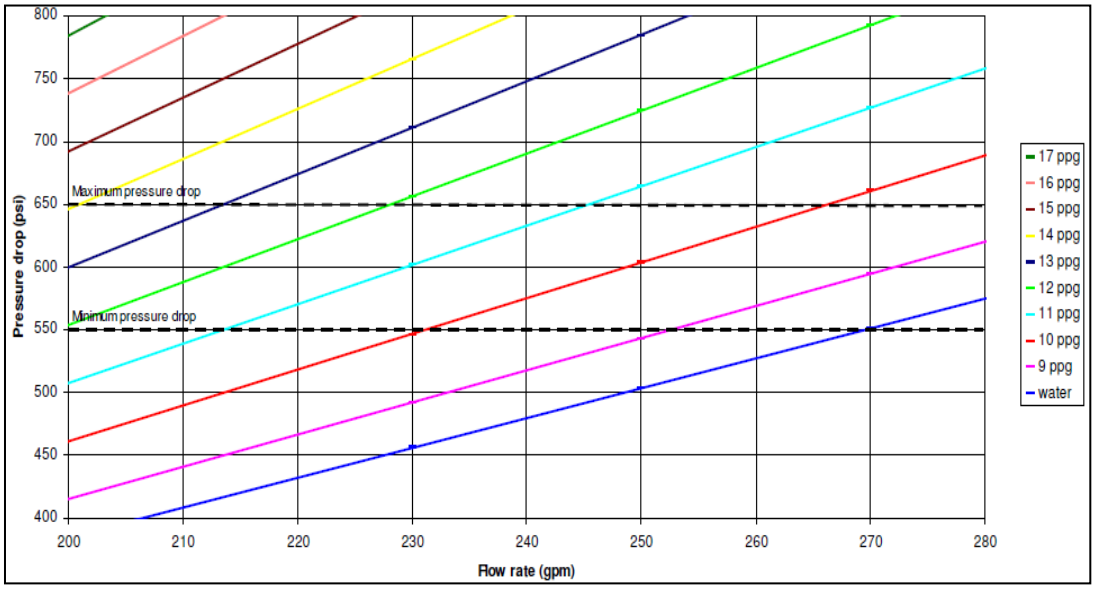

Figure 2. 9: Relationship between pressure drop and flow rate for different mud weights (valve size = 1.03 inches) (Robertson, 2006)

Valve/orifice flow area: The variation in valve/orifice flow area between the stationary plate and oscillating valve creates the restriction to fluid flow with the AOT, thereby generating pressure pulses. **Figure 2.10** shows the relationship between the flow area and the valve rotation angle.

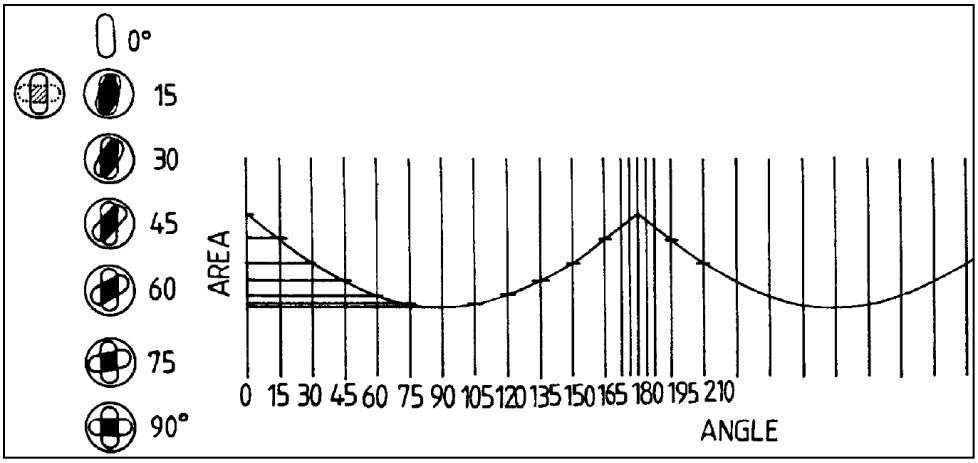

Figure 2. 10: Relationship between flow area and rotation angle (Eddison and Hardie, 2001)

The AOT is designed with a unique feature that provides the shop technicians and field operators the capability to adjust the orifice/valve setting of the AOT to match specific flow rates, mud weights, and rig pump pressures. **Figure 2.11** shows the theoretical relationship between pressure drop and flow rate for different oscillating valve diameters and specific mud weight of 8.6 ppg.

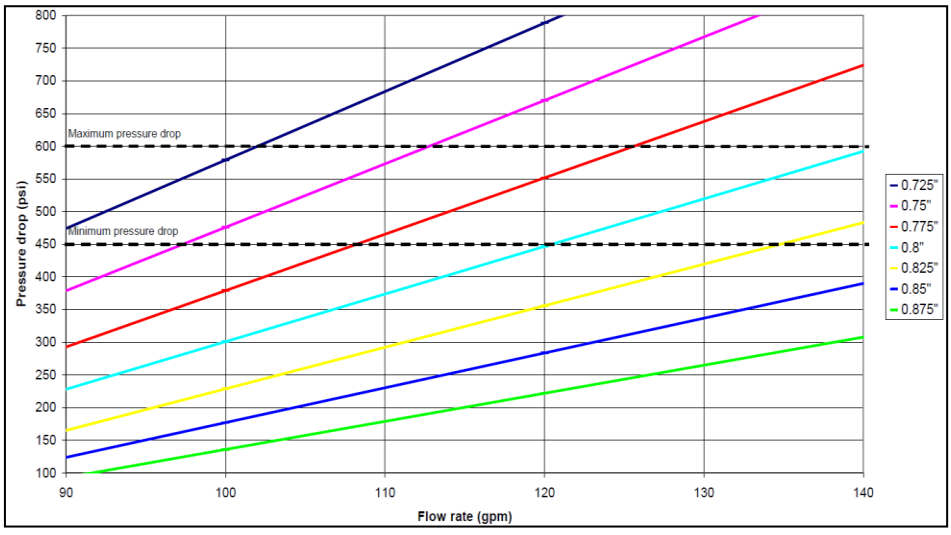

Figure 2. 11: Theoretical relationship between pressure drop and flow rate for different valve sizing (mud weight = 8.66 ppg) (Robertson et al., 2004)

Pressure drop across the AOT: The AOT pressure drop ΔP indicates the hydraulic resistance of the AOT to the mud flow. It is the difference between the inlet and outlet pressure

of the AOT. **Figure 2.12** shows the pressure drop and pressure pulses generated within and behind the AOT, represented as harmonic waves. This pressure drop acts as pressure pulses on the pump open area (POA) of the shock-sub or oscillation section of the AOT. The effectiveness of AOTs depends on the pressure drop generated across the AOT, which in turn depends on the drilling fluid density and flow rate (NOV, 2016). Experimental testing of AOTs has shown that other parameters contribute to the magnitude of pressure drop include: valve/orifice dimensions (Robertson et al., 2004), internal geometry and relative movement of the AOT spring stacking against the drilling fluid. Therefore, AOT pressure drop ΔP is defined as:

$$\Delta \mathrm{P} = f \left\{ \begin{array}{c} \text{Operating flow rate} \\ \text{Drilling fluid density} \\ \text{Valve/orifice flow area} \\ \text{AOT internal geometry} \\ \text{Movement of AOT spring stacking} \end{array} \right\}$$

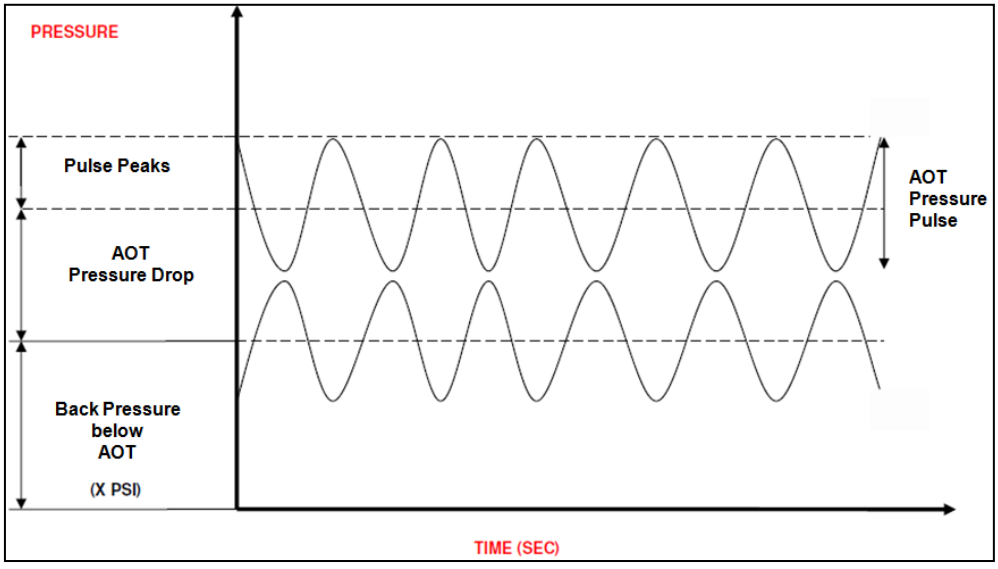

Figure 2. 12: Pressure drop and pressure pulses generated within and behind the AOT (Robertson, 2006)

The pressure drop across AOTs ranges from 300 to 900 psi depending on set up in the shop. The addition of these pressure drop to drillstring pressure loss increases the standpipe pressure while drilling (Martinez et al., 2013), and can be enormous to the rig pump pressure

capacity (Gee et al., 2015). The pressure limitation hinders a segment of the drilling market from using the AOTs (Martinez et al., 2013; Robertson et al., 2004). Therefore, there is a need for low-pressure AOTs that can effectively break static friction without contributing significant pressure to the drilling system. One of the improvements was to redesign the valve/orifice sizes (to reduce the pressure drop) and increase the pump open area, allowing the AOT to generate magnitudes of oscillations similar to the standard AOT at a much lower pressure drop (Martinez et al., 2013; NOV, 2016).

AOT spring rate or spring constant: AOT spring rate or spring constant is the force required to compress the spring by a given length. The value of the AOT spring rate is provided by the tool manufacturer. The load versus displacement relationship of the AOT spring is linear and the slope or spring rate can be found using a bench press test. The spring constant of the Belleville springs loaded on the mandrel of the oscillation section can be varied by changing the disc spring stacking, as shown in Figure 2.7. As discussed earlier, the movement of the mandrel on the oscillation section can be controlled and optimized by increasing or decreasing the spring rate.

Pump open area (POA): The pump open area (POA), which is the area of the internal piston where the pressure pulses act upon (**Figure 2.13**). As the pressure pulses act on the pump open area, the mandrel of the AOT is extended (Martinez et al., 2013). When aggressive pressure pulses are generated at the valve section of the AOT, the pump open area needs to be reduced to minimize the oscillations generated by the AOT.

Types of drilling fluid: The elastomers of power sections of AOTs are affected by the composition of drilling fluids. Certain additives in oil-based muds (OBMs) and synthetic based muds (SBMs) have the ability to chemically and thermally degrade AOT elastomers by altering

the elastomer properties, such as changes in volume, hardness, tensile strength. This results in severe damage to the tool (Bodepudi et al., 1998).

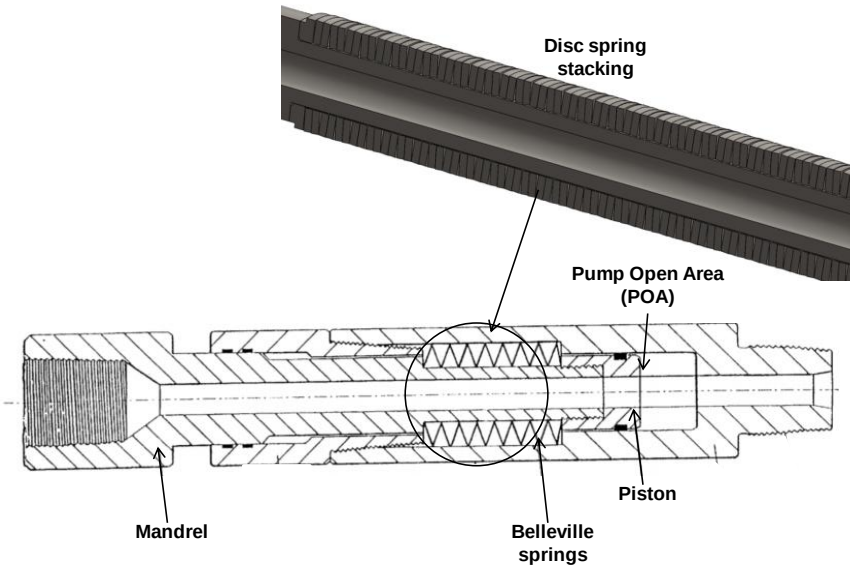

Figure 2. 13: Belleville spring stacking in the oscillation section (Eddison and Hardie, 2006)

Downhole temperature: Temperature affects power section elastomers and density of the drilling fluid. Shrinkage and swelling of elastomer occur as temperature changes, leading to fatigue and damage of the elastomer rubber. At higher downhole temperature, the elastomer swells increasing the pressure drop across the power section of the AOT. Higher temperatures can also lead to a breakdown in density flowing across the AOT, leading to a reduction in pressure drop below the desired level. Also, the lubricity of drilling fluids reduces at high temperatures, which leads to an increase in the frictional force between the drillstring and the wellbore (Abdo and Al-Sharji, 2015).

The operating parameters of axial oscillation tools need to be optimized and rightly configured to improve efficiency and effectiveness of axial oscillation-supported drilling system, without causing dynamic instabilities to the drilling system (Baez and Alali, 2011). Typical sizes

and specification of an AOT are shown in **Table 2.2**. **Table 2.3** shows a typical BHA including an AOT placed at 120.12 m behind the bit.

Table 2. 2: Typical sizes and technical specification of an AOT (Azike-Akubue, 2012)

Tool Size (OD)	3-3/4"	4-3/4" (HF)	5" (HF)	6-1/2"	6-3/4"	8"	9-5/8"
Overall Length	12-1/2 ft.	8-3/4 ft.	8-3/4 ft.	6 ft.	9 ft.	11 ft.	12 ft.
Weight	240 lbs	310 lbs	498 lbs	900 lbs	1,000 lbs	1,600 lbs	2,000 lbs
Recommended Flow Range	90-140 gpm	150-270 gpm 250-330 gpm	150-270 gpm 250-330 gpm	375-475gpm	400-600 gpm	500-1,000 gpm	600-1100 gpm
Temp Range*	302°F (150°C)	302°F (150°C)	302°F (150°C)	302°F(150°C)	302°F (150°C)	302°F (150°C)	302°F (150°C)
Operating Frequency	26 Hz @ 120 gpm	18-19 Hz @ 250 gpm 16-17 Hz @ 250 gpm	18-19 Hz @ 250 gpm 16-17 Hz @ 250 gpm	15 Hz @ 400 gpm	16-17 Hz @ 500 gpm	16 Hz @ 900 gpm	12-13 Hz @ 900 gpm
Operational Pressure drop generated	500-600 psi*	500-600 psi*	500-600 psi*	500-600 psi*	500-600 psi*	500-600 psi*	500-600 psi*

Table 2. 3: Typical BHA including an AOT (Azike-Akubue, 2012)

Element	Top Connection	OD(in.)	ID(in)	NONMAG	Length(m)	Cum. Length (m)
8"3/4 Bit	4"1/2 Reg Pin	8.750		ST	0.26	0.26
8 11/16" Turbo Back Stab	4"1/2 Reg Pin	6.000 6.688	2.250	ST	0.34	0.60
7" SperryDrill Lobe 7/8, 83/8" Sleeve, AKO 1.15 deg	4"1/2 IF Box	6.750 8.375	4.753	ST	7.71	8.31
6"1/2 Float Sub	4"1/2 IF Box	6.750	2.750	ST	0.96	9.27
6"3/4 Pony NMDC	4"1/2 IF Box	6.750	3.100	NM	1.50	10.77
6"1/2 Pony NMDC - MWD	4"1/2 IF Box	6.625	3.250	NM	1.81	12.58
6"3/4 MWD NM HOS	4"1/2 IF Box	6.750	3.250	NM	1.62	14.20
7"1/4 IB Steel Stab	4"1/2 IF Box	6.500 7.250	2.875	ST	1.80	16.00
9 x 5" HWDP (Rig)	4"1/2 IF Box	5.000	3.000	ST	83.39	99.39
Agitator	4"1/2 IF Box	6.750		ST	2.74	102.13
Shock sub	4"1/2 IF Box	6.750		ST	2.74	104.87
4 x 5" HWDP (Rig)	4"1/2 IF Box	5.000	3.000	ST	37.06	141.93
6"1/2 Drilling Jars	4"1/2 IF Box	6.500	2.500	ST	9.64	151.57
1 x HWDP (Rig)	4"1/2 IF Box	5.000	3.000	ST	9.27	160.84

2.3.2. Effects of Drilling Parameters

The drilling parameters applicable to directional drilling are weight-on-bit (WOB), rotational speed or RPM and flow rate. As WOB increases at the bit, a compressive force is transferred from the bit towards the surface. Placing the AOT in the compressive region along the drillstring limits the extension of the oscillation section or shock-sub of AOTs (Martinez et

al., 2013). Also, the spring stiffness or spring rate of AOT need to be able to withstand high compressive forces generated from higher downhole weight-on-bit. The effect of RPM on the performance of axial oscillation-supported drillstring can be linked to rotary drilling operations, where frictional force is reduced with increasing RPM coupled with oscillations from the AOT (Samuel, 2010).

Field and experimental results show that the rotation of drillpipe has a remarkable effect on hole cleaning and friction reduction during directional drilling. The level of improvement due to pipe rotation is a function of the combined effects of mud rheology, cuttings size, and flow rate (Sanchez et al., 1997). However, AOTs are mostly needed in slide drilling operations with steerable BHAs where surface RPM is non-existent. Field studies also show that percentage improvement in ROP with AOT is generally higher during slide drilling than rotary drilling (Robertson et al., 2009; Barton et al., 2011). The effect of flow rate has been explained earlier as part of the operating parameters of AOTs that need to be optimized.

2.3.3. Other Parameters Affecting the Performance of AOT

Borehole Geometry: The complexity of borehole geometry affects the performance of AOTs in axial oscillation-supported drilling systems. As it is known, normal contact loads contribute to the frictional forces while drilling. From the equations of torque and drag, the magnitude of normal contact loads increases with increasing borehole inclination, azimuth, and doglegs (Johancsik et al., 1984). As borehole inclination starts to deviate from the vertical, normal contact loads or side forces increases. Frictional forces increases in the curve and lateral sections, thereby damping the axial displacement response of AOTs as a result of Coulomb friction (Gee et al., 2015). Higher friction factors are generally assumed in the curve and lateral sections to account for the additional contact forces due to buckling (Forster, 2015).

Friction: The friction factor used for torque and drag and vibration analysis is a term that accounts for the coefficient of friction between contacting surfaces and other uncertainties such as cuttings characteristics, mud type, mud lubricity, hole tortuosity, pipe buckling (Samuel, 2010). The frictional force opposing the drillstring motion or Coulomb friction defined as $F_c = \mu F_N$ contributes to the damping of oscillations generated by the AOTs in axial oscillation-supported drillstrings. Theoretical model shows higher vibrating forces and accelerations when the AOTs are located in the vertical section than when located in the lateral section (Shor et al., 2015).

Drillstring Characteristics: Drillstring stiffness (modulus of elasticity and inertia) and length to diameter ratio affects axial displacement and acceleration of axial oscillation-supported drilling systems when excited by AOTs. Vibration studies show that increasing drillstring stiffness provides more resistance to vibrations (Larsen, 2014). For a particular drillstring material, e.g. steel, stiffness increase requires increasing the cross-sectional area or a thicker pipe, which results in pipe weight increase (Tian et al. 2015). Therefore, drillstrings with lesser stiffness tend to oscillate at higher amplitudes. There is a compromise in reducing drillstring stiffness to increase axial displacement response and accelerations or increasing tendency of buckling due to increasing compressive forces. In addition, increasing ratios of length to diameter of drillstrings reduces vibration stability (Tian et al. 2015). Hence, drillstrings with high length to diameter ratio oscillate with higher amplitude when subjected to AOT excitation, but reduces the stability to overall vibrations, which can be damaging.

2.4. Methods Used to Evaluate the Effectiveness of AOTs

The application of axial oscillation tools often provides effective solutions to problems related to low ROP, buckling, erratic reactive torque, unstable toolface control, short bit life,

high tortuosity and poor borehole quality associated with high friction in high-angle and extended-reach wells (Baez and Alali, 2011). The methods used in evaluating the effectiveness of axial oscillation-supported drilling system involve measurements and monitoring of several parameters. The measured parameters are (i) weight transfer, rate of penetration, ROP and drag; (ii) stick-slip and torsional vibrations; (iii) mechanical specific energy (MSE); (iv) toolface control; and (v) drilling dynamics.

2.4.1. Weight Transfer and Rate of Penetration (ROP)

Weight stacking occurs downhole when the cumulative static frictional force along the entire drillstring is greater than the applied downward force (Skyles et al., 2012). The downward force stacks uphole and hinders the amount of weight transferred to the drill bit. **Figure 2.14** shows the description of weight stacking. Robertson (2006) was one of the first to study and evaluate the effectiveness of AOTs using mathematical modeling and verification with field results. The work of Robertson (2006) provided a simple methodology for evaluating the effectiveness of an AOT between sliding and rotating drilling. The primary goal of the study was to determine if AOTs improve slide drilling performance and determine actual friction factors for slide drilling. Field data showing ROP values with and without AOT were compared to assess the effectiveness of the tool. **Tables 2.4** and **2.5** show the field ROP data with and without AOT.

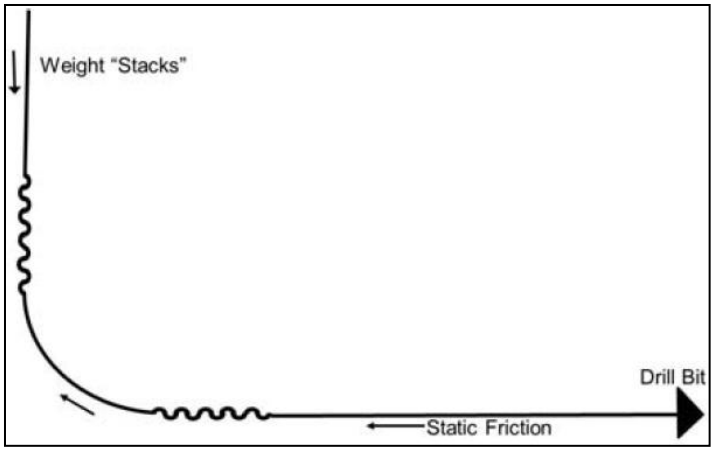

Figure 2. 14: Description of weight stacking (Skyles et al., 2012)

Table 2. 4: ROP data without axial oscillation tool (Robertson, 2006)

Without Axial Oscillation Tool (at end of Bit 5-D)	Average ROP (m/h)
Rotary Drilling	2.81
Slide Drilling	1.02

Table 2. 5: ROP data with axial oscillation tool (Robertson, 2006)

With Axial Oscillation Tool (at end of Bit 6-D)	Average ROP (m/h)
Rotary Drilling	2.69
Slide Drilling	2.42

Using ROP as a measure of the effectiveness of the AOT in an axial oscillation-supported system, Eq. 2.1 is proposed (Robertson, 2006) for assessing the performance of the tool.

$$ROP = \left(\frac{WOB}{d_B}\right)^{a_5} \cdot RPM^{a_6} \cdot K \qquad (2.1)$$

where ROP is the rate of penetration (m/h), WOB is the weight-on-bit $(kDaN)$, d_B is the bit diameter (mm), RPM is the bit rotational speed (RPM), K is the formation constant, a_5 is the WOB exponent (0.8 - 2.0) and a_6 is the RPM exponent.

The following expression, which is used to calculate the formation constant, can be obtained by rearranging Eq. 2.1,

$$K = \frac{ROP}{\left(\frac{WOB}{d_B}\right)^{a_5} \cdot RPM^{\,a_6}} \tag{2.2}$$

The formation constant is considered to be an invariable in homogeneous-formation over very short intervals of rotary and slide drilling. Since the constant is a formation property it is considered to be independent of the type of drilling operation. Hence, K for rotating operation is equated to K for sliding operation in Eq. 2.3.

$$\frac{ROP_{rot}}{\left(\frac{WOB_{rot}}{d_B}\right)^{a_5} \cdot (RPM_{rot})^{a_6}} = \frac{ROP_{slide}}{\left(\frac{WOB_{slide}}{d_B}\right)^{a_5} \cdot (RPM_{slide})^{a_6}} \tag{2.3}$$

WOB for sliding operation is evaluated using Eq. 2.4.

$$WOB_{slide} = d_B \left[\left(\frac{RPM_{rot}}{RPM_{slide}}\right)^{a_6} \cdot \left(\frac{ROP_{slide}}{ROP_{rot}}\right) \cdot \left(\frac{WOB_{rot}}{d_B}\right)^{a_5}\right]^{1/a_5} \tag{2.4}$$

The average percentage of WOB transferred over different homogeneous intervals drilled with different bits with the same design were calculated for cases with and without the tool. **Table 2.6** and **2.7** show the average percentage of WOB transferred with and without the tool.

Table 2. 6: Percentage of WOB transferred with AOT at 280 m from Bit (Robertson, 2006)

Mode	From (m)	To (m)	ROP (m/h)	Motor RPM	Total RPM	WOB (rig) (kDaN)	WOB (calc) (kDaN)	WOB % Transfer
Slide	4529.2	4532.0	2.42	65.84	65.84	25.12	18.03	71.77%
Rotary	4532.2	4535.0	2.69	66.17	101.93	12.95		
Rotary	4534.0	4536.8	2.71	66.41	102.34	13.24		
Slide	4537.6	4541.0	2.18	67.31	67.64	22.31	16.13	72.31%
Slide	4542.0	4544.4	2.18	68.06	68.06	22.96	15.68	68.29%
Rotary	4544.6	4545.6	2.93	67.32	103.54	13.83		
Rotary	4544.6	4545.6	2.93	67.32	103.54	13.83		
Slide	4546.6	4548.0	1.73	67.30	67.87	21.68	12.48	57.58%
Rotary	4544.6	4545.6	2.93	67.32	103.54	13.83		
Slide	4549.0	4553.0	2.07	68.26	68.39	21.55	14.80	68.66%
Slide	4549.0	4553.0	2.07	68.26	68.39	21.55	16.89	78.35%
Rotary	4553.2	4556.2	2.48	67.73	101.92	13.60		
Rotary	4573.0	4575.2	2.61	66.53	101.30	14.24		
Slide	4576.4	4579.4	2.28	65.29	65.59	25.07	19.17	76.47%

Table 2. 7: Percentage of WOB transferred without AOT (Robertson, 2006)

Mode	From (m)	To (m)	ROP (m/h)	Motor RPM	Total RPM	WOB (rig) (kDaN)	WOB (calc) (kDaN)	WOB % Transfer
Rotary	4482.0	4482.6	3.27	66.58	98.71	14.54		
Slide	4483.8	4484.5	1.04	66.94	66.94	29.89	6.79	22.73%
Rotary	4512.0	4515.4	2.81	67.54	100.62	13.76		
Slide	4518.4	4519.0	1.20	67.34	67.34	33.59	8.77	26.11%
Rotary	4512.0	4515.4	2.81	67.54	100.62	13.76		
Slide	4519.4	4521.6	0.97	67.32	67.32	33.56	7.10	21.14%

2.4.2. Stick-slip and Torsional Vibrations

During the stick-slip phase, the bit rotational speed changes from zero to several times the surface speed. The stick-slip phase imposes torsional fatigue in the drillstring components. One of the methods of mitigating stick-slip is to use axial oscillation tools to break static friction during the stick phase of the stick-slip process. During field operations, stick-slip is measured by the variation in BHA or drillbit speed (Patil and Teodoriu, 2012). The variation in RPMs of a standard BHA (without AOT) and a BHA (with AOT) drilling in the same formation is shown in **Figures 2.15** and **2.16**.

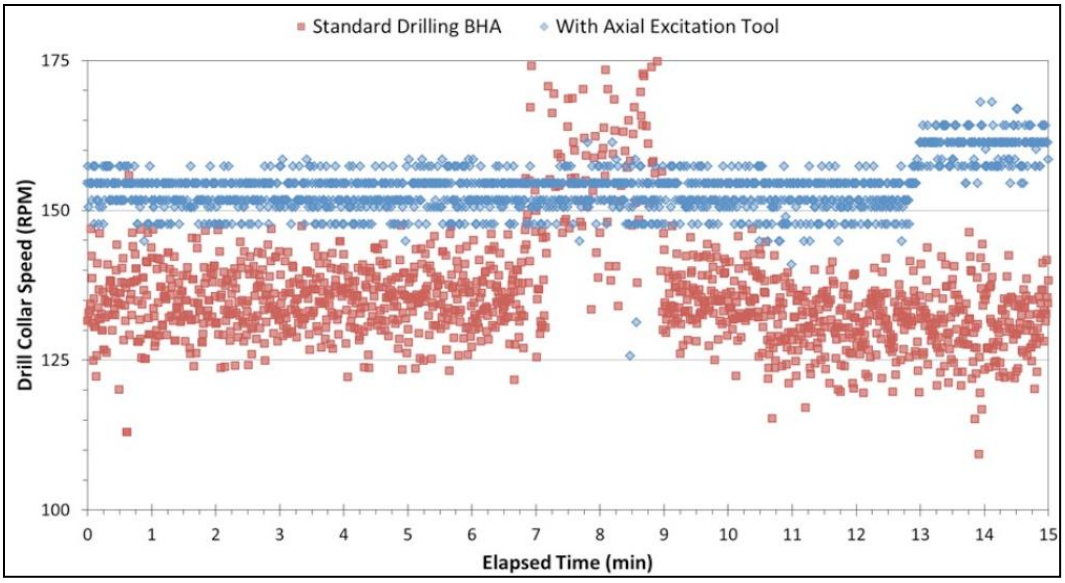

Figure 2. 15: Variation in RPM on drill collar (Clausen et al., 2014)

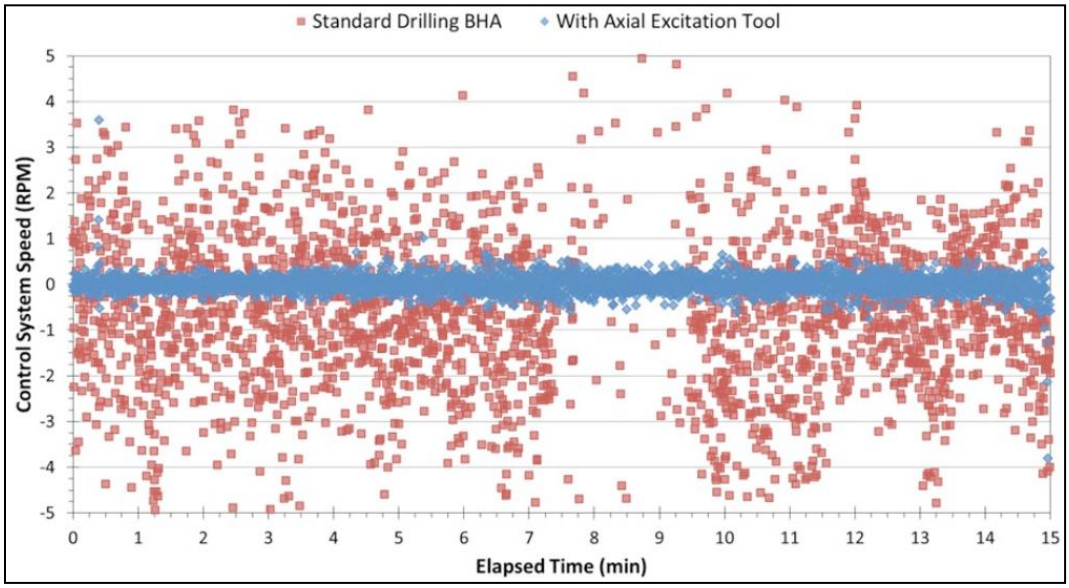

Figure 2. 16: Variation in RPM on RSS internal control system (Clausen et al., 2014)

It can be observed that stick-slip was reduced with the use of AOT in the BHA. Also, the reduction in the variation of the RPM on the RSS internal control system allows better holding of geostationary position within the RSS and control of toolface (Clausen et al., 2014). The application of axial oscillation tool (AOT) in conjunction with the standard rotary steerable

system (RSS) has been effective in mitigating downhole torsional vibrations, stick-slip, and lateral vibrations.

2.4.3. Mechanical Specific Energy (MSE)

The friction reduction provided by AOT decreases the mechanical specific energy (MSE). The MSE is the amount of work done by the bit per unit volume of rock drilled. It is expressed mathematically as (Azike-Akubue et al. 2012):

$$MSE = \frac{W}{A_X} + \frac{120\pi NT}{A_X R} \quad (2.5)$$

where W is the weight-on-bit (lbf), A_X is the cross-sectional area (in^2), N is the rotary speed (RPM), T is the drilling torque ($ft.lbf$) and R is the rate of penetration (ft/hr).

Assuming the rotary speed N and borehole cross-sectional area are constant at all time, increasing the rate of penetration R while a decrease in applied weight-on-bit W and torque T to achieve the same rate of penetration results in decreased MSE. Increasing weight transfer through the use of AOT improves ROP, reduces MSE and enhances drilling efficiency.

2.4.4. Toolface Control

In addition to weight transfer, toolface control (**Figure 2.17**) is an important variable that needs to be controlled by drilling engineers and directional drillers while sliding in high-angle and extended reach wells. Both toolface control and weight transfer are dependent on each other due to the reactive torque generated by the motor (Jones et al., 2015). Erratic toolface control occurs due to unsteady weight transfer to the bit, leading to tortuous doglegs and poor wellbore quality. The application of axial oscillation tools in slide drilling and rotation operations leads to steady toolface control. Hence, operators of axial oscillation-supported drillstrings use

measurement and monitoring of changes in toolface control to measure the effectiveness of AOTs and the entire system.

Figure 2. 17: Toolface control (Skyles et al., 2012)

2.4.5. Drilling Dynamics

An observation from the data (**Figures 2.18** and **2.19**) presented by McCarthy et al. (2009) showed a minimal increase in axial accelerations with AOT as compared to without AOT. Maximum axial accelerations during the slide run with AOT was 4.5 *g* while without AOT was close to 3 *g*.

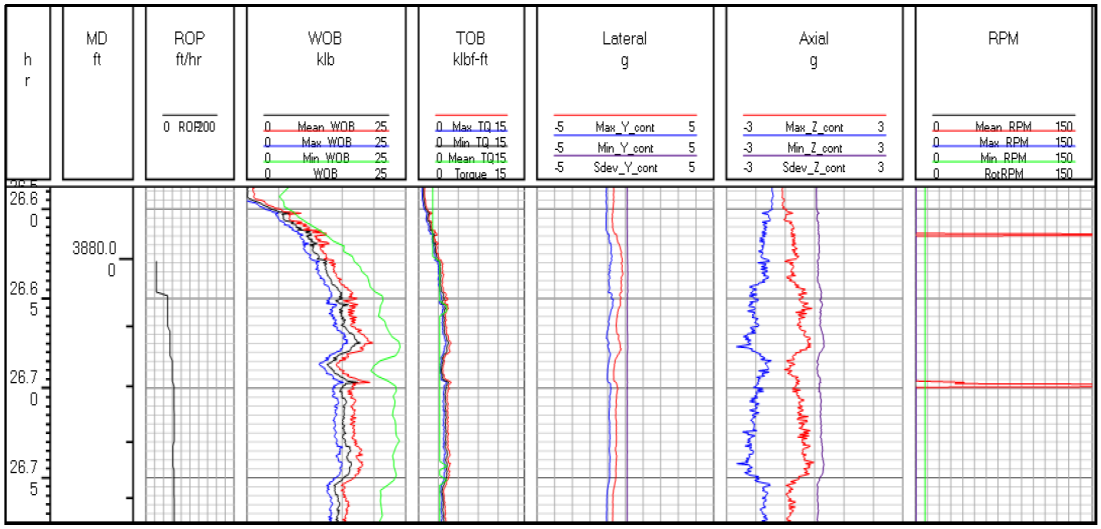

Figure 2. 18: Slide drilling at the end of run 1 without AOT (McCarthy et al., 2009)

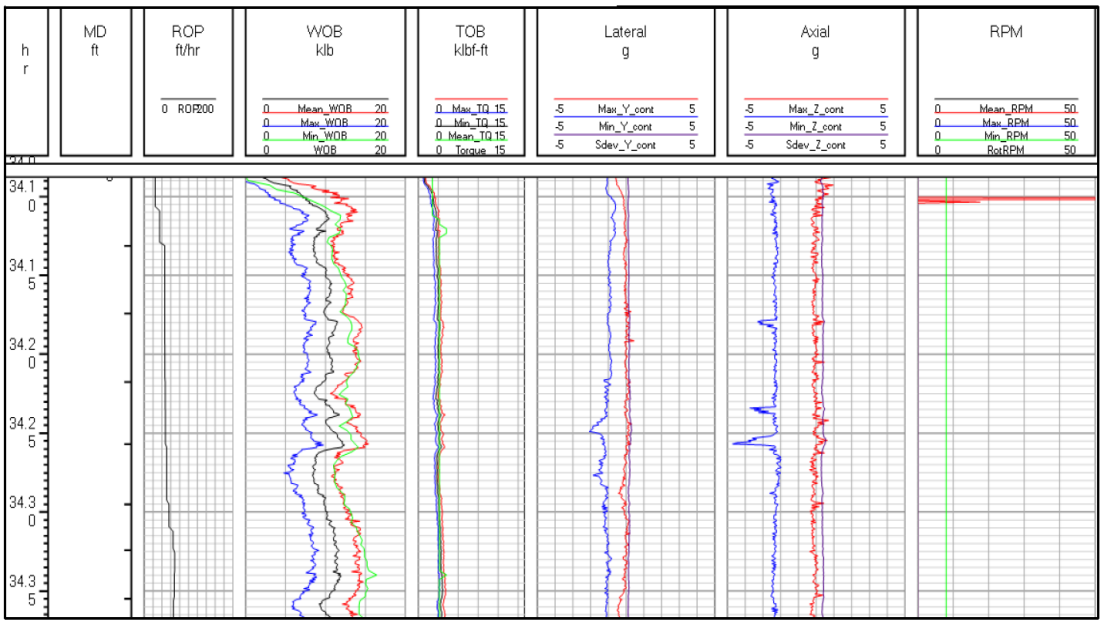

Figure 2. 19: Slide drilling at the beginning of run 2 with AOT (McCarthy et al., 2009)

Gee et. al (2015) presented a case study showing the back and forth transfer of oscillations generated by AOT along the length of drillstring while reducing friction over a major portion of the drillstring. The axial oscillations generated by the AOT can be measured over several hundred feet or close to over a thousand feet away from the tool (Gee et. Al, 2015). The case study presented by Gee et. Al (2015) was a tangent well drilled in the Middle East with five (5) high-frequency measurement devices (HFMD) included in the drillstring.

2.5. Experimental and Modeling Studies of AOT-Supported Drillstrings

Several experimental, mathematical and numerical models have been developed to investigate and evaluate the performance of axial oscillation tools (AOTs) in the axial oscillation-supported drillstrings. The focus of most of the existing models is directed towards: (i) predicting and simulating the dynamic response of AOTs; (ii) placement analysis of AOTs; and (iii) evaluating the friction-reducing performance of AOTs. The need to develop practical models, which precisely simulates the effect of AOTs cannot be overemphasized. The literature

review discusses the contributions of existing models in the dynamic analysis of axial oscillation-supported drilling systems and opportunities for improvements of the models.

2.5.1. Experimental Studies

Barakat et al. (2007) performed experiments to examine the influence of hydraulic vibrations on the transfer of axial loads in horizontal wellbores. Parameters such as frequency, flow rate and axial loads were varied to investigate their effects on the force transfer. The results showed a reduction in friction force between 30% and 100%. Higher flow rates of water increased axial force transfer which is similar to the effect of an increase in the frequency of pressure pulses. Increasing the viscosity of water reduced axial force transfer due to the viscous damping effect, especially under laminar flow conditions. A similar study (Abdo and Al-Sharji, 2015) was conducted to investigate the effects of amplitudes and frequencies of vibrations on frictional force, axial load transfer, and lock-up load of buckled rod confined in a horizontal cylinder for dissimilar fluids at normal and high temperature. Results show a reduction in axial force transfer with temperature for cases with and without vibrations.

Another study performed by Newman et al. (2009) to investigate the effects of vibrations while drilling using coiled tubing (CT) strings showed a reduction in friction with vibration frequency. The results also indicated that axial vibration of the CT drillstring was more effective in reducing friction than torsional vibration. Martinez et al. (2013) conducted testing focused on the development of a modified axial oscillation tool (AOT) designed to operate at a low-pressure drop, that is, decreasing the magnitude of pressure added to the standpipe by the AOT from the range of 500-600 *psi* to the range of 300-400 *ps*i. The results demonstrated a reduction in the pressure drop with the pump open area, resulting in greater AOT displacements. This is beneficial for rigs with limited pump pressure capabilities. However, increasing the pump area of

an AOT can lead to further compression and accelerated fatigue of the springs in the "Low Pressure" AOT due to the longer extension of the shock tool mandrel (Martinez et al., 2013). A recent laboratory study (Clausen et al., 2014) on the effect of an axial oscillation tool on ROP showed higher gains in ROP at a lower vibrating frequency, which could be due to a decrease in amplitude of excitation at higher frequencies.

Schultz (2015) conducted experimental studies on two downhole vibration tools (AOT and fluid hammer vibrating tools) for performance comparison. The results show similar performance for both tools in terms of pressure pulse height and frequency. This peak-to-peak pressure has a direct impact on the vibratory force. The peak-to-peak pressure change shown in **Figures 2.20** and **2.21** can be used to determine vibratory force for a specific coiled tubing size. The results from the study indicate that the pressure pulses or waves are sinusoidal and can be represented by harmonics of Fourier sine or cosine series. The force and frequency of the vibratory load exerted on the drillstring increased with flow rate through the tool. Hence, there is a cost associated with increasing the flow rate as it increases the average circulating pressure drop and subsequently the required hydraulic horsepower.

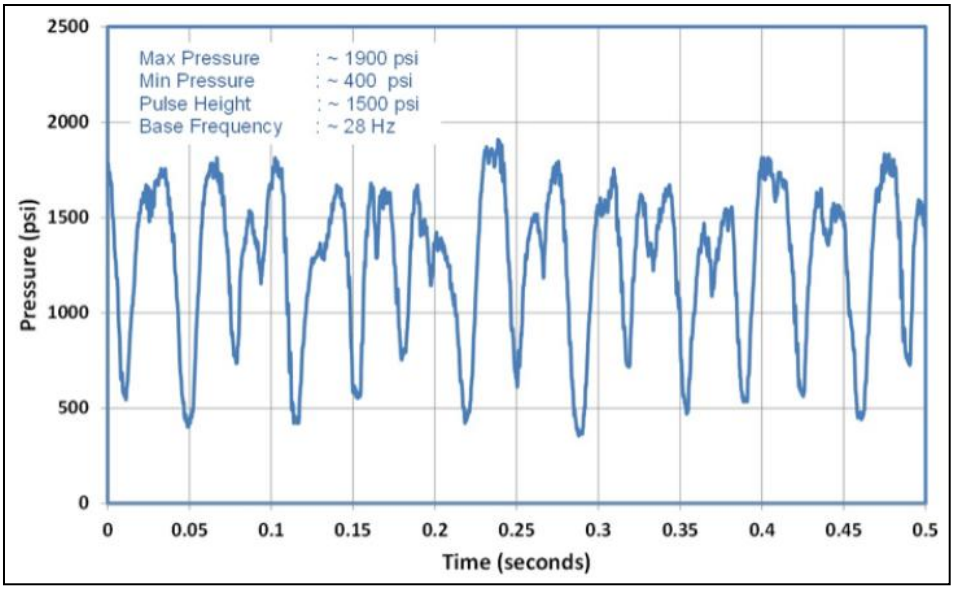

Figure 2. 20: Backpressure of fluid hammer vibrating tool at 3 bbl/min (Schultz, 2015)

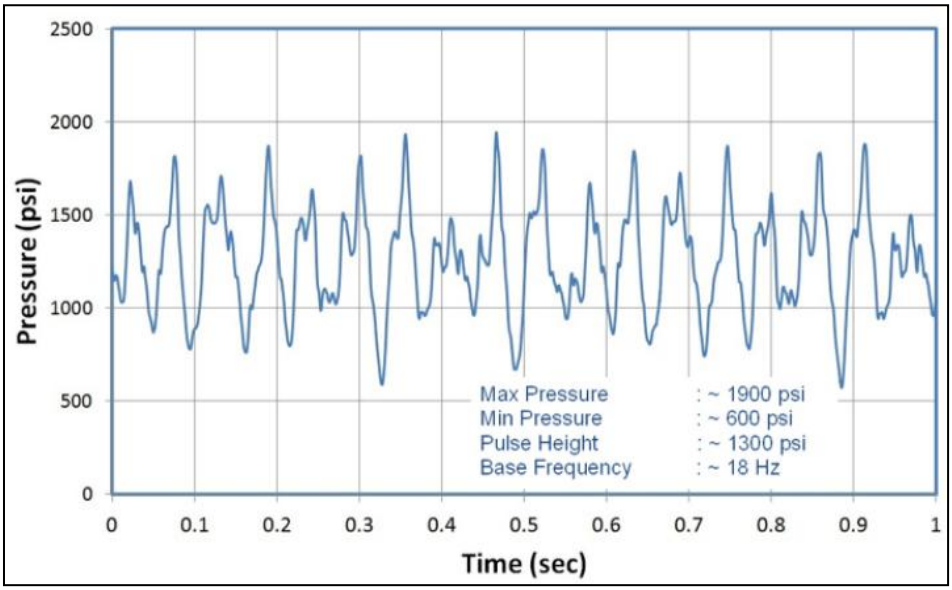

Figure 2. 21: Backpressure for AOT tool at 3 bbl/min (Schultz, 2015)

More recently, an experimental investigation (Tian et al., 2016) was conducted to evaluate the accuracy of a newly developed analytical model. Experimental measurements obtained from the study of Tian et al. (2016) is shown in **Figure 2.22**.

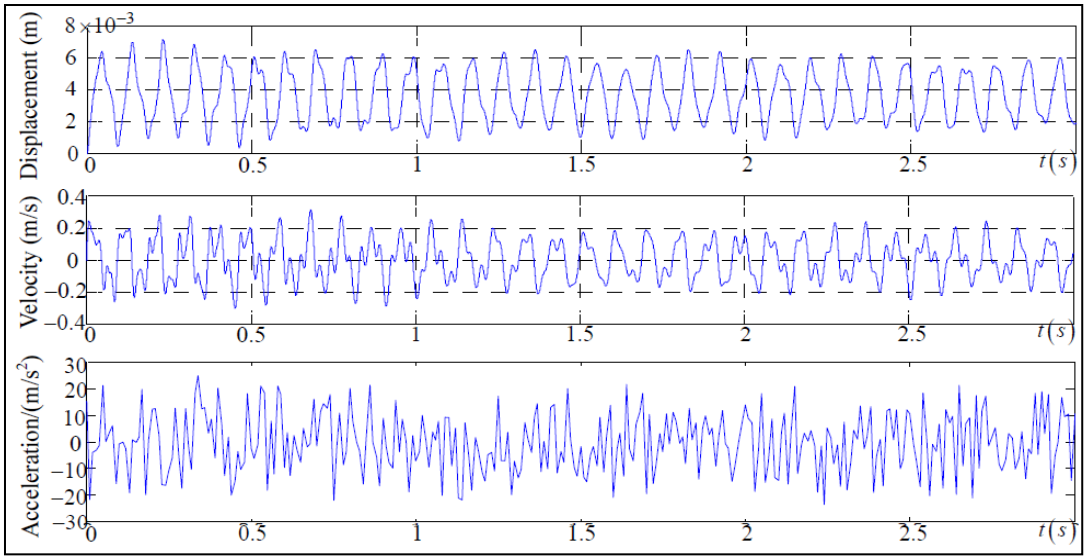

Figure 2. 22: Measured displacement, velocity and acceleration of AOT (Tian et al., 2016)

2.5.2. Analytical Modeling

The theory of axial vibrations of drillstrings is primarily used to model the response of axial oscillation-supported drillstrings subjected to either force or displacement excitations. A variety of analytical axial vibration models (Bailey and Finnie, 1960; Khan, 1983; Rashed et al., 2007; Li et al., 2007; Clausen et al., 2014; Forster and Grant, 2012; Forster, 2015; Shor et al., 2015; Tian et al., 2016; Bu et al., 2016; Al Dushaishi et al., 2017) have been formulated to study the axial vibrations of drillstrings. This study will focus on pure axial oscillations and will review uncoupled axial vibration models.

Longitudinal (or axial) and torsional vibrations in drillstrings are analogous and governed by similar equations (Bailey and Finnie, 1960; Khan, 1983). The undamped wave equation is used as the governing equation of the longitudinal motion of stepped drillstrings. The general solution to this equation is obtained by applying the method of separation of variables. The natural frequencies of the drillstring are obtained by finding the values of ω that match the required boundary conditions. Unlike other models, Bailey and Finnie (1960) defined x as zero

at the bottom of the drillstring and increasing towards the top of the string. The boundary condition at the bottom of the string is assumed to be fixed, and the boundary condition at the top of the string is assumed to be free. The top boundary condition is estimated from the motion of the derrick and travelling block which seems complicated.

Khan (1983) estimated the longitudinal natural frequencies and mode shapes of drillstrings for various boundary conditions at the bit and at the top of the string. For simplicity, equivalent viscous damping is used as an approximation for effects of different types of frictional resistances (contact, fluid, and material) along the drillstring. The longitudinal vibration of a steel bar is considered and described by the damped wave equation. The solution for the wave equation is obtained using the method of separation of variable to compute the natural frequencies and mode shapes. Three different boundary conditions (fixed-top and fixed-bottom, fixed-top and free-bottom, and mass-spring-at-top and spring-at-bottom) are considered in the analysis. The third boundary condition is the most realistic one because it accounts for the mass and stiffness of the drawworks and derrick at the top (Khan, 1983). The boundary condition with the spring at the bottom provides a means of varying the bottom end condition from fixed to free or to any intermediate value by choosing an appropriate value of the spring constant.

Another study (Li, 1987) modeled the longitudinal vibrations of drillstrings using the undamped wave equation. The wellbore-bit contact is considered as the source of excitation and the drillstrings is modeled as a continuous rod. Distance or velocity of slip between the bit tooth and the hole bottom is assumed negligible. The method of separation of variables is applied to solve the undamped wave equation. The boundary condition at the top of drillstring is assumed to be fixed. At the bottom of the string, it is assumed to be free with an inertial motion. A

frequency model is also developed. The source of excitation is modeled as a periodic and harmonic force function, which is expanded using Fourier series.

Shor et al. (2015) modeled the source of damping in the vertical well as mainly viscous damping due to the interaction of the drillstring with the drilling fluid and material hysteresis using a velocity-dependent term. Once the borehole begins deviation from vertical, the frictional contact between the borehole and the drillstring becomes prevalent. The frictional contact force is modeled as an equivalent viscous damping force with a damping coefficient, $c_c = \frac{4F_c}{\pi\omega X} = \frac{4\mu F_N}{\pi\omega X}$. The equivalent viscous damping coefficient c_c is defined as a function of normal contact force F_N, friction factor μ, and an assumed displacement amplitude, X.

2.5.3. Numerical or Finite Element Modeling

A number of finite element models (Apostal et al. 1990; Soni and Bogner 1982; Gee et al. 2015; Wilson and Heisig, 2015; Wilson and Heisig 2015; Ghasemloonia et al. 2014) have been developed to predict the forced frequency response of a drillstring or axial oscillation-supported drillstrings.

The finite element model presented by Apostal et al. (1990) was developed to predict the forced frequency response of a drillstring in an arbitrary curved 3D wellbore. Although the study is not directly related to axial oscillation-supported drillstrings, the finite element analysis provides a forced frequency response (FFR) or critical speeds of the drilling assembly subjected to force and/or displacement excitations along the drillstring. The stiffness matrix used in the solution contains contact effects and friction. The model considers damping in the solution of steady-state response. The benefit of the model is that it aids in evaluating the effect of damping in conventional drilling assemblies forced frequency response finite element analysis. A notable effect of damping is that the response of the drilling assembly and excitation force does not

necessarily need to be in phase, though the response and excitation operate at the same frequency (Apostal et al.,1990). According to the model, the excitation may be applied as direct nodal forces or nodal displacements. In addition, the applied inputs can be multiple excitations at differing phase angles. The full transient dynamic response analysis of any nonlinear finite element model requires time integration of the equations of motion written in matrix form.

Chapter 3: Experimental Testing of an Axial Oscillation Tool

3.1. Experimental Setup

Prior to mathematical modeling of axial oscillation-supported drillstrings, experimental testing was carried out in the shop to determine the performance and feasibility of downhole applications of an axial oscillation tool. A test fixture for flow testing was designed to hold the axial oscillation tool in place. The text fixture consists of a chain vise and pipe support welded to an I-beam to secure the test tool (**Figure 3.1**).

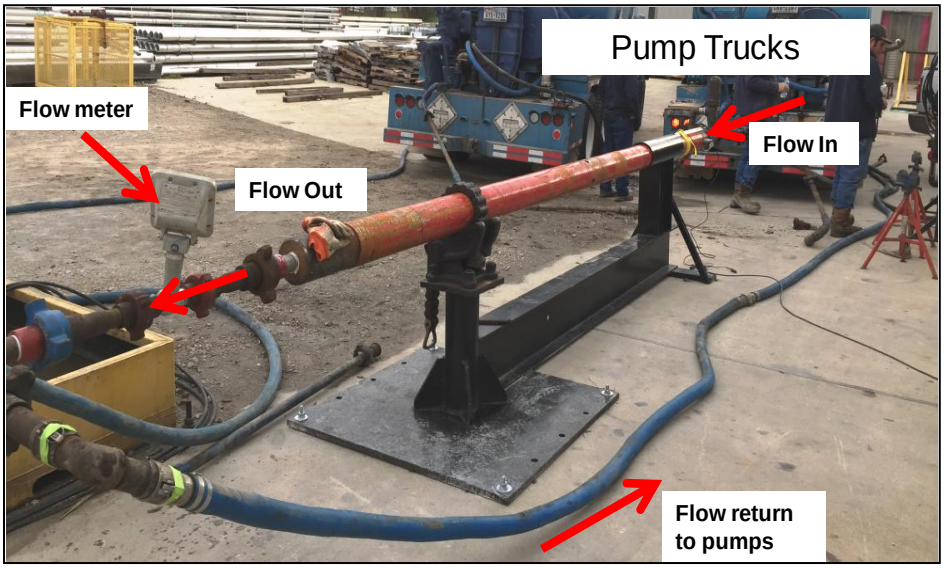

Figure 3. 1: Experimental setup used for testing AOT

Two triplex pump trucks were connected to water tanks (**Figure 3.2**). Each pump was rated for 5000 psi and 200 *gpm*. The test tool was connected to the pump trucks where the flow from the two trucks was combined before entering the test tool and splits after exiting the tool returning to each truck's water tank, thereby forming a closed flow loop. The experimental test setup involved the installation of dynamic pressure sensors at the upstream and downstream ends of the tool to measure pressure drop data. Measurements of the axial displacement of the

oscillation section were obtained using a displacement marker (**Figure 3.3**). Water was pumped through the tool at a steady-state flow rate. The flow rates used were 200 and 400 *gpm* and the Belleville spring stacking tested were 2x2 and 3x3 stacks.

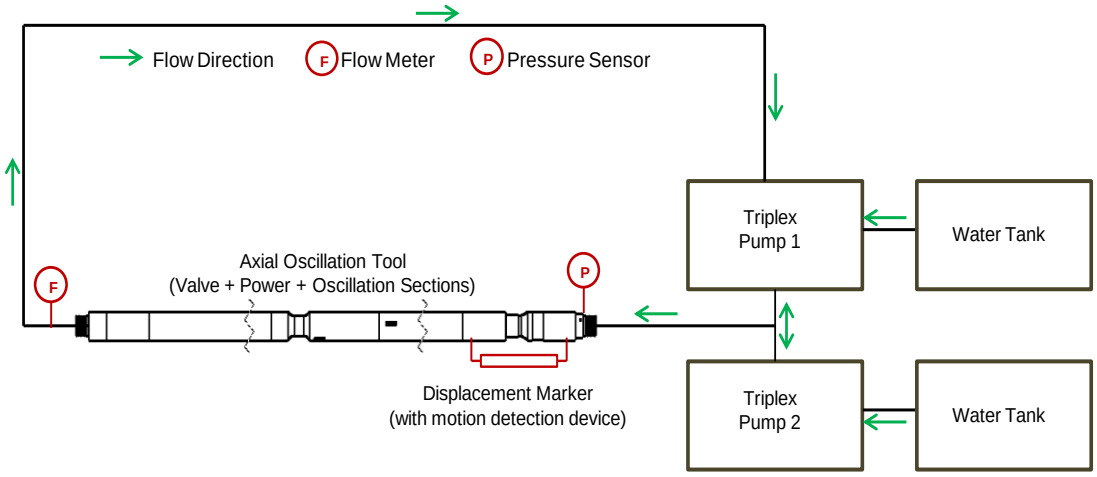

Figure 3. 2: Schematic of the flow loop

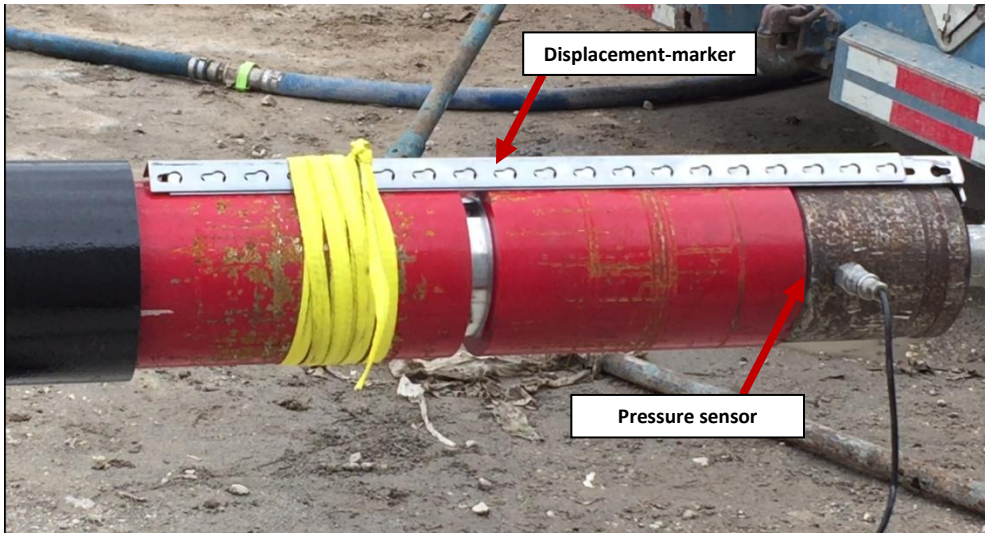

Figure 3. 3: Displacement-marker attached to the test tool

Varying the spring stacking changed the spring rate or stiffness of the oscillation section of the test tool. The load versus displacement plots of the 2x2 and 3x3 spring stackings are shown in **Figure 3.4**. The spring rate of the test tool is derived from the slope of the load versus displacement graph.

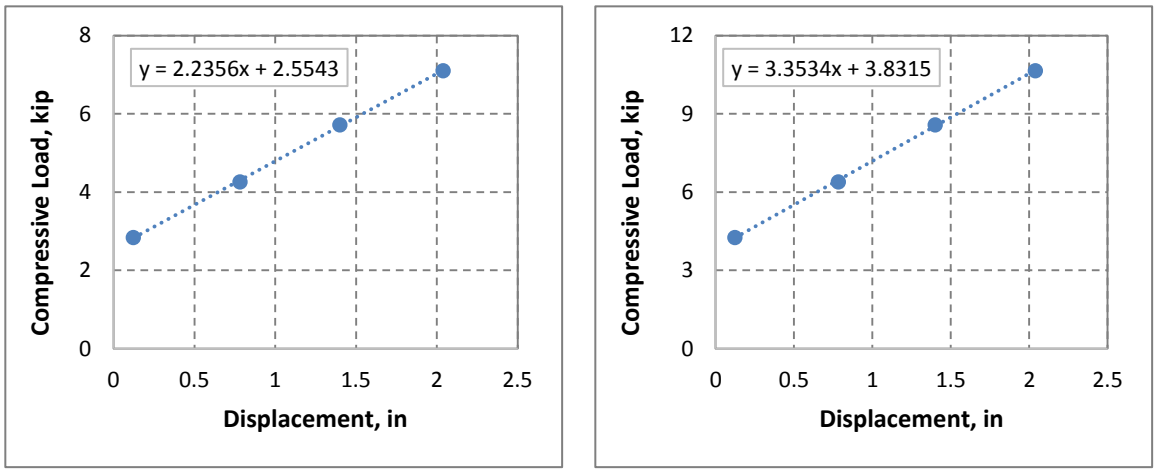

(a) **(b)**

Figure 3. 4: Load versus displacement of spring stacking of: a) 2×2 stack; and b) 3×3 stack

3.2. Test Procedure

The following experimental procedures were utilized in the testing of the axial oscillation tool for each spring configuration. First, the dynamic pressure sensor and flow meter were positioned to measure the pressure drop and flow rate, respectively. The recording device was initialized to record the motion of the displacement marker located at the top of the test tool. The required flow rate through the flow loop was maintained by controlling pump speed. At each experiment, steady-state flow is established prior to taking the pressure and flow rate measurements, and video recording. Slow motion playback of the recorded video was used to obtain displacement data. The procedure was repeated for different flow rates and spring stack configuration.

3.3. Test Results

Results obtained from the experiments are presented in **Table 3.**1. Minimum displacement is the least actuated position while the maximum displacement is the farthest

actuated position. The frequency of the pressure pulse is determined over a five-second interval. The flow rate-frequency relationship of the test tool was tested using the 2x2 spring stack. **Figure 3.5** shows the observed linear relationship between frequency and flow rate, which is due to the linear relationship between the rotor speed of the power section and flow rate. Table 3.1 demonstrates that the pressure differential increased with flow rate for each spring stacking. At higher spring rate (3x3 stacking), the magnitudes of displacement and pressure differential were reduced. This indicates that the pressure differential is affected by the spring configuration.

Table 3. 1: Results from experimental testing of an axial oscillation tool

Stack Type	Flow rate (gpm)	Pressure (psi)			Frequency (Hz)	Displacement (inches)	
		Minimum	Maximum	Differential		Minimum	Maximum
2×2 Stack	200	190	300	110	11	0.281	0.598
	400	475	625	150	19	1.125	1.343
3×3 Stack	200	120	210	90	10.2	0.250	0.457
	400	380	475	95	19.5	0.443	0.625

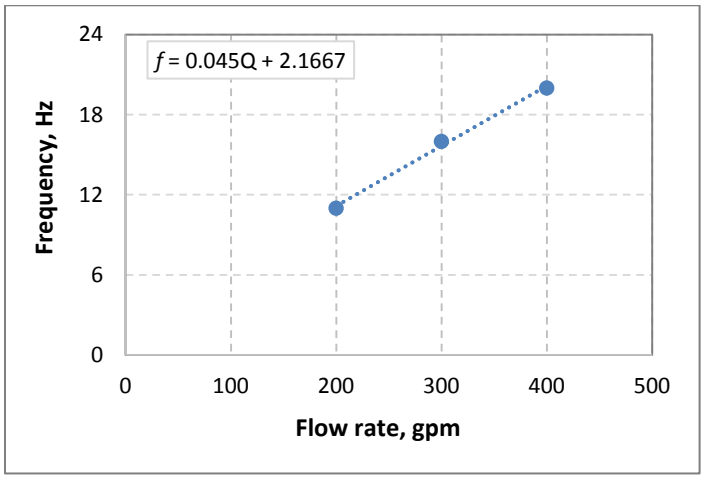

Figure 3. 5: Relationship between the frequency of pressure fluctuation and flow rate

Figure 3.6 shows the pressure drop fluctuations observed during the experimental testing of the axial oscillation tool. Two identifiable frequencies (from the test tool and noise from the triplex pumps) were observed in the pressure data when operating at 200 gpm (Figures 3.6a and 3.6c). Noise from the triplex pumps is relatively insignificant in the pressure fluctuation when

operating at 400 gpm (Figure 3.6b and 3.6d). The frequency of pressure pulses should be doubled when the flow rate is doubled but due to noise effects, the frequency of pressure pulses at 200 *gpm* (~10-11 Hz) is not doubled when flowing at 400 *gpm* (~18-19 Hz).

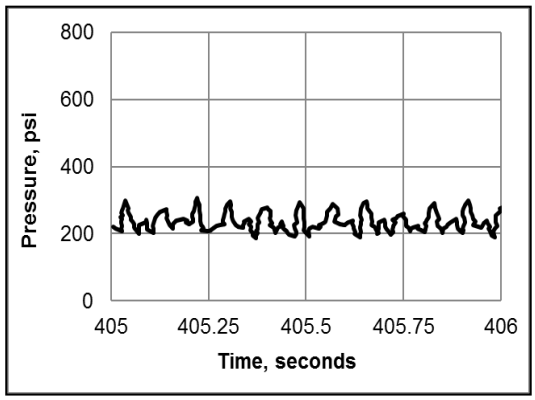

(a) 2x2 spring stacking configuration at 200 gpm

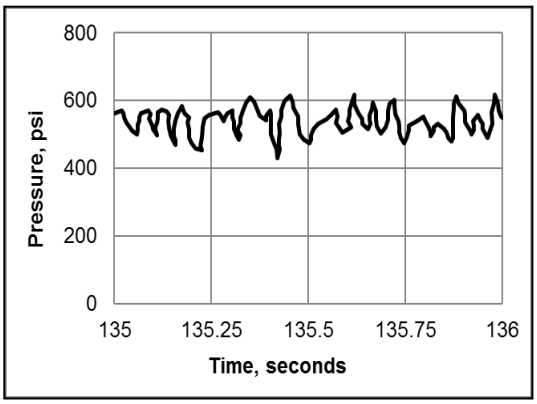

(b) 2x2 spring stacking configuration at 400 gpm

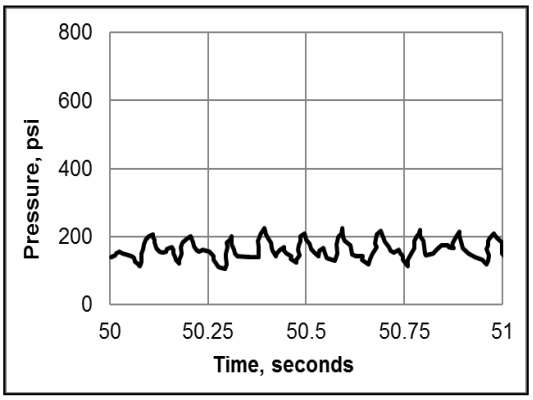

(c) 3x3 spring stacking configuration at 200 gpm

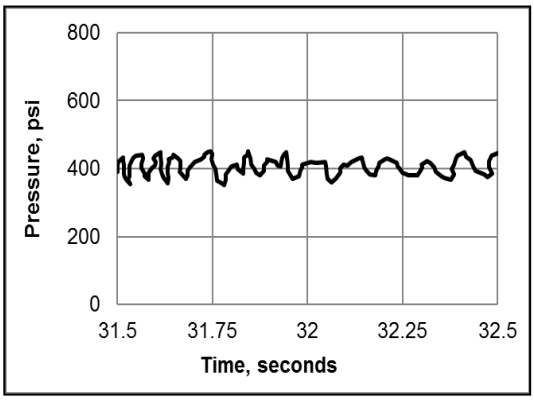

(d) 3x3 spring stacking configuration at 400 gpm

Figure 3. 6: Pressure drop vs. time for different stacking configurations and flow rates

Chapter 4: Mathematical Modeling of Axial Oscillation-Supported Drillstrings

4.1. Dynamic Modeling of AOT Excited Drillstrings

A dynamic model will be developed to simulate the response of a drillstring excited by an axial oscillation tool (AOT) operating at the surface and downhole conditions. The goal of this study is to develop a practical mathematical model to predict the axial displacement of axial oscillation-supported drillstrings as a function of:

- The flow rate or frequency of pressure pulse
- The magnitude of pressure pulses
- Spring rate or stiffness of axial oscillation tool (AOT)
- Elastic properties of the drilling assembly
- Damping mechanism (viscous and Coulomb damping)

The theory of vibration is used to study the oscillatory response of the axial oscillation-supported drilling system due to excitation displacements generated by the AOT and the associated forces acting on the tool and drillstring while in operation. The vibrations of axial oscillation-supported drillstrings can be modeled as a discrete system (mass-spring-damper) with predetermined degrees of freedom or as a continuous system (rod or bar) with distributed mass, elasticity and damping to derive the equations that simulate the behavior of the system.

4.1.1. Assumptions and Limitations

The following assumptions are made in the development of the new model used in this study are:

- The motion of the axial oscillation-supported drillstring is purely axial and uncoupled (i.e. does not include lateral or torsional motions).

- The motion of the system is periodic, that is, motion repeats itself after regular time intervals.
- The axial displacement created by the axial excitation from the bit-rock interaction is not considered.
- The developed dynamic model covers a few thousand feet of drillstring length, while the rest of the drillstring length up to surface is represented as a stiffness boundary condition.
- Viscous and Coulomb damping are the only types of damping considered. However, Coulomb damping is the dominant damping mechanism.
- Steady-state behavior is considered due to the continuous action of the excitation force.
- The drillstring is made of an elastic and homogeneous material.
- The hydrodynamic force due to the inertia of the internal fluid is not considered.
- The temperature effect is not considered.

4.1.2. Model Formulation

An axial oscillation-supported drillstring (**Figure 4.1**) consists of an axial oscillation tool (AOT) connected to bottomhole assemblies on both sides of the tool is considered for model formulation. As stated earlier, the oscillations generated by the AOT are transmitted uphole and downhole. The uphole oscillations are primarily excited by the longitudinal motion of the support (spring and piston) while the downhole oscillations are excited by the transmitted elastic force from upward oscillations. This study focuses on the displacement excitations generated by the compression and tension of the spring (support) within the axial oscillation tool. The system is modeled as a continuous concentric cylindrical bar (or rod) that can deform longitudinally or axially along the longitudinal axis. The displacement excitation or support excitation model and free body diagram are presented in **Figure 4.2**.

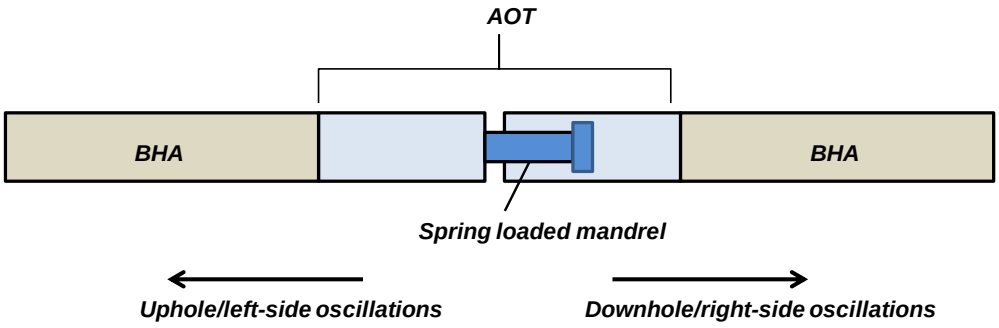

Figure 4. 1: Schematic of the axial oscillation-supported drillstring

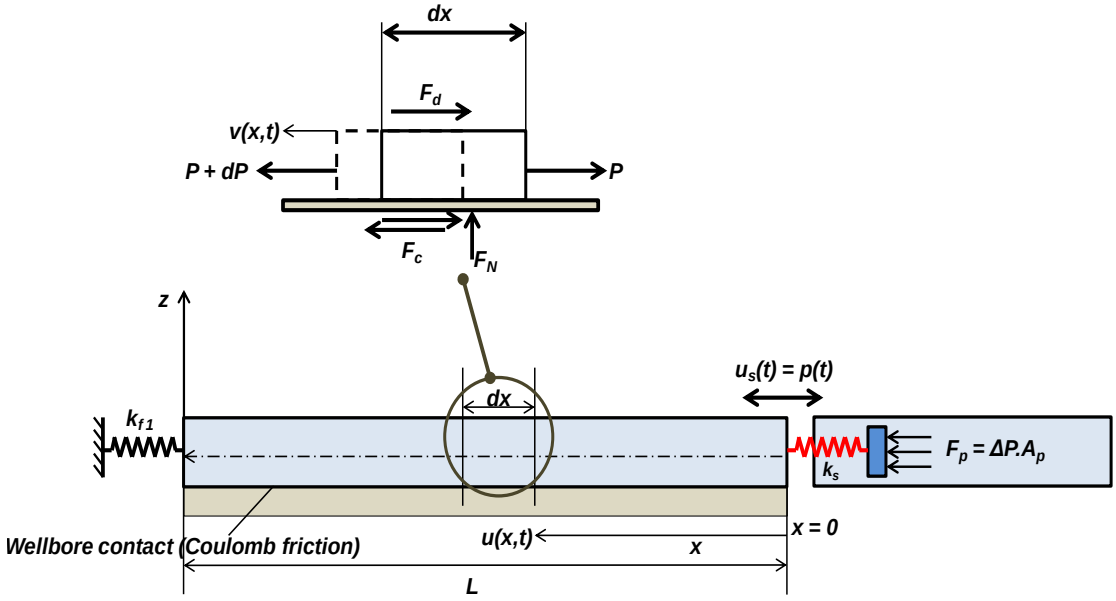

Figure 4. 2: Displacement (support) excitation model and free body diagram

Figure 4.2 shows a continuous cylindrical bar model subjected to support excitation or spring motion, $u_s(t) = p(t)$ in the axial direction. The cross sections of the differential element (Figure 4.2) is acted upon by internal axial forces within the bar due to axial excitations. The internal axial forces are given as P and $P + dP$ with:

$$P = \sigma A = EA\left(\partial v/\partial x\right) \tag{4.1}$$

where σ is the axial stress, E is Young's modulus, v is the axial displacement at a specific location, and $\partial v/\partial x$ is the axial strain. Damping force per unit length F_d and Coulomb damping or friction force F_c act on the differential element. The source of viscous damping force is the

viscous fluid surrounding the vibrating bar (Dareing and Livesay, 1968) and Coulomb or dry friction force is due to the contact between the wellbore with the cylindrical bar (Paranjpe, 1990). The boundary or end conditions of the model are dependent on the stiffness k_{f1} of the pipe and BHA fittings connected to the left end of the axial oscillation-supported drillstring.

Using Newton's second law of motion to derive the equation of motion for the longitudinal vibrations of the axial oscillation-supported drillstring, that is,

$$\sum(mass \times acceleration) = resultant\ force$$

$$(P + dP) - P - [F_d \pm F_c]dx = \rho A dx \left({}^{\partial^2 u}/_{\partial t^2} \right) \qquad (4.2)$$

The force of damping per unit length, $F_d = c\,{}^{\partial v}/_{\partial t}$ is proportional and linear to the velocity ${}^{\partial v}/_{\partial t}$, where c is the viscous damping coefficient. The energy dissipated in one cycle of forced harmonic free vibration is measured by the damping coefficient c. The Coulomb (or friction) damping force is a constant value, independent of the quantity of displacement and velocity, but depends on the friction factor μ and normal contact load F_N. The normal friction force F_N is distributed along the cylindrical bar element. The Coulomb damping force acts in the opposite direction of the element's velocity, where the damping force reverses sign when the element's velocity changes signs. A discontinuity (**Figure 4.3**) is created by the Coulomb frictional force at the change of sign, which makes it a nonlinear damping force, defined as:

$$\pm F_c = \pm \left(\frac{\partial v}{\partial t}\right) \mu F_N = sgn\left(\frac{\partial v}{\partial t}\right) \mu F_N \qquad (4.3)$$

where $sgn\left(\frac{\partial v}{\partial t}\right) = +1\ \left(\frac{\partial v}{\partial t} \geq 0\right)$and $sgn\left(\frac{\partial v}{\partial t}\right) = -1\ \left(\frac{\partial v}{\partial t} < 0\right)$.

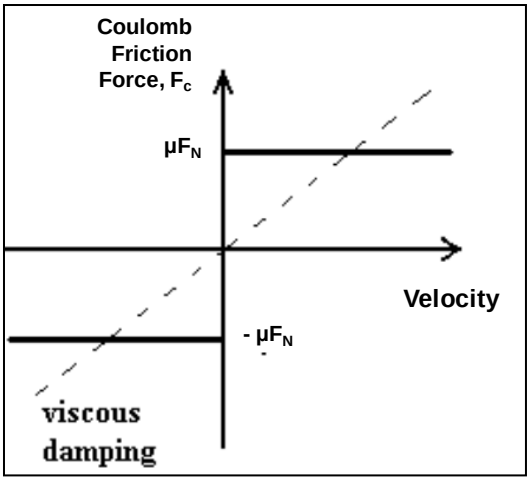

Figure 4. 3: Representation of Coulomb friction

Figure 4.4 shows the representation of the total axial displacement $u(x,t)$ measured from the springs supports (where $x = 0$) to a position of interest on the cylindrical bar model and instant or relative displacement $v(x,t)$ measured at a position of interest relative to the spring or support motion. These displacements are of interest to this study.

$$u(x,t) = v(x,t) + u_s(t) \qquad (4.4)$$

$u(x,t)$ is total axial displacement of the cylindrical bar model measured from the support of springs. $v(x,t)$ is instantaneous or relative displacement of any point on the bar relative to the support (formation). $u_s(t)$ is displacement excitation function or p(t).

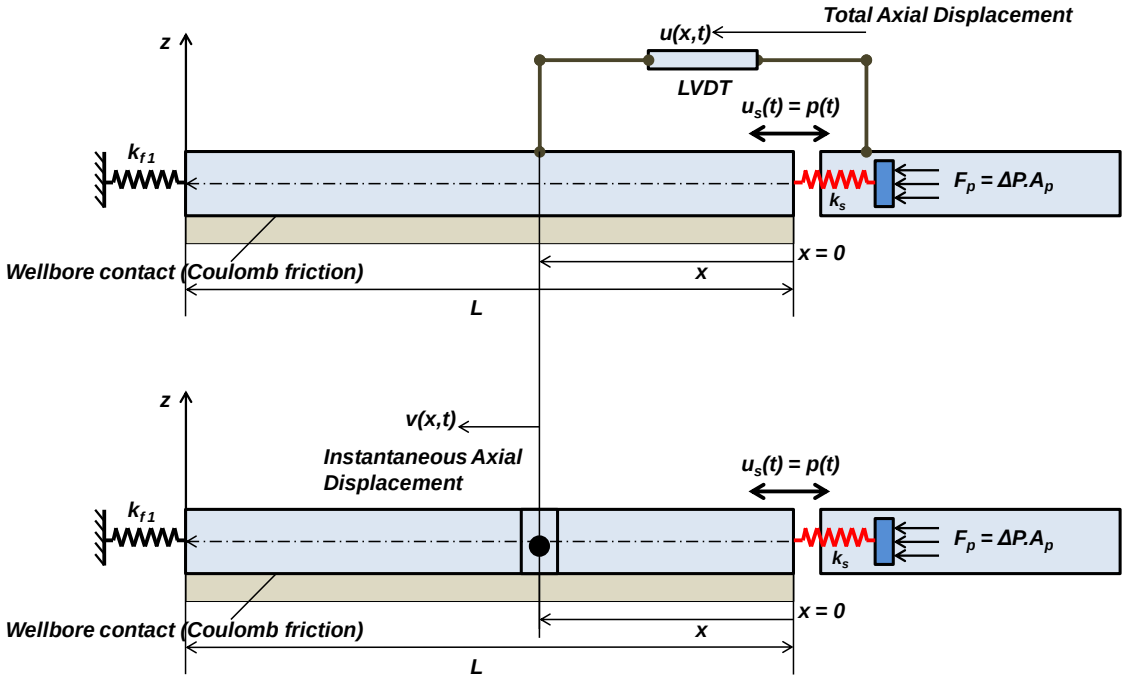

Figure 4. 4: Representation of total and instant (relative) axial displacements

The longitudinal motion of a continuous cylindrical bar under the influence of viscous and Coulomb damping, and longitudinal support excitation is represented by the equation of motion:

$$\rho A \frac{\partial^2 u}{\partial t^2}(x,t) + c\frac{\partial v}{\partial t}(x,t) + sgn\left(\partial v/_{dt}\right)\mu F_N = EA\frac{\partial^2 v}{\partial x^2}(x,t) \qquad (4.5)$$

$$\rho A \frac{\partial^2 (v+u_s)}{\partial t^2} + c\frac{\partial v}{\partial t}(x,t) - EA\frac{\partial^2 v}{\partial x^2}(x,t) + sgn\left(\partial v/_{dt}\right)\mu F_N = 0 \qquad (4.6)$$

where $\rho A = M$ and $EA = K$.

For the case of an inclined drillstring in a deviated wellbore with inclination angle I and buoyed weight W, the free body diagram in Figure 4.2 can be modified into **Figure 4.5**. The equation of motion in Eq. 4.6 is also modified into Eq. 4.7.

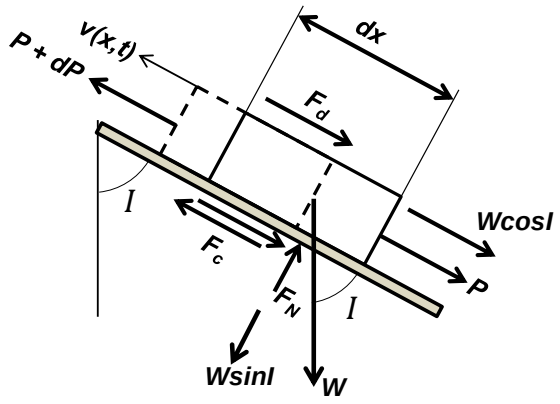

Figure 4. 5: Modified free body diagram for an inclined drillstring model

$$M\frac{\partial^2(v+u_s)}{\partial t^2} + c\frac{\partial v}{\partial t}(x,t) - K\frac{\partial^2 v}{\partial x^2}(x,t) + sgn\left(\partial v/_{dt}\right)\mu F_N + Mf_c g\cos I = 0 \tag{4.7}$$

The normal contact force F_N is expressed in Appendix B as:

$$F_N = Mf_c g\sin I + 2T\sin{}^{\delta}/_{2} \tag{4.8}$$

Therefore,

$$M\frac{\partial^2 v}{\partial t^2} + c\frac{\partial v}{\partial t}(x,t) - K\frac{\partial^2 v}{\partial x^2} + sgn\left(\frac{\partial v}{\partial t}\right)\mu F_N = -M\frac{\partial^2 u_s}{\partial t^2} - Mf_c g\cos I \tag{4.9}$$

$$u_s(x,t) = p(t) = \delta_a\cos\omega t \tag{4.10}$$

$$\delta_a = F_p/k_s \tag{4.11}$$

where δ_a is the displacement of the AOT spring due to the hydraulic excitation force F_p and AOT spring rate k_s. The excitation force F_p is due to fluid pressure change (ΔP) acting against the pump open area (A_p) pushing the springs or support $(F_p = \Delta P A_p)$. Dividing Eq. 4.9 by M:

$$\frac{\partial^2 v}{\partial t^2} + \frac{c}{M}\frac{\partial v}{\partial \mathrm{t}} - \frac{K}{M}\frac{\partial^2 v}{\partial x^2} + sgn\left(\frac{\partial v}{\partial t}\right)\mu\frac{F_N}{M} = -\frac{\partial^2 p}{\partial t^2} - f_c g\cos I \qquad (4.12)$$

The magnitude of viscous damping force is relatively small when compared to Coulomb (friction) damping and it can be neglected. Thus, Eq. 4.12 can be simplified to:

$$\frac{\partial^2 v}{\partial t^2} - \frac{K}{M}\frac{\partial^2 v}{\partial x^2} + sgn\left(\frac{\partial v}{\partial t}\right)\mu\frac{F_N}{M} = -\frac{\partial^2 p}{\partial t^2} - f_c g\cos I \qquad (4.13)$$

A closed-form solution of Eq. 4.12 is difficult to derive analytically due to the nonlinearity of the equation. Notwithstanding, Eq. 4.13 can be solved analytically by linearizing the equation with the equivalent viscous damping coefficient c_{eq}, where the quantity of energy dissipated per cycle with Coulomb damping is equated to the quantity of energy dissipated per cycle with an equivalent viscous damper. Although Coulomb (friction) damping is the dominant damping mechanism in this model, as applied in several vibration studies (Bandstra, 1983; Rao, 2007; Rao, 2011; Shor et al., 2015), the equivalent viscous damping force can be used as an approximation. This procedure is sufficiently accurate when the magnitude of Coulomb damping (friction) force is less than the equivalent excitation force. As the equivalent excitation force increases, the effect of Coulomb damping on axial oscillations reduces. The details of the concept of equivalent viscous damping are presented in Appendix A. Hence:

$$c_{eq} = {4F_c}/{\pi\omega X} = {4\mu F_N}/{\pi\omega X} = {4\mu_c Mg}/{\pi\omega X} \qquad (4.14)$$

where μ_c is the product of μ and f_c. Therefore, Eq. 4.9 can be rewritten as:

$$\frac{\partial^2 v}{\partial t^2} + \frac{c_{eq}}{M}\frac{\partial v}{\partial \mathrm{t}} - \frac{K}{M}\frac{\partial^2 v}{\partial x^2} = -\frac{\partial^2 p}{\partial t^2} - f_c g\cos I \qquad (4.15)$$

From the geometry of the continuous cylindrical bar model in Figure 4.2, boundary conditions are depicted in **Figure 4.6** as: At $x = 0$,

$$EA\frac{\partial v}{\partial x}(0,t) = 0 \tag{4.16}$$

At $x = l$,

$$EA\frac{\partial v}{\partial x}(l,t) = -k_{f1}v(l,t) \tag{4.17}$$

where k_{f1} is the stiffness of the drillstring components at the boundary of the model in Figure 4.2.

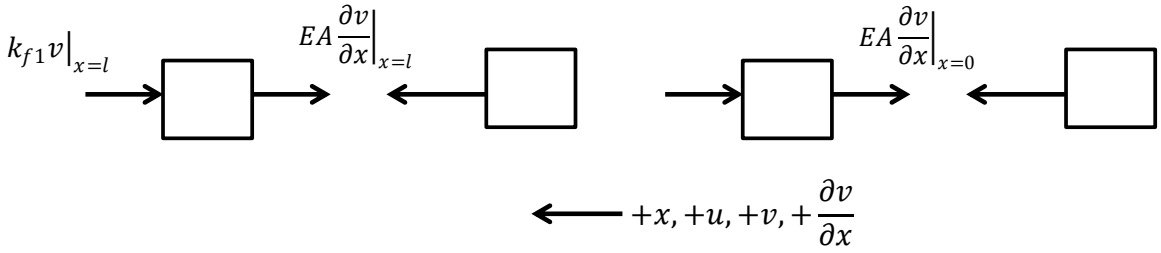

Figure 4. 6: Boundary conditions for displacement excitation model

4.1.3. Frequency Solution of Equation of Motion and Natural Frequencies

The equation of motion of free vibrations of the continuous cylindrical bar model is obtained by substituting $-\frac{\partial^2 p}{\partial t^2} - f_c g \cos I = 0$ in Eq. 4.15. Gravitational force does not influence the natural frequency, but rather offsets the equilibrium position at which the drillstring will oscillate. Therefore:

$$\frac{\partial^2 v}{\partial t^2} + \frac{c_{eq}}{M}\frac{\partial v}{\partial \mathrm{t}} = \frac{K}{M}\frac{\partial^2 v}{\partial x^2} \tag{4.18}$$

Eq. 4.18 is a boundary value problem (BVP) expressed as:

$$v_{tt} + Cv_t = B^2 v_{xx} \quad \text{for } 0 < x < l,\ t > 0 \tag{4.19}$$

where $B = \sqrt{E/\rho}$ is the velocity of sound in steel.

$$EAv_x(0,t) = 0 \tag{4.20}$$

$$EAv_x(l,t) = -k_{f1} v(l,t) \tag{4.21}$$

Using the method of separation of variables (Strauss, 2008; Rao, 2007), the solution of $v(x,t)$ is assumed to be of the form: $v(x,t) = U(x)\,T(t)$; and subsequently $v_t = UT'; v_{tt} = UT''; v_x = U'T; v_{xx} = U''T$. Eq. 4.19 becomes:

$$UT'' + CUT' = B^2 U''T \tag{4.22}$$

Dividing Eq. 4.22 by $-UT$ yields $-\frac{T''}{T} - \frac{CT'}{T} = -B^2 \frac{U''}{U}$ and further simplification results in $-B^2 \frac{U''}{U} = -\left(\frac{T''+CT'}{T}\right) = \lambda$. The constant λ is called Eigenvalue. $\lambda > 0$ and $\lambda = \omega^2$(ω is the frequency of excitation). Therefore, $-B^2 \frac{U''}{U} = \omega^2$

$$U'' + \frac{\omega^2}{B^2} U = 0 \tag{4.23}$$

The general solution of Eq. 4.23 is expressed as:

$$U(x) = G\cos\frac{\omega}{B}x + H\sin\frac{\omega}{B}x \tag{4.24}$$

$$U'(x) = -\frac{\omega}{B} G\sin\frac{\omega}{B}x + \frac{\omega}{B} H\cos\frac{\omega}{B}x \tag{4.25}$$

where G and H are arbitrary constants. From the boundary condition at $x = 0$,

$$EAu_x(0,t) = 0 \tag{4.26}$$

$$EAU'(0)T = 0 \tag{4.27}$$

$$U'(0) = 0 \tag{4.28}$$

$$-\frac{\omega}{B} G \sin 0 + \frac{\omega}{B} H \cos 0 = 0 \tag{4.29}$$

$$H = 0 \tag{4.30}$$

From the boundary condition at $x = l$,

$$EAu_x(l,t) = -k_{f1} u(l,t) \tag{4.31}$$

$$EAU'(l)T = -k_{f1} U(l)T \tag{4.32}$$

$$EA\left(-\frac{\omega}{B} G \sin\frac{\omega}{B} l\right) = -k_{f1}\left(G \cos\frac{\omega}{B} l\right) \tag{4.33}$$

$$\tan\frac{\omega l}{B} = \frac{Bk_{f1}}{EA\omega} \tag{4.34}$$

$$\alpha \tan\alpha = k_{f1}/K_1 \tag{4.35a}$$

where: $\alpha = \omega l/B$ and $K_1 = \frac{EA}{l}$ (stiffness of the bar). Eq. 4.25 is the frequency equation in the form of a transcendental equation with a multiple number of roots. For the n^{th} root, Eq. 4.35a can be expressed as:

$$\alpha_n \tan\alpha_n = k_{f1}/K_1, \qquad n = 1,2,\ldots \tag{4.35b}$$

With $\alpha_n = \omega_n l/B$ or $\omega_n = \alpha_n B/l$, the mode shapes corresponding to the natural frequencies ω_n can be expressed as:

$$U_n(x) = G_n \cos\frac{\omega_n}{B} x\,, \quad n = 1,2,\ldots \tag{4.36}$$

4.2. A solution of Linear Wave Equation

The equation of motion governing periodic displacement or support excitation of a cylindrical bar model subjected to damping (equivalent viscous damping) and longitudinal support excitation (Figure 4.2) is expressed in Eq. 4.14 with initial conditions: $v(x,0) = 0$ and

$\frac{\partial v}{\partial t}(x,0) = 0$. The Eigenfunction Superposition Method is used to obtain the steady-state solution (Leissa and Qatu, 2011). The periodic harmonic equivalent loading induced by the support or spring motion $\left(-\frac{\partial^2 p}{\partial t^2}\right)$ and the gravitational component $f_c g \cos I$ in the modified equation of motion (Eq. 4.15) are expanded with Fourier cosine series:

$$-\frac{\partial^2 p}{\partial t^2} - f_c g \cos I \cong \sum_{n=1}^{\infty} R_n(t) \cos\frac{\omega_n}{B} x \qquad (4.37)$$

The equivalent loading due to support excitation and gravitational component are assumed to contain components which have a similar shape as an Eigenfunction of the free damped vibration case and each has the possibility of independently varying with time.

$$R_n(t) = \frac{2}{l}\int_0^l \left(-\frac{\partial^2 p}{\partial t^2} - f_c g \cos I\right) \cos\frac{\omega_n}{B} x \, dx \qquad (4.38)$$

$R_n(t)$ is the Fourier coefficient representing the magnitude of each component of the equivalent loading.

$$R_n(t) = \frac{2}{l}\int_0^l (\omega^2 \delta_a \cos\omega t - f_c g \cos I) \cos\frac{\omega_n}{B} x \, dx \qquad (4.39)$$

The hydraulic force F_p is generated from fluid pressure difference, ΔP acting on the pump open area A_p pushing the springs or support. That is, $F_p = \Delta P A_p$. Thus:

$$R_n(t) = \frac{2\omega^2 \Delta P A_p \cos\omega t}{k_s l}\int_0^l \cos\frac{\omega_n}{B} x \, dx - \frac{2 f_c g \cos I}{l}\int_0^l \cos\frac{\omega_n}{B} x \, dx \qquad (4.40)$$

$$R_n(t) = \frac{2\omega^2 \Delta P A_p B}{k_s \omega_n l}\sin\frac{\omega_n}{B} l \cos\omega t - \frac{2 f_c g B \cos I}{\omega_n l}\sin\frac{\omega_n}{B} l \qquad (4.41)$$

$$-\frac{\partial^2 p}{\partial t^2} - f_c g \cos I \cong \sum_{n=1}^{\infty} \left(\frac{2\omega^2 \Delta P A_p B}{k_s \omega_n l} \sin \frac{\omega_n}{B} l \cos \omega t - \frac{2 f_c g B \cos I}{\omega_n l} \sin \frac{\omega_n}{B} l \right) \cos \frac{\omega_n}{B} x \tag{4.42}$$

The form of Eq. 4.15 is assumed as:

$$v(x,t) = \sum_{n=1}^{\infty} \bar{T}_n(t) \cos \frac{\omega_n}{B} x \tag{4.43}$$

where $\bar{T}_n(t)$ is the time-dependent solution due to longitudinal support motion.

$$v_t(x,t) = \sum_{n=1}^{\infty} \bar{T}_n'(t) \cos \frac{\omega_n}{B} x \tag{4.44}$$

$$v_{tt}(x,t) = \sum_{n=1}^{\infty} \bar{T}_n''(t) \cos \frac{\omega_n}{B} x \tag{4.45}$$

$$v_x(x,t) = -\frac{\omega_n}{B} \sum_{n=1}^{\infty} \bar{T}_n(t) \sin \frac{\omega_n}{B} x \tag{4.46}$$

$$v_{xx}(x,t) = -\left(\frac{\omega_n}{B}\right)^2 \sum_{n=1}^{\infty} \bar{T}_n(t) \cos \frac{\omega_n}{B} x \tag{4.47}$$

Substituting v_t, v_{tt}, v_x and v_{xx} and $-\frac{\partial^2 p}{\partial t^2} - f_c g \cos I$ into Eq. 4.15:

$$\sum_{n=1}^{\infty} \left[\bar{T}_n''(t) + \frac{c_{eq}}{M} T_n'(t) + \frac{K}{M} \left(\frac{\omega_n}{B}\right)^2 T_n(t) \right] \cos \frac{\omega_n}{B} x =$$

$$\sum_{n=1}^{\infty} \left(\frac{2\omega^2 \Delta P A_p B}{k_s \omega_n l} \sin \frac{\omega_n}{B} l \cos \omega t - \frac{2 f_c g B \cos I}{\omega_n l} \sin \frac{\omega_n}{B} l \right) \cos \frac{\omega_n}{B} x \tag{4.48}$$

$$\bar{T}_n''(t) + \frac{4\mu_c g \sin I}{\pi \omega X} \bar{T}_n'(t) + B^2 \left(\frac{\omega_n}{B}\right)^2 \bar{T}_n(t) = \frac{2\omega^2 \Delta P A_p B}{k_s \omega_n l} \sin \frac{\omega_n}{B} l \cos \omega t - \frac{2 f_c g B \cos I}{\omega_n l} \sin \frac{\omega_n}{B} l \tag{4.49}$$

$$\bar{T}_n''(t) + \beta \bar{T}_n'(t) + \omega_n^2 \bar{T}_n(t) = R_{n1} \cos \omega t - R_{n2} \tag{4.50}$$

where R_{n1}, R_{n2} and β terms expressed in the following equations:

$$\bar{R}_{n1} = \frac{2\omega^2 \Delta P A_p B}{k_s \omega_n l} \sin \frac{\omega_n}{B} l \tag{4.51}$$

$$\bar{R}_{n2} = \frac{2 f_c g B \cos I}{\omega_n l} \sin \frac{\omega_n}{B} l \tag{4.52}$$

$$\beta = \frac{4\mu_c g \sin I}{\pi \omega X} \tag{4.53}$$

The right-hand side of Eq. 4.50 can be interpreted as an excitation (acceleration) parameter with an amplitude of $\bar{R}_{n1}$ and a shift in the initial location of the spring ($x = 0$ in Figure 4.2) due to gravity effect from zero by $\bar{R}_{n2}$ in the negative direction (**Figure 4.7**).

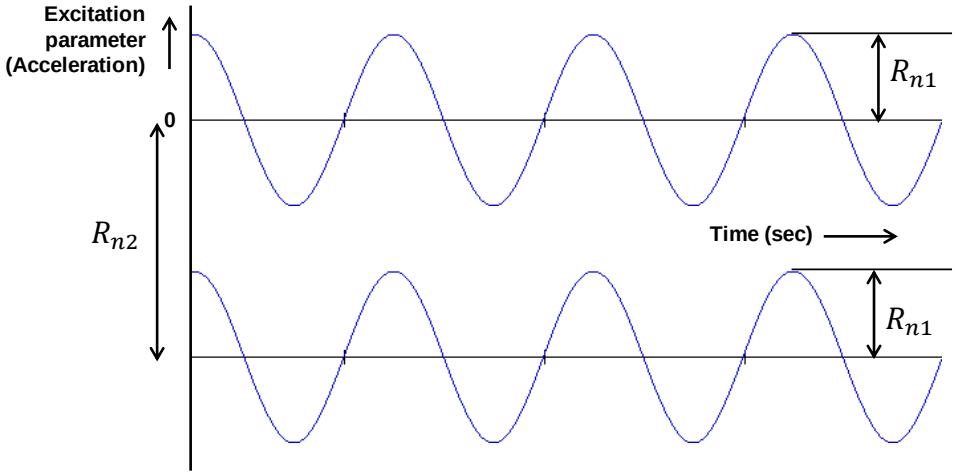

Figure 4. 7: **Shift in initial location of the spring due to gravity effect**

The amplitude of the excitation parameter is of interest to this study, therefore Eq. 4.50 can be rewritten as:

$$\bar{T}_n''(t) + \beta \bar{T}_n'(t) + \omega_n^2 \bar{T}_n(t) = R_{n1} \cos \omega t \tag{4.54}$$

The particular solution of Eq. 4.54 is assumed to be of the form:

$$\bar{T}_n(t) = D_n \sin \omega t + E_n \cos \omega t \tag{4.55}$$

The constants D_n and E_n can be expressed as:

$$D_n = \frac{\bar{R}_{n1}(\omega_n^2 - \omega^2)}{(\omega_n^2 - \omega^2)^2 + (\beta\omega)^2} \tag{4.56}$$

$$E_n = \frac{\bar{R}_{n1} \cdot \beta\omega}{(\omega_n^2 - \omega^2)^2 + (\beta\omega)^2} \tag{4.57}$$

The particular solution $\bar{T}_n(t)$ in Eq. 4.54 can also be expressed in terms of an amplitude $\bar{A}_n$ and a phase angle $\bar{\varphi}_n$:

$$\bar{T}_n(t) = \bar{A}_n \cos(\omega t - \bar{\varphi}_n) \tag{4.58}$$

$$\bar{A}_n = \sqrt{{D_n}^2 + {E_n}^2} \tag{4.59}$$

$$\tan \bar{\varphi}_n = \frac{E_n}{D_n} \tag{4.60}$$

The total steady-state motion of the bar subjected to damping and longitudinal harmonic support motion can be expressed as:

$$u(x,t) = \frac{\Delta P A_p}{k_s} \cos \omega t + \sum_{n=1}^{\infty} \bar{T}_n(t) \cos \frac{\omega_n}{B} x \tag{4.61}$$

or

$$u(x,t) = \frac{\Delta P A_p}{k_s} \cos \omega t + \sum_{n=1}^{\infty} [D_n \cos \omega t + E_n \sin \omega t] \cos \frac{\omega_n}{B} x \tag{4.62}$$

or

$$u(x,t) = \frac{\Delta P A_p}{k_s} \cos \omega t + \sum_{n=1}^{\infty} \bar{A}_n \cos(\omega t - \bar{\varphi}_n) \cos \frac{\omega_n}{B} x \tag{4.63}$$

The 1st mode shape or first natural frequency is considered and used in this study (i.e. only $n = 1$ is considered. The full modal solution (from $n = 1,2,3$ ...) is beyond this study.

Chapter 5: Numerical Calculations and Discussion of Results

5.1. Numerical Procedure

The numerical procedure used in calculating instant (or relative) and total axial displacements of the axial oscillation-supported drillstring using the model developed in this study is described here. The flowchart of the numerical procedure is also displayed in Figure 5.1.

1. Input cross-sectional area of drillstring A, modulus of elasticity E, the speed of sound in steel B, boundary stiffness k_{f1} and length of drillstring in consideration l.
2. Calculate the natural frequency ω_n from Eq. 4.35b.
3. Input pressure differential within AOT, pump open area A_p, excitation frequency ω and AOT spring rate k_s.
4. Calculate the excitation parameter $\bar{R}_{n1}$ from Eq. 4.51.
5. Input density of steel ρ, mud density ρ_m, friction factor μ, the acceleration due to gravity g, maximum spring displacement X and well survey data.
6. Calculate the equivalent viscous damping parameter β from Eq. 4.53.
7. Calculate constants D_n, and E_n using Eq. 4.56 and Eq. 4.57 respectively.
8. Output time-dependent solution using Eq. 4.58.
9. Output instant (or relative) displacement $v(x,t)$ from Eq. 4.43.
10. Output total displacement $u(x,t)$ from Eq. 4.63.

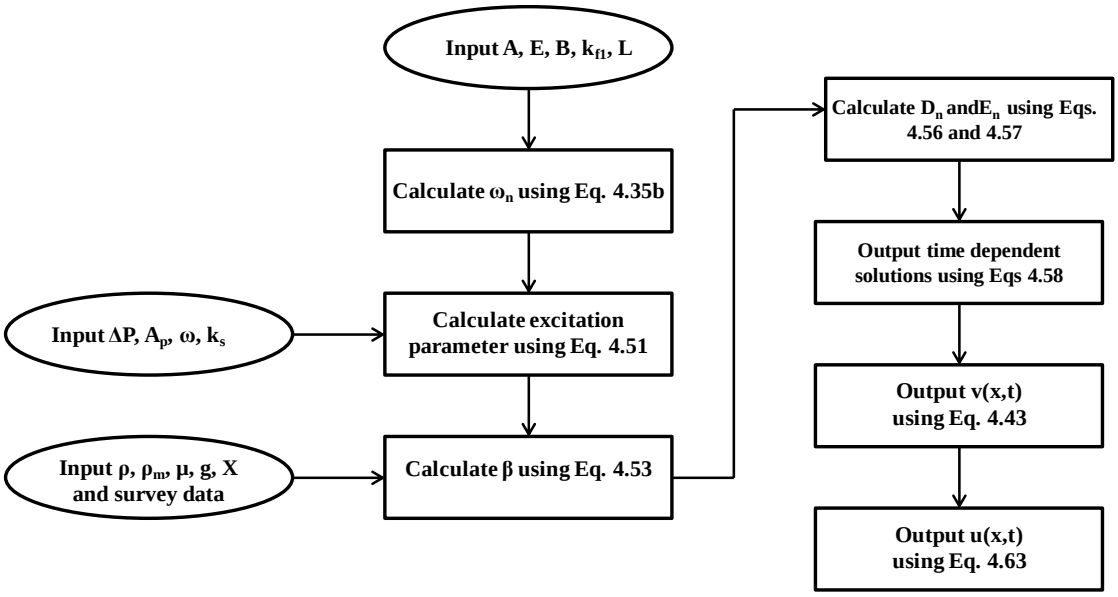

Figure 5. 1: Flowchart of the numerical procedure

5.2. Model Validation Using Current Experimental Data

The axial or longitudinal response equation derived in Chapter 4 will be used to calculate displacement and accelerations of axial oscillation-supported drillstrings and validated with data obtained from experimental testing.

5.2.1. Input Parameters for AOT-1

The input parameters for AOT-1 were obtained from the experimental test presented in Chapter 3 and presented in **Table 5.1**.

Table 5. 1: Input parameters for experimental testing of AOT-1

Parameters	Values	Units
Length, l	7	ft
Average Outer Diameter, d_o	6.50	in.
Average Inner Diameter, d_i	2.81	in.
Stiffness of pipe fittings, k_{f1}	100,000	lbf/in
Modulus of Elasticity, E	200	GPa
Density of Steel, ρ	0.284	lbs/in^3
Excitation or operating frequency ω	11-19	Hz
AOT Pressure Drop, ΔP	90-150	psi
AOT Spring Rate, k_s	2,235-3,353	lbf/in
Pump open area, A_p	12	in^2

5.2.2. Natural Frequencies

The natural frequencies of the axial oscillation-supported drilling system can be calculated from the n^{th} root of Eq. 4.35b which is expressed as:

$$\alpha_n \tan \alpha_n = k_{f1}/K_1 \,, \qquad n = 1,2, \ldots$$

$$K_1 = \frac{EA}{l} = \frac{200 \times 10^9 \times 0.017}{2.25} = 1.511 \times 10^9 \; N/m$$

$$\frac{k_{f1}}{K_1} = \frac{2.011 \times 10^7 \;\; {}^{N}/_{m}}{1.511 \times 10^9 \;\; {}^{N}/_{m}} = 0.0116$$

Therefore, find α_n where $\alpha_n \tan \alpha_n = 0.0116$. The first 3 roots of Eq. 4.35b for stiffness ratio $k_{f1}/K_1 = 0.0116$ are given in **Table 5.2**.

Table 5. 2: First 3 natural frequencies for k_{f1}/K =0.0116 (AOT-1)

n	α_n (radians)	Natural frequency (rad/s)	Natural frequency (Hz)
1	0.1068	237.79	37.84
2	3.1453	7,055.94	1,122.99
3	6.2851	14,099.63	2,244.03

$$B = \sqrt{\frac{E}{\rho}} = \sqrt{\frac{200 \times 10^9}{7{,}850}} = 5{,}047.54 \; m/s$$

$$\omega_1 = \frac{\alpha_1 B}{l} = \frac{0.106 \times 5{,}047.54}{2.25} = 239.62 \; rad/s$$

$$Natural \; frequency \; (Hz) = \frac{Natural \; frequency \; (rad/s)}{2\pi} = \frac{237.8}{2\pi} = 38.14 \; Hz$$

The mode shapes corresponding to the natural frequencies ω_n with the spring end boundary condition in Figure 4.2 can be expressed as:

$$U_n(x) = \cos \frac{\omega_n}{B} x \,, \quad n = 1,2, \ldots$$

$$U_n(x) = \cos\frac{\alpha_n}{l}x\,, \quad n = 1,2,\ldots$$

The mode shapes are shown in **Figure 5.2** to **Figure 5.4**.

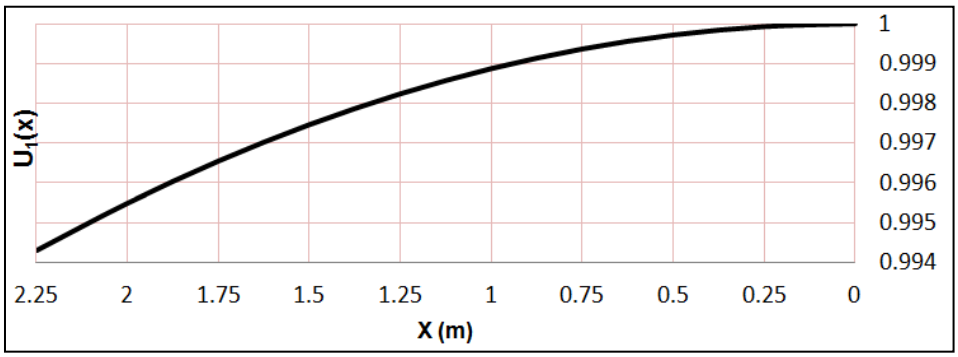

Figure 5. 2: 1st mode shape for AOT-1

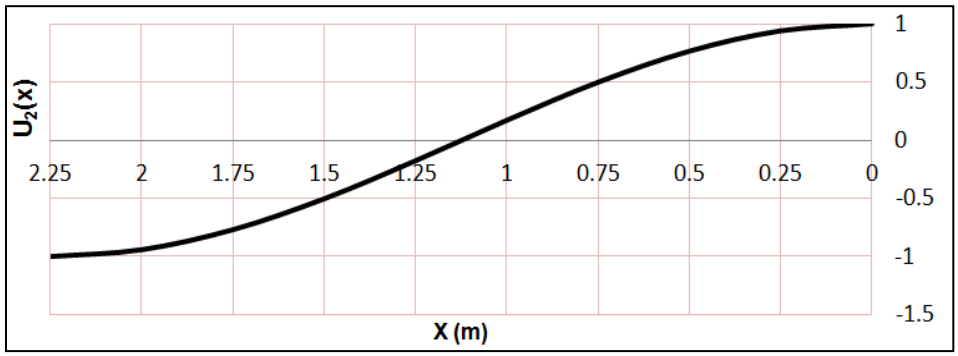

Figure 5. 3: 2nd mode shape for AOT-1

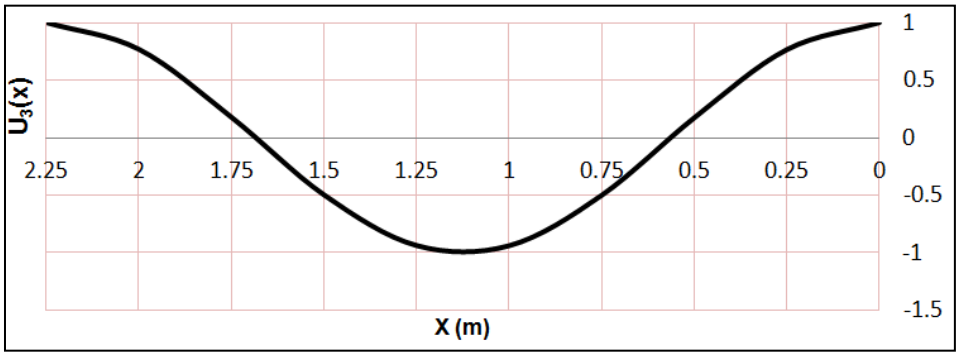

Figure 5. 4: 3rd mode shape for AOT-1

The mode shapes of uphole longitudinal oscillations are a transverse representation of the longitudinal motion of points or positions on the continuous cylindrical bar. The motion of points towards the left or tensile response is represented as a positive value on the mode shape

while the motion of points toward the right or compressive response is represented as a negative value on the mode shape. **Figure 5.2** shows one tensile region when operating at the 1st natural frequency but the displacement reduces as length increased. **Figure 5.3** shows one tensile region and one compressive region per half cycle when operating at the 2nd natural frequency. **Figure 5.4** shows two tensile regions and one compressive region per cycle when operating at the 3rd natural frequency.

5.2.3. Axial Displacement

From the experimental test data of AOT-1, four data points were collected. The first two data points displayed in **Table 5.3** were obtained using the 2x2 spring stacking and the next two data points shown in **Table 5.4** were obtained using the 3x3 spring stacking. **Figure 5.5** shows the model versus test results using the data in Tables 5.3 and 5.4.

Table 5. 3: Test and model data for AOT-1 with 2x2 stacking

2X2 Spring Stacking						
Flow rate (gpm)	**Pressure drop (psi)**	**Operating frequency (Hz)**	**AOT spring rate (lbf/in)**	**Test maximum displacement (in)**	**Test minimum displacement (in)**	**Model maximum amplitude (in)**
200	110	11	2,235	0.598	0.468	0.643
400	150	19	2,235	1.343	1.125	1.251

Table 5. 4: Test and model data for AOT-1 with 3x3 stacking

3X3 Spring Stacking						
Flow rate (gpm)	**Pressure drop (psi)**	**Operating frequency (Hz)**	**AOT spring rate (lbf/in)**	**Test maximum displacement (in)**	**Test minimum displacement (in)**	**Model maximum amplitude (in)**
200	90	11	3,353	0.457	0.250	0.429
400	95	19	3,353	0.625	0.443	0.520

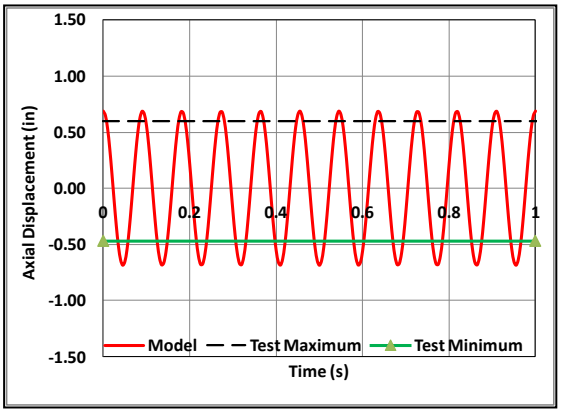

(a) 2x2 stacking at 200 gpm

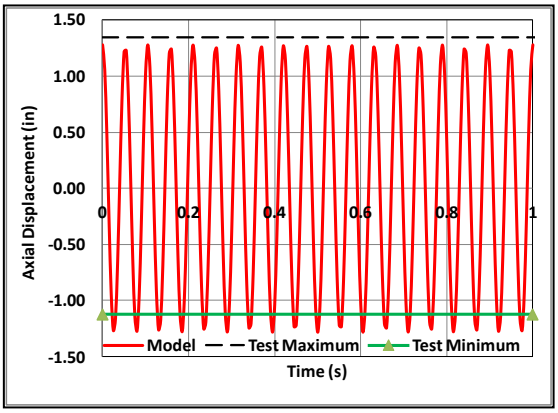

(b) 2x2 stacking at 400 gpm

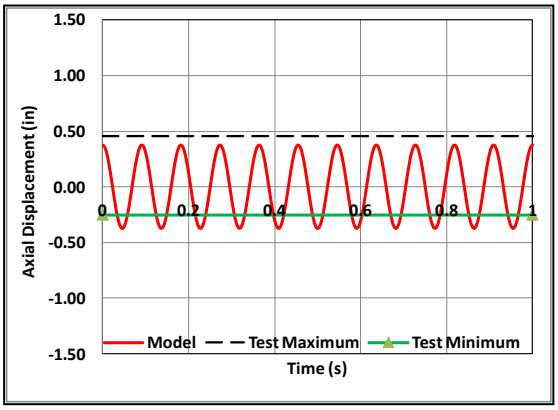

(c) 3x3 stacking at 200 gpm

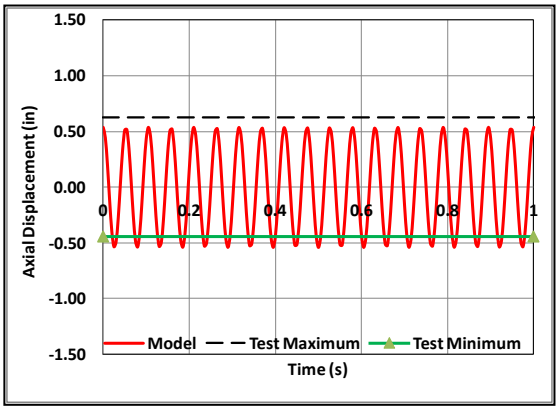

(d) 3x3 stacking at 400 gpm

Figure 5. 5: Model versus test data for AOT-1

The model predictions and test measurements presented in Figure 5.5 show increase in axial displacement as the flow rate (or frequency) increases. This shows that the flow rate is a critical parameter because it influences pressure drop across AOT and operating frequency. Theoretically, the oscillating response of output axial displacement should have the same

frequency as the pressure pulse. However, the slight variation in the frequency of actual input pressure (Figure 3.6) and theoretical (modeled) displacement frequency is due to noise effects. This effect is also the cause of variation between measured and modeled axial displacements. Increasing the spring rate of the AOT's oscillation section results in a decrease in axial displacement for a constant flow rate and valve configuration. The decrease in axial displacement is due to the reduction in pressure drop (Figure 3.6), which is the result of reduced hydraulic resistance within the test tool.

5.3. Model Validation Using Published Experimental Data

The axial or longitudinal response equation derived in chapter 4 will be used to calculate displacement and accelerations of axial oscillation-supported drillstrings and validated with published experimental data.

5.3.1. Input Parameters for AOT-2

The model input parameters for AOT-2 (**Table 5.5**) were obtained from the experimental data published by Martinez et al., 2013.

Table 5. 5: Input parameters for experimental testing of AOT-2

Parameters	**Values**	**Units**
Length, l	7	ft
Average Outer Diameter, d_o	6.50	in.
Average Inner Diameter, d_i	2.81	in.
Stiffness of pipe fittings, k_{f1}	100,000	lbf/in
Modulus of Elasticity, E	200	GPa
Density of Steel, ρ	0.284	lbs/in^3
Excitation or operating frequency ω	9.5-19	Hz
AOT Pressure Drop, ΔP	280-900	psi
AOT Spring Rate, k_s	35,000	lbf/in
Pump open area, A_p	15.9	in^2

5.3.2. Axial Displacement for AOT-2

A linear variable displacement transducer (LVDT) was used to record the average displacement of the mandrel of AOT-2. The displacement excitation model was used to predict the amplitude of oscillations and compared results to the average displacement data from the functional test of AOT-2, and presented in **Table 5.6** and **Figure 5.6**. The graph presented in Figure 5.6 represents the performance or characteristic curves for an axial oscillation tool plotted for specific mud weight, valve sizing, and spring stiffness. It is recommended that drilling engineers request for these performance curve from AOT suppliers or service companies for managing expectations. As expected, Figure 5.8 shows that as flow rate increases (which increases operating frequency), pressure drop and axial displacement are both increased. The deviation of model amplitude from test displacement increased from 5.6% to 22% as flow rate and pressure drop increased, but starts to reduce at higher flow rates and pressure drops. The average deviation is approximately 14.5%, that is, the predicted displacement by the model on average is approximately 14.5% less than the test displacement. These deviations could be ascribed to the coupled motion of the axial oscillation tool or overestimation of the boundary stiffness.

Table 5. 6: Test and model data for AOT-2

Flow rate (gpm)	Frequency (Hz)	Pressure Drop (psi)	Test (Average Displacement) (in)	Model Amplitude (in)	Deviation (%)
250	9.5	280	0.16	0.151	5.6
300	11.4	380	0.24	0.209	12.9
350	13.3	540	0.40	0.324	19
400	15.2	660	0.54	0.421	22
450	17.1	780	0.64	0.545	14.8
500	19	900	0.80	0.697	12.9

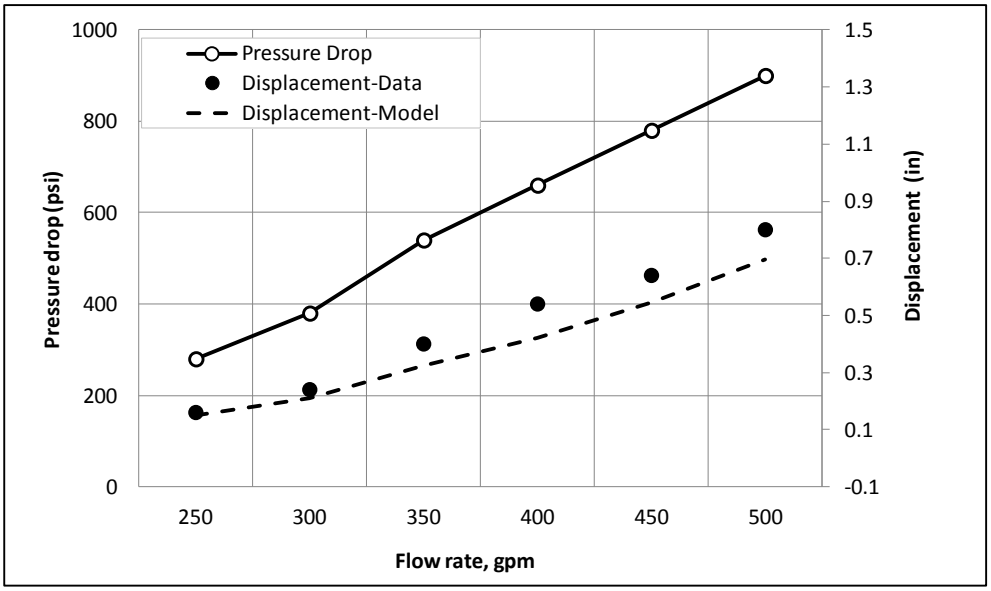

Figure 5. 6: Model versus test data for AOT-2

5.3.3. Input Parameters for AOT-3

The input parameters for the model evaluation on AOT-3 was obtained from to the experimental and analytical data from testing an "hydro-oscillator tool" as presented in the study of Tian et al. (2016) and shown in **Table 5.7**.

Table 5. 7: **Input parameters for experimental testing of AOT-3**

Parameters	**Values**	**Units**
Length, l	15.5	ft
Average Outer Diameter, d_o	4.50	in.
Average Inner Diameter, d_i	2.81	in.
Stiffness of pipe fittings, k_{f1}	100,000	lbf/in
Modulus of Elasticity, E	210	GPa
Density of Steel, ρ	0.284	lbs/in^3
Excitation or operating frequency ω	6.07	Hz
AOT Pressure Drop, ΔP	464	psi
AOT Spring Rate, k_s	25,696	lbf/in
Pump open area, A_p	10	in^2

5.3.4. Axial Displacement and Acceleration for AOT-3

The amplitude of the support excitation model applied to AOT-3 was compared to the amplitude obtained from the analytical model and experimental testing published in the study of Tian et al. (2016). The comparison is presented in **Table 5.8**.

Table 5. 8: Axial displacement results for AOT-3

Model amplitude	**Amplitude from analytical model (Tian et al., 2016)**	**Amplitude from experiment (Tian et al., 2016)**
0.1686 in	0.1457 in	0.1575 in

The amplitude of acceleration can be calculated from:

$$Acceleration\ amplitude = (Frequency)^2 \times Displacement\ amplitude$$

The magnitude of accelerations from axial oscillation tools can be expressed in m/s^2 or in g's (1 g = 9.8 m/s^2). **Table 5.9** presents the acceleration amplitude from this model of this study compared to the analytical and experimental data presented by Tian et al. (2016).

Table 5. 9: Acceleration results for AOT-3

Model amplitude	Amplitude from analytical model (Tian et al., 2016)	Amplitude from experimental model (Tian et al., 2016)
2.54 g	2.24 g	2.24 g

Graphically, **Figure 5.7** shows the comparison of the maximum axial displacement and acceleration measurements with modeled data of the current and existing models. Predictions of the axial displacements by the current model is approximately 7% above the measured displacements by Tian et al. (2016) while the predicted axial accelerations by the current model is approximately 13% above the measured accelerations. The difference in measured and predicted values of axial displacements and accelerations can be related to experimental conditions and structural damping of generated oscillations.

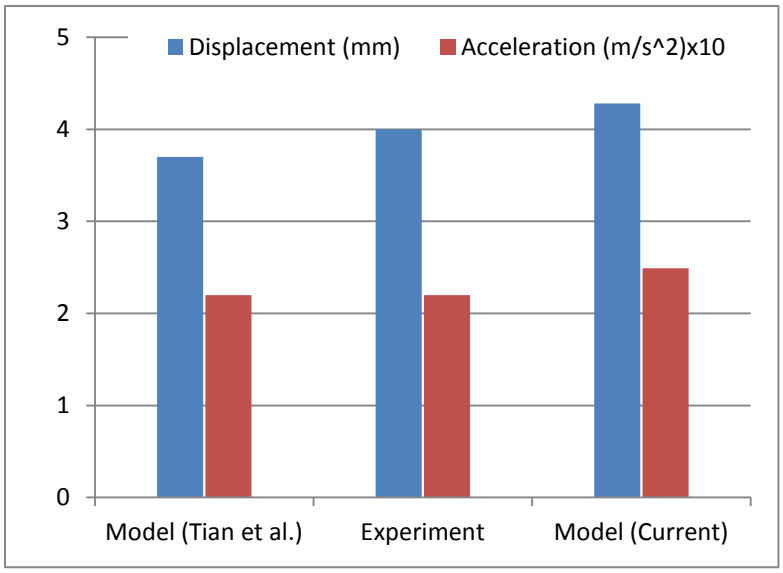

Figure 5. 7: Comparison of model predictions with measurements for of AOT-3

5.4. Parametric Study

The axial or longitudinal response equations derived in Chapter 4 is used to perform a parametric study in a horizontal well to examine the influence of pressure drop, flow rate,

friction factors and distance from the axial oscillation tool on the amplitude of axial oscillations. Simulations are performed on a drillstring excited by axial oscillation tool in two sections of the horizontal well (tangent and lateral section).

5.4.1. Input Parameters

The BHA and input parameters of the axial oscillation tool used for the parametric study are displayed in **Table 5.10** and **Table 5.11** respectively.

Table 5. 10: BHA used for parametric study

	OD (in)	ID (in)	Length (ft)	Length (m)	Cumulative Length (ft)	Cumulative Length (m)
Bit	8.5	2.25	0.85	0.26	0.85	0.26
Motor	6.75	4.75	25.3	7.71	26.15	7.97
Float Sub	6.75	2.75	3.15	0.96	29.3	8.93
UBHO	6.75	3.1	3	0.91	32.3	9.85
2 x NMDC	6.625	3.25	60	18.29	92.3	28.13
Flex Joint	6.75	3	7	2.13	99.3	30.27
Crossover Sub	6.75	3	3	0.91	102.3	31.18
81 x Drillpipe	5	4.276	2400	731.52	2502.3	762.70
AOT	6.75	2.81	14	4.27	2516.3	766.97
DP to Surface	5	4.276	10696	3260.14	13212.3	4027.10

Table 5. 11: Input parameters for parametric study of AOT

Parameters	Values	Units
Length, l	1,500	ft
Average Outer Diameter, d_o	6.5	in.
Average Inner Diameter, d_i	2.81	in.
Stiffness of pipe fittings, k_{f1}	150,000	lbf/in
Modulus of Elasticity, E	210	GPa
Density of Steel, ρ	0.284	lbs/in^3
Mud density, ρ_m	9	ppg
Excitation or operating frequency ω	9.5-13.3	Hz
AOT Pressure Drop, ΔP	280-540	psi
AOT Spring Rate, k_s	35,000	lbf/in
Pump open area, A_p	15.9	in^2

The operating regions of the axial oscillation tool are provided in **Table 5.12**.

Table 5. 12: Operating regions for a parametric study of AOT-1 (Martinez et al. ,2013)

Flow rate (gpm)	Frequency (Hz)	Pressure Drop (psi)
250	9.5	280
300	11.4	380
350	13.3	540

Figure 5.8 displays the well profile of the horizontal well used for the parametric study.

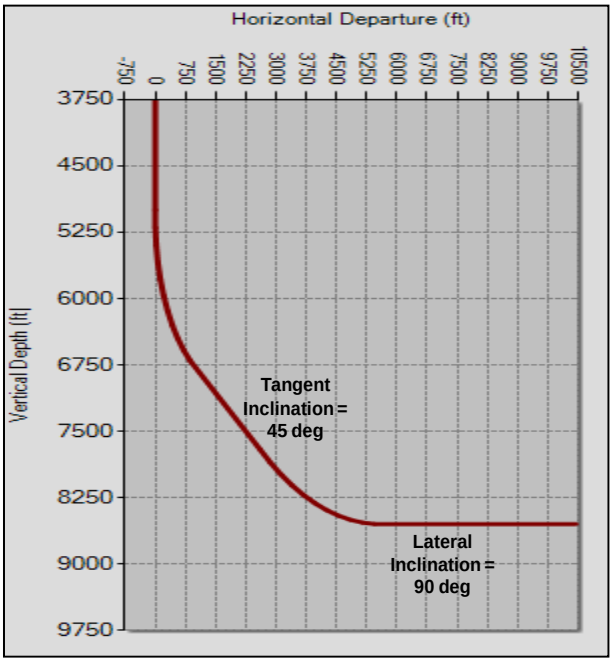

Figure 5. 8: Well profile used for parametric study

5.4.2. Natural Frequencies

The natural frequencies of the axial oscillation-supported drilling system can be calculated from the nth root of Eq. 4.22 which is expressed as:

$$\alpha_n \tan \alpha_n = k_{f1}/K_1, \qquad n = 1,2, \ldots$$

$$K_1 = \frac{EA}{l} = \frac{210 \times 10^9 \times 0.00354}{461.46} = 1.626 \times 10^6\ N/m$$

$$\frac{k_{f1}}{K_1} = \frac{2.627 \times 10^7\ {}^{N}/_{m}}{1.626 \times 10^6\ N/m} = 16.3$$

Therefore, find α_n where $\alpha_n \tan \alpha_n = 16.3$

$$B = \sqrt{\frac{E}{\rho}} = \sqrt{\frac{210 \times 10^9}{7{,}861}} = 5{,}168.54\ m/s$$

$$\omega_1 = \frac{\alpha_1 B}{l} = \frac{1.4803 \times 5{,}168.54}{461.46} = 16.58\, rad/s$$

$$Natural\ frequency\ (Hz) = \frac{Natural\ frequency\ (rad/s)}{2\pi} = \frac{16.58}{2\pi} = 2.64\ Hz$$

The first 5 roots of Eq.4.35b for stiffness ratio $k_{f1}/K_1 = 16.3$ are given in **Table 5.13**.

Table 5. 13: First 5 natural frequencies for $k_{f1}/K = 16.3$

n	α_n (radians)	Natural frequency (rad/s)	Natural frequency (Hz)
1	1.3673	15.46	2.64
2	4.4453	49.78	7.92
3	7.4299	83.22	13.24
4	10.4300	116.82	18.59
5	13.4460	150.60	23.97

5.4.3. Axial Displacement

Vertical Section

The axial oscillation-supported drillstring in the vertical section of the well trajectory is shown in **Figure 5.9**. The plot of axial displacement responses of the drillstring at different AOT operating parameters with varying distance from the axial oscillation tool are shown in **Figures 5.10, 5.11 and 5.12**.

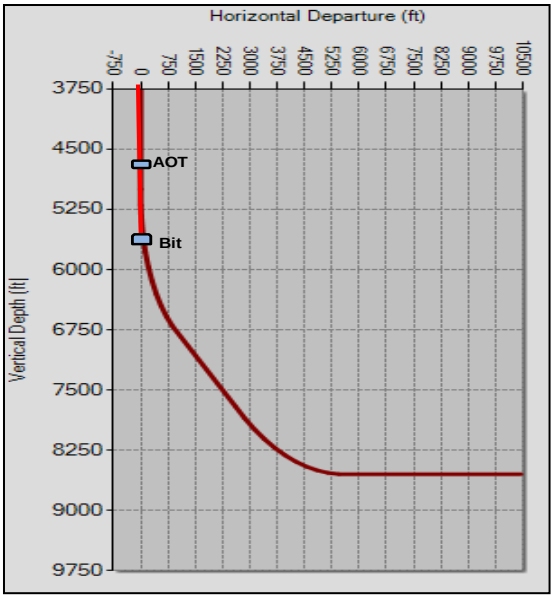

Figure 5. 9: Axial oscillation-supported drillstring in the vertical section

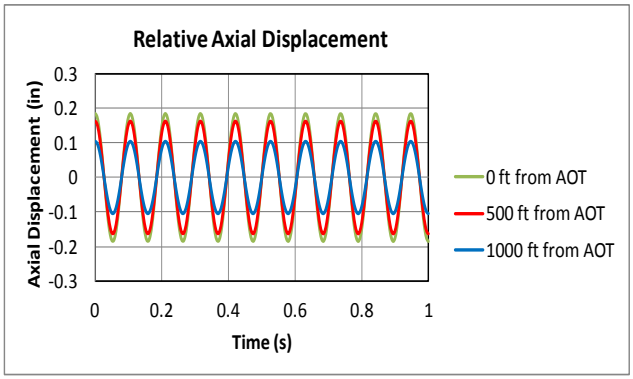

Figure 5. 10: Predicted relative axial displacements at 250 gpm, 9.5 Hz and 280 psi in the vertical section

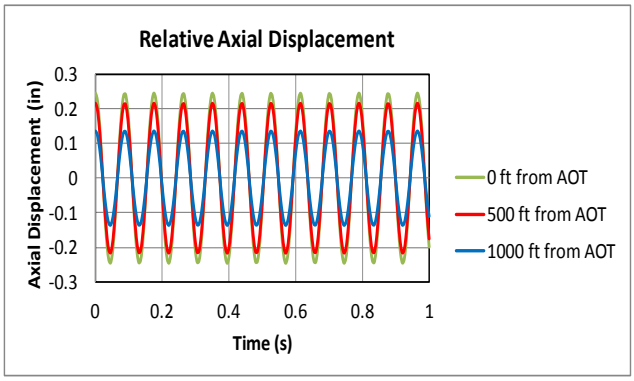

Figure 5. 11: Predicted relative axial displacements at 300 gpm, 11.4 Hz and 380 psi in the vertical section

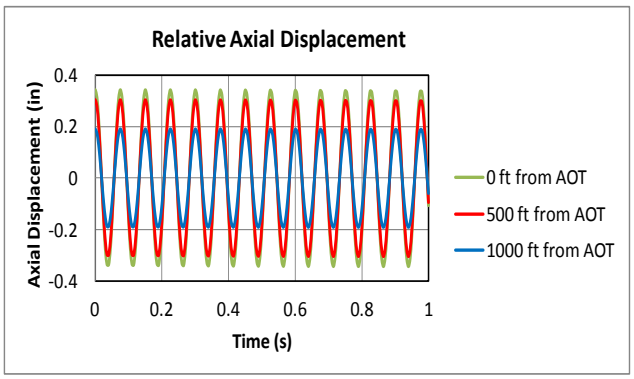

Figure 5. 12: Predicted relative axial displacements at 350 gpm, 13.3 Hz and 540 psi in the vertical section

Model predictions show axial displacement of the drillstring increases as the flow rate (frequency) and pressure drop within the AOT are simultaneously increased in the vertical section of the well trajectory. The effects of damping from Coulomb friction is negligible in the vertical section because the weight of the drillstring is not in contact with the wellbore, assuming the drillstring is centered in the wellbore. This observation is supported with the decrease in the equivalent viscous damping parameter β defined in Eq. 4.53 as wellbore inclination decreases..

Tangent Section

The axial oscillation-supported drillstring in the tangent section of the well trajectory is shown in **Figure 5.13**. The axial displacement responses of the drillstring at different values of friction factors with varying distance from the axial oscillation tool are shown in **Figure 5.14**.

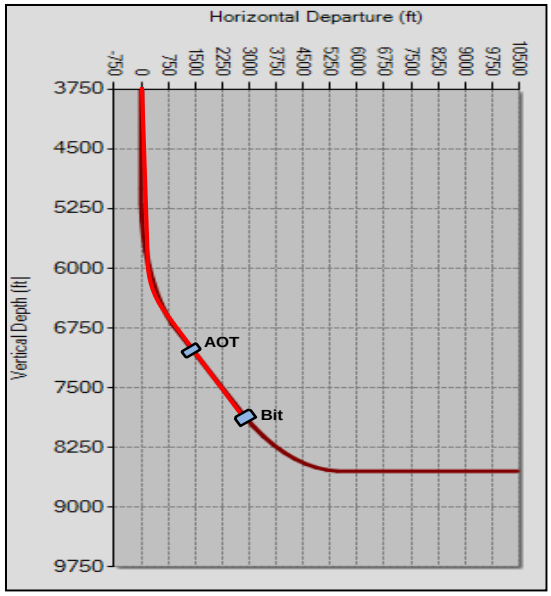

Figure 5. 13: Axial oscillation-supported drillstring in the tangent section

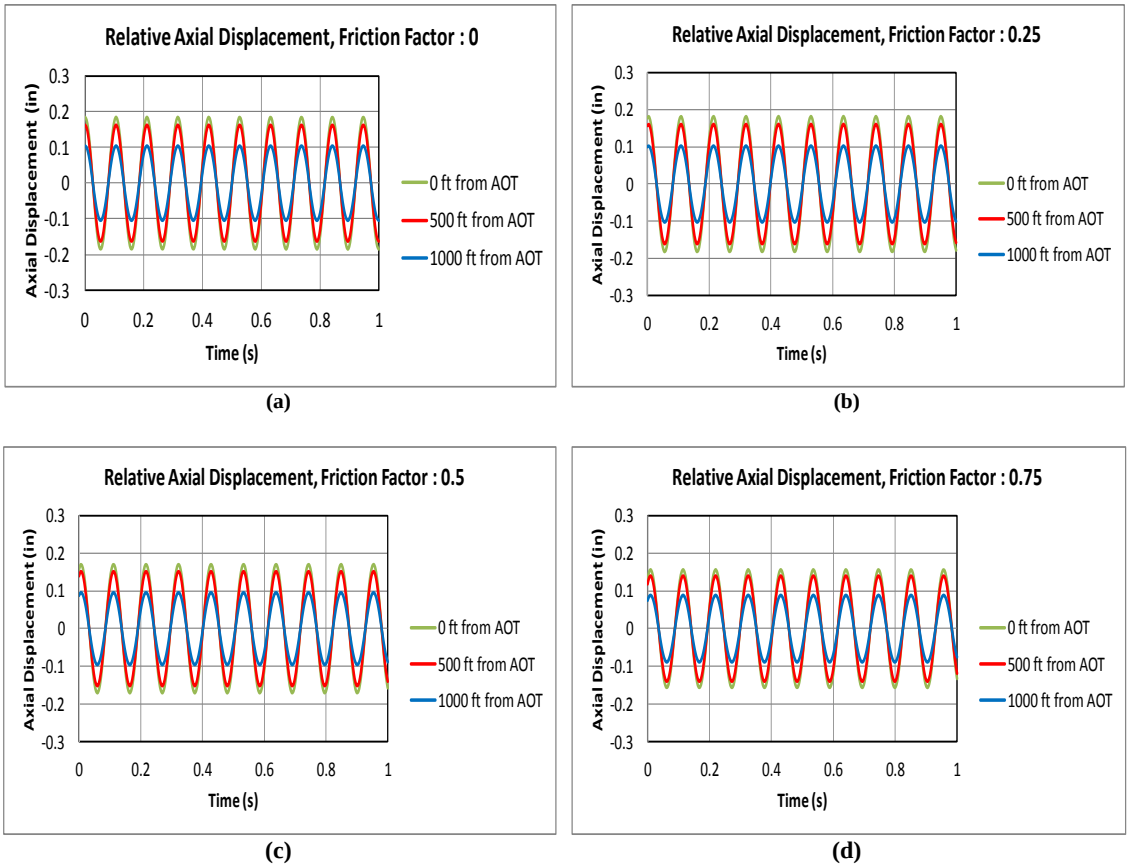

Figure 5. 14: Predicted relative axial displacements at 250 gpm, 9.5 Hz and 280 psi

As anticipated, the magnitude of the axial displacement of the drillstring decreases with distance from AOT. The decrease in the magnitude of axial displacement is primarily due to the loss of vibrational energy along the length of the drillstring. In addition, the magnitude of axial displacement decreased with increasing friction factor. An important observation from plots is the reduced effect of friction factor on axial displacement (**Figures 5.15** and **5.16**) as pressure drop and operating flow rates (frequencies) are simultaneously increased. An increase in both pressure drop and frequency increases the excitation parameter in Eq. 4.39 and increases the vibrating force and energy. It should be noted that AOTs have the excitation frequencies increase alongside with pressure drop; therefore, as the system energy increases with frequency, the effect of Coulomb damping on the axial displacement of drillstring diminishes.

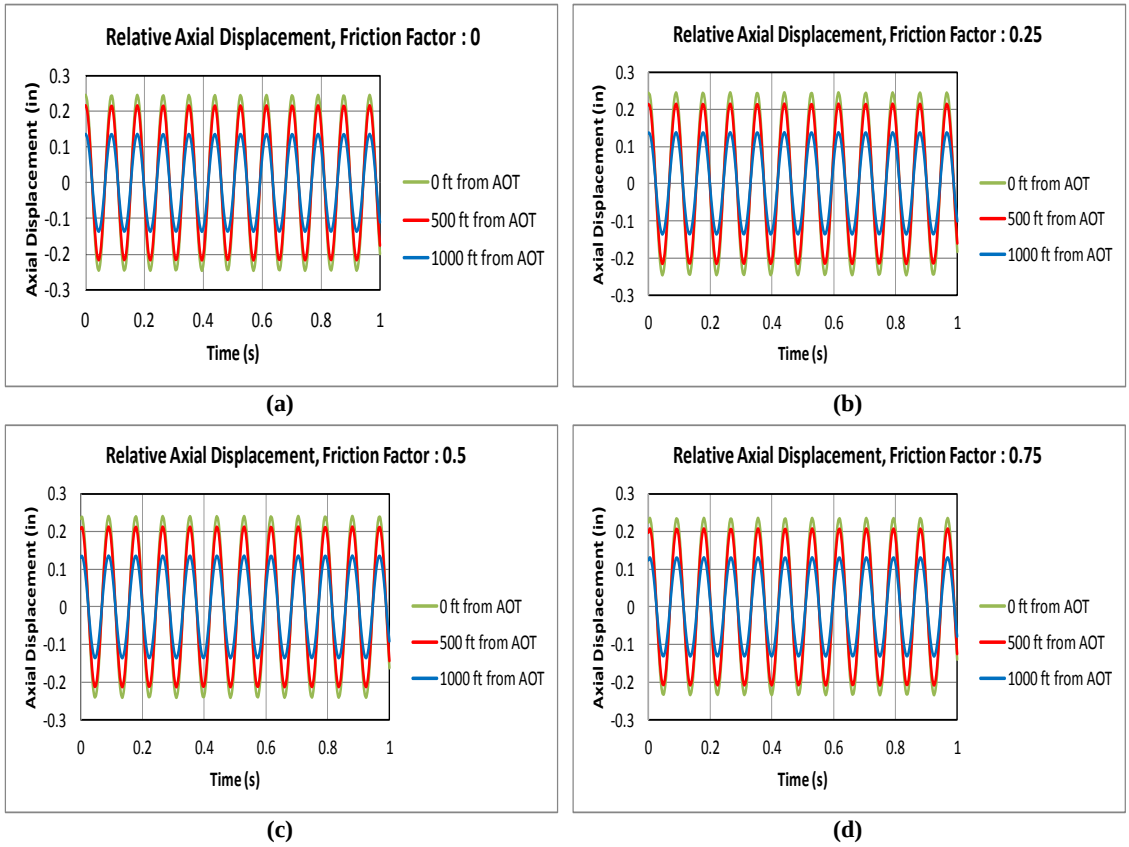

Figure 5. 15: Predicted relative axial displacements at 300 gpm, 11.4 Hz and 380 psi

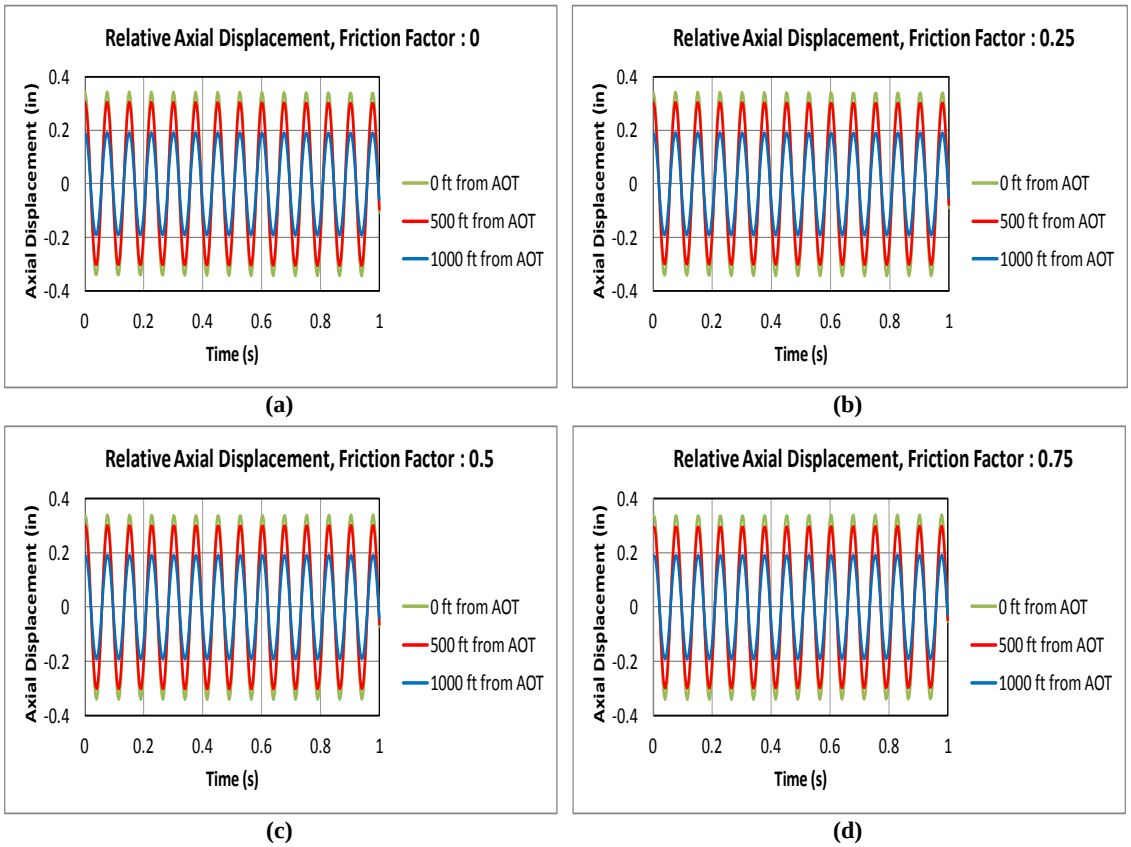

Figure 5. 16: Predicted relative axial displacements at 350 gpm, 13.3 Hz and 540 psi

Lateral Section

The axial oscillation-supported drillstring in the tangent section of the well trajectory is shown in **Figure 5.17**.

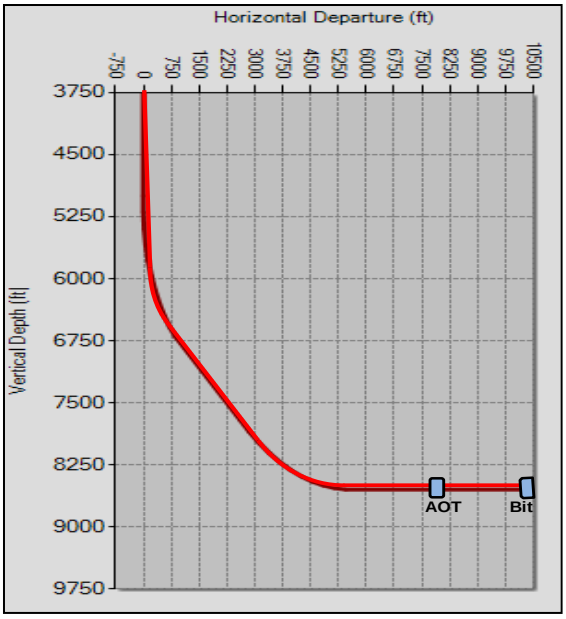

Figure 5. 17: Axial oscillation-supported drillstring in the lateral section

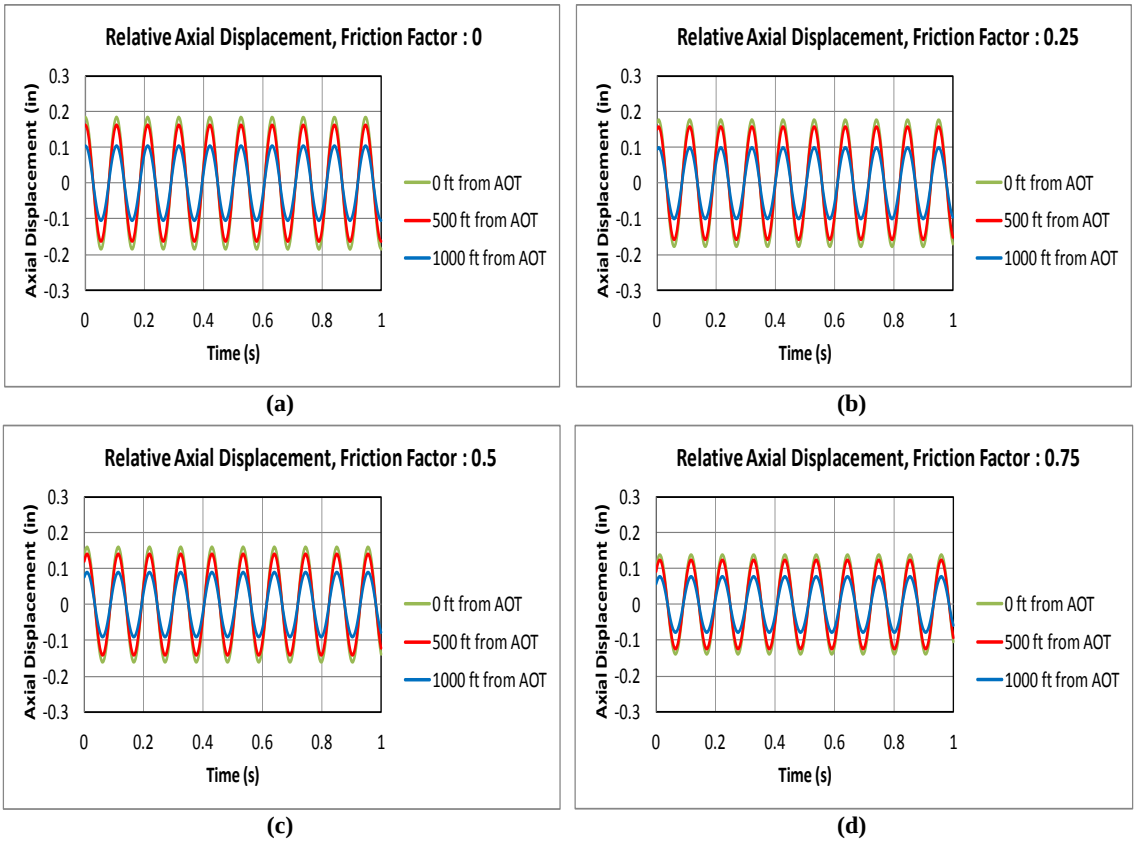

Figure 5. 18: Predicted relative axial displacements at 250 gpm, 9.5 Hz and 280 psi

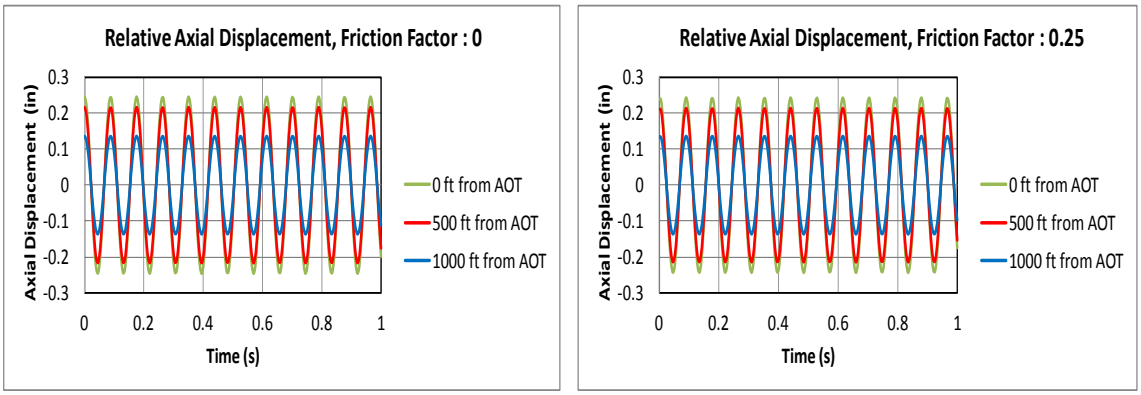

(a)

(b)

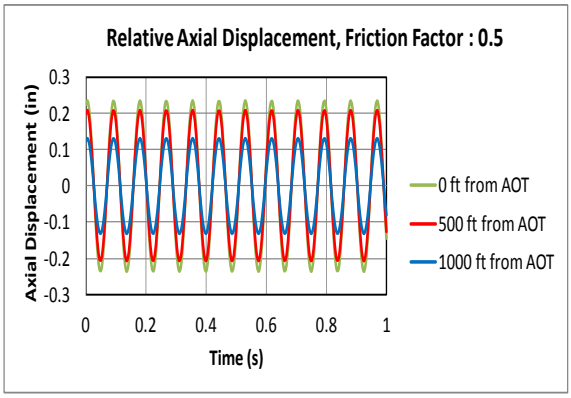

(c)

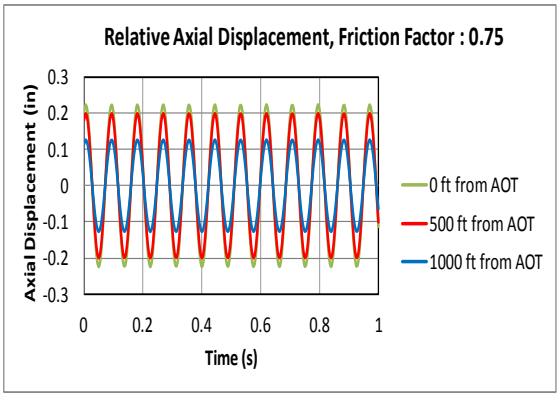

(d)

Figure 5. 19: Predicted relative axial displacements at 300 gpm, 11.4 Hz and 380 psi

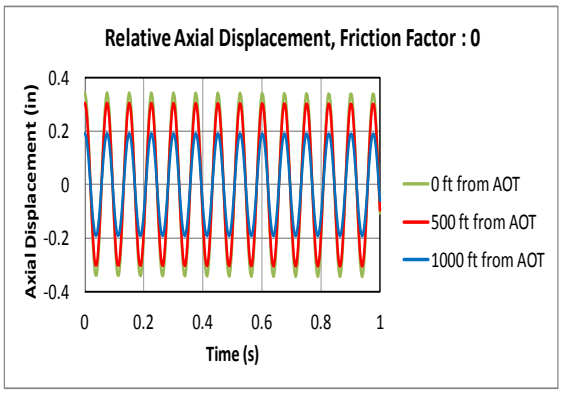

(a)

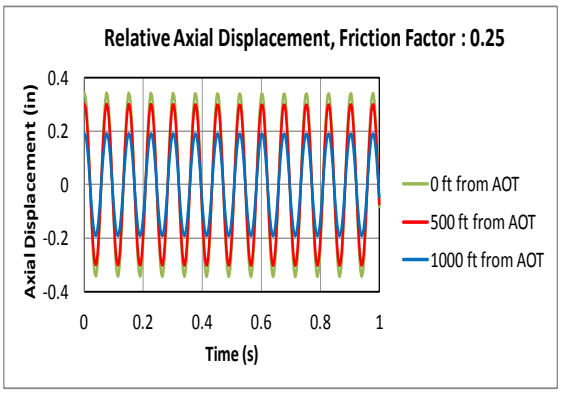

(b)

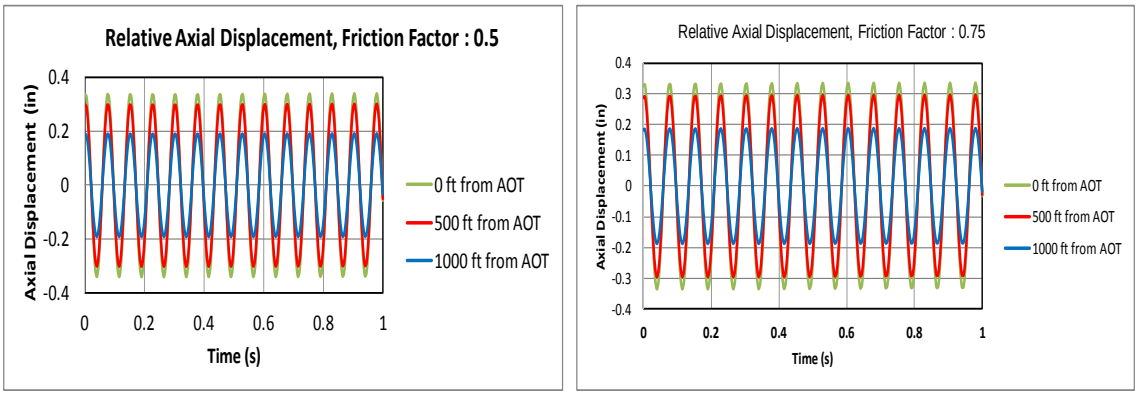

(c) **(d)**

Figure 5. 20: Predicted relative axial displacements at 350 gpm, 13.3 Hz and 540 psi

The calculated amplitudes of axial displacement in the lateral section of the horizontal well are plotted in **Figures 5.18** to **5.20**. Similar to the response in the tangent section, the magnitude of the axial displacement of the drillstring decreases with distance from AOT. Also, the magnitude of axial displacement decreased with increasing friction factor. As pressure drop and frequency increases simultaneously, the damping effect of friction on the axial displacement of drillstring diminishes. The plots in Figures 5.18 to 5.20 show the effect of an increase in wellbore inclination (90 degrees) on the axial displacement when compared to the plots in Figures 5.14 and 5.16 (at 45 degrees). Increasing the wellbore inclination dampens the axial displacement due to an increase in the normal contact load contributing to the Coulomb damping force and increase in the equivalent viscous damping parameter in Eq. 4.53 as wellbore inclination increases. **Figures 5.21** to **5.23** compare the amplitudes of axial displacement in the tangent and lateral sections at 0 ft, 500 ft and 1,000 ft from the AOT towards the surface, with friction factors of 0, 0.25, 0.5 and 0.75. These plots show that axial displacements or dynamic response of axial oscillation-supported drillstrings are significantly damped by Coulomb friction at low operating regions of the AOT.

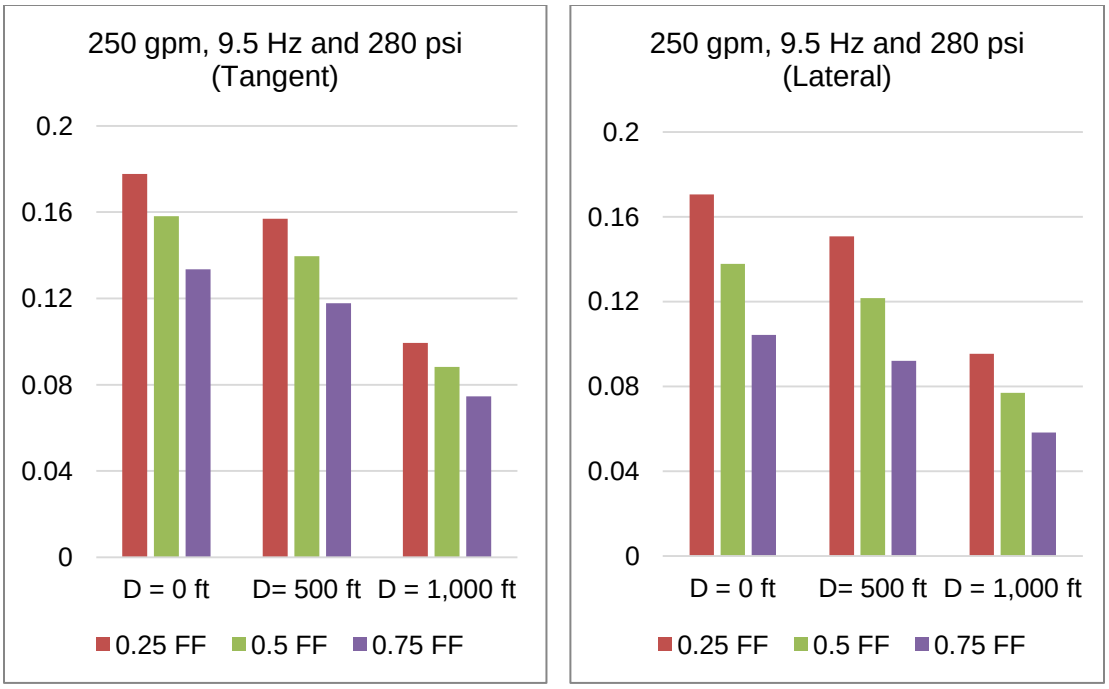

Figure 5. 21: Amplitudes of relative axial displacement at 250 gpm, 9.5 Hz and 280 psi

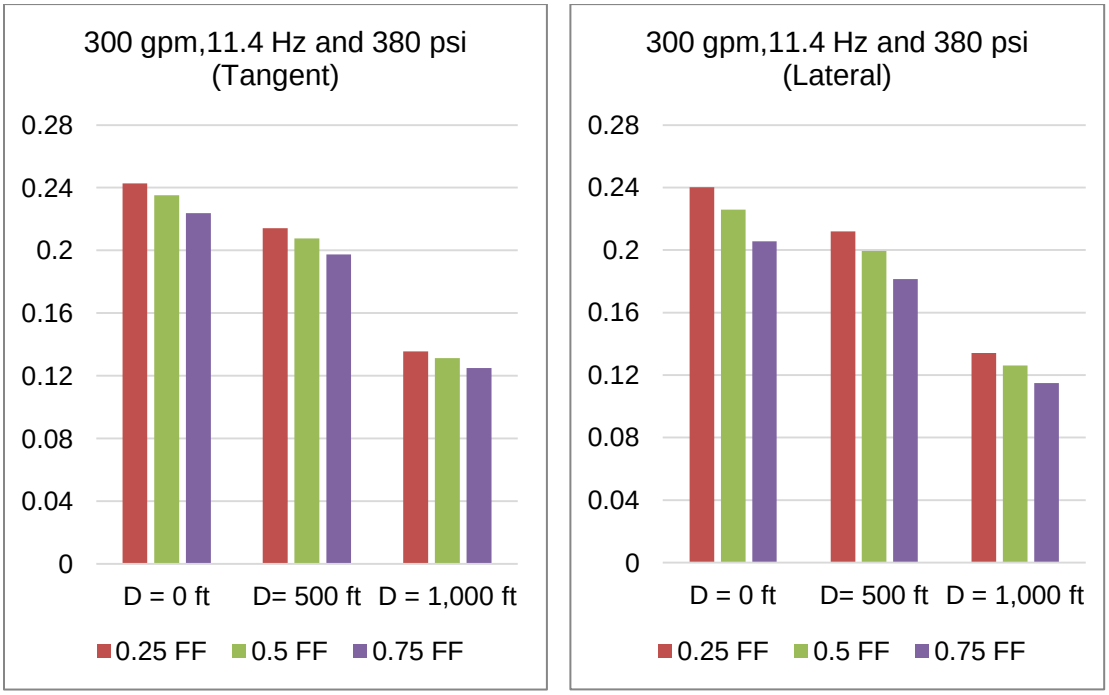

Figure 5. 22: Amplitudes of relative axial displacement at 300 gpm, 11.4 Hz and 380 psi

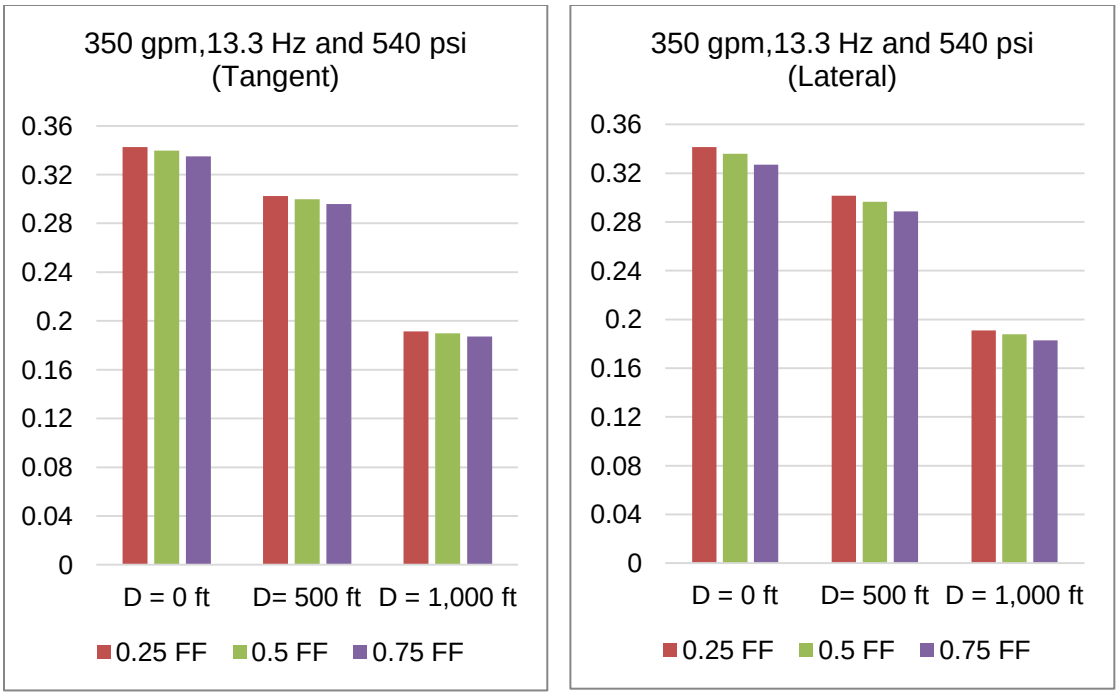

Figure 5. 23: Amplitudes of relative axial displacement at 350 gpm, 13.3 Hz and 540 psi

5.5. Downhole Data Matching

The displacement excitation model can also be used in downhole data matching when some of the data required are known. In matching, unknown input data will be assumed in order to obtain predicted displacements or accelerations that match downhole measurements.

5.5.1. Downhole Acceleration Matching

The data used for downhole acceleration matching was provided by Jones et al. (2016). The data provided are that of the bottomhole assembly (**Table 5.17**) and downhole accelerations (**Figure 5.21**).

Table 5. 14: BHA used for downhole acceleration matching

Description	Length (ft.)	Total Length (ft.)
8 ¾″ Bit	0.7	0.7
6 ¾″ 7/8 5.0, 1.83 FBH	27.8	28.5
8″ NM Stab	6.1	34.6
NM Pony DC	15.6	50.2
MWD	19.3	69.5
NM Flex DC	60.2	129.7
16 × 5″ HWDP	1508.3	1638.0
Shock & Vib Sub	2.1	1640.1
5 × 5″ DP	470.8	2110.9
6 ¾″ FRT	25.7	2136.6
5 × 5″ DP	472.5	2609.1
Shock & Vib Sub	2.1	2611.2

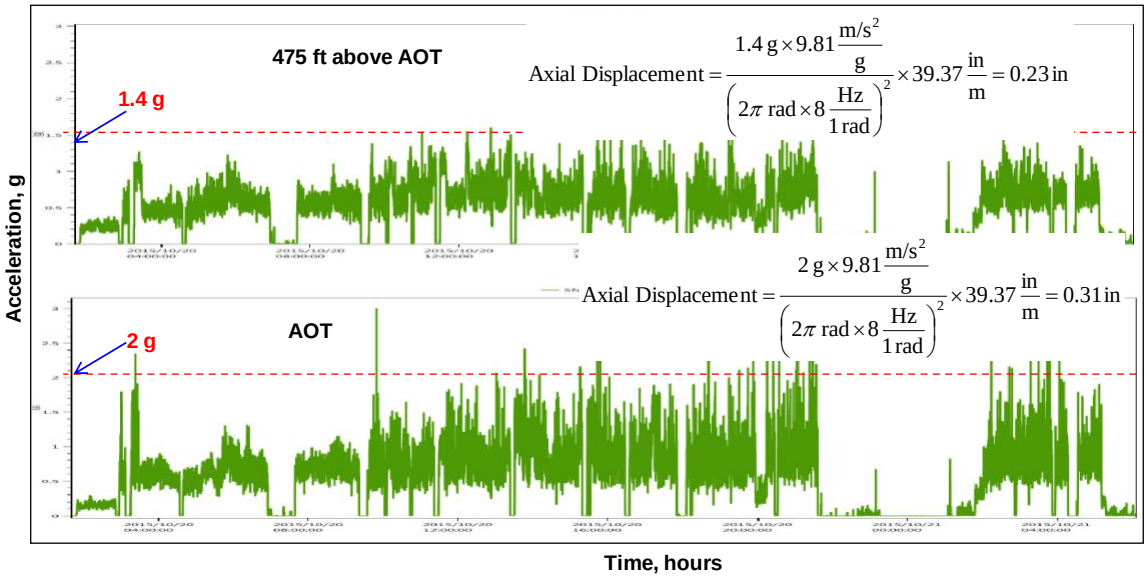

Figure 5. 24: Downhole acceleration data

The following data were not provided in the study of Jones et al. (2016): input parameters of the axial oscillation tool (AOT), mud density and well survey. Input parameters of AOT are assumed based on a comparable 6.75 inches AOT operating at the given frequency of 8 Hz. **Table 5.18** shows the assumed input parameters of AOT. Since well trajectory is not provided, it is assumed that the downhole acceleration matching is performed on a horizontal drillstring in the lateral section.

Table 5. 15: Input parameters of AOT for downhole acceleration matching

Parameters	Values	Units
Length, l	1,500	ft
Average Outer Diameter, d_o	6.75	in.
Average Inner Diameter, d_i	2.81	in.
Stiffness of pipe fittings, k_{f1}	150,000	lbf/in
Modulus of Elasticity, E	210	GPa
Density of Steel, ρ	0.284	lbs/in^3
Mud density	10	ppg
Excitation or operating frequency ω	8	Hz
AOT Pressure Drop, ΔP	500	psi
AOT Spring Rate, k_s	35,000	lbf/in
Pump open area, A_p	14	in^2

The predicted axial displacements from the displacement excitation model at the AOT is 0.286 inches and 475 ft away from the AOT is 0.255 inches (**Figure 5.22**). The discrepancies in matching the measured and predicted axial displacements are due to the uncertainties in assumed data (AOT parameters, friction factor, and wellbore trajectory) which were not provided by the authors of the published data.

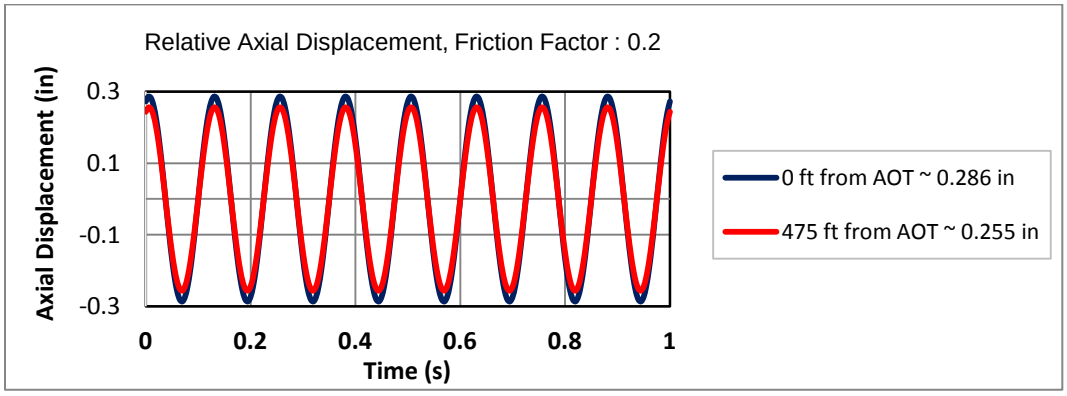

Figure 5. 25: Predicted axial displacements from downhole acceleration data

5.5.2. Downhole Displacement Matching

The displacement excitation model was used in estimating axial displacement in the lateral section of a horizontal well using the limited data provided in the study of Khan et al. (2019). Few of the input parameters of the AOT were provided (**Table 5.19**), while the rest of

the input parameters will be assumed to match the amplitude of axial displacement of 0.02 inches reported by Khan et al. (2019) in **Figure 5.19**. It should be noted that the displacement measurement device was placed directly above the AOT.

Table 5. 16: Input parameters of AOT for downhole displacement matching

Parameters	Values	Units
Length, l	1,500	ft
Excitation or operating frequency ω	16	Hz
AOT Pressure Drop, ΔP	420	psi
Mud density	9	ppg

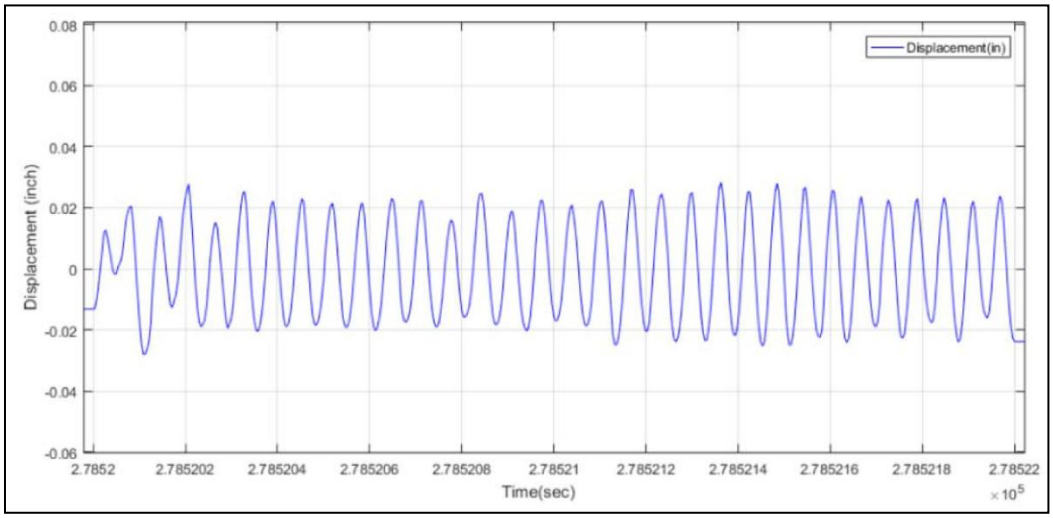

Figure 5. 26: Measured axial displacement of the AOT in the lateral section (Khan et al., 2019)

In an attempt to match the amplitude of axial displacement, the following parameters were varied: boundary stiffness k_{f1}, pump open area A_p, AOT spring rate k_s and friction factor. However, the measured amplitude of axial displacement could not be closely matched. The assumed input parameters are shown in **Table 5.20** and the predicted axial displacement is displayed in **Figure 5.20**. Some of the assumed input data were outside the practical operational limits in an attempt to match the downhole measured displacements.

Table 5. 17: Assumed parameters of AOT for downhole displacement matching

Parameters	Values	Units
Average Outer Diameter, d_o	6.75	in.
Average Inner Diameter, d_i	2.81	in.
Stiffness of pipe fittings, k_{f1}	300,000	lbf/in
Modulus of Elasticity, E	210	GPa
Density of Steel, ρ	0.284	lbs/in^3
AOT Spring Rate, k_s	60,000	lbf/in
Pump open area, A_p	12	in^2
Friction Factor	0.75	

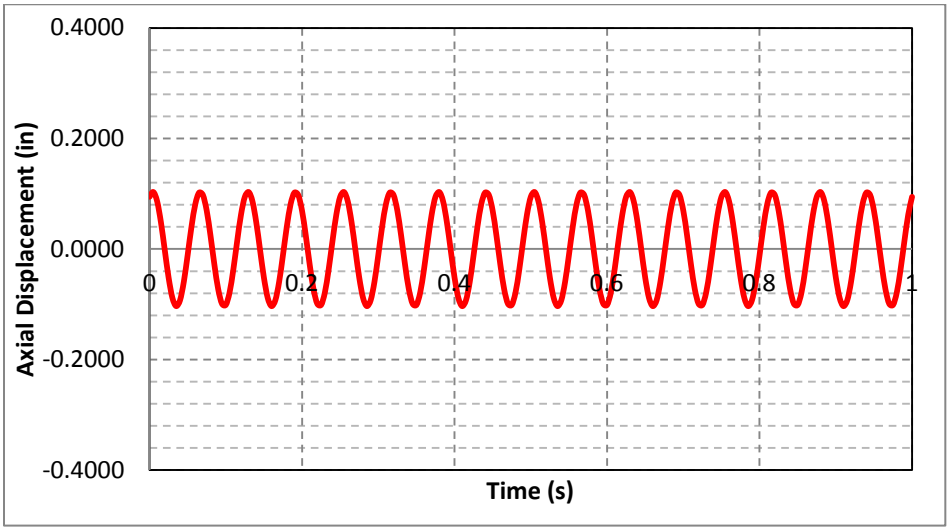

Figure 5. 27: Predicted axial displacement of the AOT in the lateral section

The large discrepancy in measured and predicted axial displacements could be due to the following reasons: (i) the magnitude of measured axial displacement of 0.02 in seems too low for the reported input pressure and frequency; and (ii) lack of sufficient data (dimensions of BHA and drillpipe, friction factor) were provided in the study of Khan et al. (2019).

Chapter 6: Conclusions and Recommendations

6.1. Conclusions

A new mathematical model based on displacement excitation of AOTs on the drillstring has been developed in this study. The model is used to compute the axial displacements and accelerations of axial oscillation-supported drillstrings. Data obtained from the model are validated with current experimental data and published measurements. The following conclusions can be made from this current study:

- The displacement or support excitation model developed in this study ensures that most of the input parameters are acquired from practical data without the use of arbitrary values (e.g. excitation force) as observed in existing models.
- Flow rate is the most fundamental parameter in the operations of axial oscillation tools because it influences pressure drop, the magnitude of excitation force and frequency of excitation of the tools.
- Introducing spring rate improves the accuracy of the support excitation model and helps optimize the axial motion of the mandrel and enhance the performance of the AOT.
- Consistent with experimental data, predicted axial displacement increases with pressure drop and flow rate. This result is a good representation of reality and a valuable output from the model.
- As anticipated, the amplitude of axial displacement generated by axial oscillation tools (AOT) decreases along the drillstring as it moves further from the AOT due to the dissipation of vibrational energy.

- As the operating frequency increased the amplitude of axial displacement increases due to the corresponding increase in pressure drop. Most of the existing models show a decrease in axial displacement as frequency increases because the models do not account for the corresponding increase in pressure drop.
- For the same input, the model shows that increasing wellbore inclination dampens axial oscillations due to an increase in the normal contact load contributing to the Coulomb damping force.

6.2. Recommendations

The drilling industry has made significant progress in harnessing the benefits of axial oscillation tools (AOTs) in providing increased axial force transfer, freeing stuck pipes, coiled tubing drilling and well intervention and in the retrieval of stuck BHA components. However, there are still opportunities for improvements to maximize the effectiveness of AOTs and overall efficiency of axial oscillation-supported drillstrings. The opportunities for improvements will be presented in this study as needs assessment and gap analysis of axial oscillation-support drilling system technology, as presented in **Table 6.1**.

Table 6. 1: Needs assessment and gap analysis

Objectives	Current approach or technology	Gap (Needs)
To monitor the effectiveness of AOTs and axial oscillation-supported drilling systems in real-time	(1) Use of surface weight-on-bit (SWOB) and downhole weight-on-bit (DWOB) measurements to monitor weight transfer (2) Use effective tension and drag charts to measure friction reduction provided by AOTs in the drilling system (3) ROP improvement between subject well and offset well (4) Monitoring levels of stick-slip and torsional vibrations (5) Real-time computation of mechanical specific energy (6) Monitoring the stability of toolface control (7) Monitoring the drilling dynamics (axial shocks and vibrations) of the overall drilling system	(1) Collaboration between MWD companies and AOT suppliers on embedding: (a) Real-time dynamic pressure transducers on AOT to measure the pressure drop across the AOT (b) Real-time strain gauges on AOT, to measure axial displacement and accelerations generated by the AOT (c) Real-time shock and vibrations measurement subs positioned at different positions on the axial-oscillation drilling system, to monitor vibration propagation in real-time These will enable a comparison of calibration and validations of dynamic models in real-time
To achieve optimal placement of AOTs in the drillstring	(1) Use of torque and drag models by drilling engineers to place AOTs close to points with high normal contact loads (side forces) in the curve and lateral sections. (2) Use of trial and error, experience and rule of thumb to place agitators at a predetermined distance away from the bit or MWD tool, to avoid signal interference	(1) Use of mathematical models to support placement analysis; predict axial displacement and accelerations based on drilling and operating parameters, then determine if AOT will be compatible with MWD. (2) MWD signal interference does not need to affect the placement of AOT, if pressure drop, frequency, and AOT spring rate are optimized
To ensure stakeholders (AOT suppliers, drilling engineers, rig hands) understand the operations of AOTs	(1) AOT suppliers are more knowledgeable than drilling engineers or rig hands on the factors affecting the performance of AOTs.	(1) Service companies need to properly train all stakeholders on operating parameters (flow rate, mud weight, spring rate, valve sizing) of AOT and optimization strategies, and effect of drilling parameters on the performance of axial oscillation-supported drilling systems
To improve the design of AOTs to achieve pressure drops within rig limits and still	(1) AOTs with low-pressure drop requirements are preferable to rigs with low pump pressure capacity (2) Re-design of valve/orifice sizes (to reduce the pressure drop)	(1) Modification of AOT power section stator-rotor fits to minimize the pressure drop transmitted from the valve section to the oscillation section (section tool) (2) Few AOT suppliers have field-adjustable AOTs, but more

Objectives	Current approach or technology	Gap (Needs)
maximize dynamic response	(3) Increase the pump open area (4) Modify AOT spring stacking to adjust the response of the drilling system to match pressure drop (5) Use of field-adjustable flow restriction to control AOT pressure drop	suppliers need to improve on the technology
To develop practical analytical and numerical models for predicting the dynamic response of AOT during functional testing and downhole operations	(1) Existing models do not account for AOT spring rate (2) Current models have some constants of uncertainties or arbitrary inputs (3) Existing models have not been used to simultaneously validate both functional test and downhole operations	(1) Dynamic models need to account for the effect of AOT spring rate on the dynamic response of axial oscillation-supported drilling systems (2) Reduce uncertainties in model inputs (3) Dynamic models should be developed to predict the response of AOTs and axial oscillation-supported drilling systems during functional testing and downhole operations. (4) Service companies need to provide performance or characteristic curves for AOTs plotted for specific mud weight, valve sizing, and spring stiffness. These curves will enable drilling engineers and rig operators managing expectations.
To achieve AOT's compatibility with MWD and other BHA components	(1) Adjust MWD operating frequency to operate away from AOT operating frequency (2) Adjust AOT flow restriction to generate a pulse with a frequency that is outside of MWD frequency bandwidth (3) Increase or decrease operating flow rates to avoid and prevent MWD signal interference (4) Tuning of AOTs valve/orifice size to control the height of pressure pulse, and minimize the shock and vibrations transferred from AOT to MWD a sensitive BHA components.	(1) Proper planning between drilling engineers and AOT suppliers for: (a) MWD companies to have specific written standard operating procedures to filter MWD signals to avoid interference. (b) Field serviceable AOTs to optimize axial shocks and vibrations transferred to BHA components

Objectives	Current approach or technology	Gap (Needs)
To design AOTs that allows passage of fishing or retrieval tools	(1) Passage of fishing tools through AOT is almost impossible due to flow restriction of valves and stator-rotor configurations (2) Safety joint is run below AOTs, because AOTs rarely have through-bore access for running fishing tools	(1) There is still no efficient AOT in the market that has through-bore access for running fishing tools.
To develop dynamic models that accurately account for damping factors	(1) Light viscous damping is mostly used to account for the fluid effect on vibrations (2) Coulomb damping is used to account for damping due to frictional contact between drillstring and borehole (3) Equivalent viscous damping is used to account for a combined effect of viscous and Coulomb damping to simplify nonlinear models	(1) Further damping studies are necessary to account for the influence of drillstring rotation, fluid circulation, fluid rheology, pipe geometry, excitation sources. on the damping function.

References

Abdo, J., Al-Sharji, H. 2015. Investigation Of Vibration Effects On Friction and Axial Force Transfer of Buckled Rod Constrained In a Horizontal Cylinder. *Tribology International* 92: 317-327. https://doi.org/10.1016/j.triboint.2015.07.015.

Al Ali, A., Barton, S., and Mohanna, A. 2011. Unique Axial Oscillation Tool Enhances Performance of Directional Tools in Extended Reach Applications. Presented at the SPE Brasil Offshore Conference and Exhibition, Macaé, Brazil, 14-17 June. SPE-143216-MS. https://doi.org/10.2118/143216-MS.

Al Dushaishi, M.F., Nygaard R., and Stutts, D.S. 2017. An Analysis of Common Drill Stem Vibration Models. *ASME Journal of Energy Resources Technology* 140(1): 012905.

Altamimi, I.M., Mokrani, S., and Zulkaf, A.H. 2015. Axial Oscillation Tool Significantly Mitigates the Vibration Level and Enhances Drilling Performance in Conjunction With Standard RSS Systems. Presented at the SPE Abu Dhabi International Petroleum Exhibition and Conference, Abu Dhabi, UAE, 9-12 November. SPE-177713-MS. https://doi.org/10.2118/177713-MS.

Apostal, M.C., Haduch, G.A., and William, J.B. 1990. A Study to Determine the Effect of Damping on Finite-Element-Based, Forced-Frequency-Response Models for Bottomhole Assembly Vibration Analysis. Presented at the SPE Annual Technical Conference and Exhibition, New Orleans, Louisiana, USA, 23-26 September. SPE-20458-MS. https://doi.org/10.2118/20458-MS.

Azike-Akubue, V., Barton, S., Gee, R. et al. 2012. Agitation Tools Enables Significant Reduction in Mechanical Specific Energy. Presented at the SPE Asia Pacific Oil and Gas

Conference and Exhibition, Perth, Australia, 22-24 October. SPE-158240-MS. https://doi.org/10.2118/158240-MS.

Baez, F. and Alali, A. 2011. Drilling Performance Improvements in Gas Shale Plays using a Novel Drilling Agitator Device. Presented at the AADE National Technical Conference and Exhibition, Houston, Texas, USA, 12-14 April. AADE-11-NTCE-47.

Bailey, J.J. and Finnie, I. 1960. An Analytical Study of Drill-String Vibration. *Journal of Engineering for Industry* 82 (2): 122-127. doi:10.1115/1.3663017.

Bandstra, J.P. 1983. Comparison of Equivalent Viscous Damping and Nonlinear Damping in Discrete and Continuous Vibrating Systems. *Journal of Vibration, Acoustics, Stress, and Reliability in Design* 105 (3): 382-392.

Barakat, E.R. 2005. An Experimental Study and Modeling of the Effect of Hydraulic Vibrations on Axial Force Transfer in Horizontal Wellbores. Report Prepared for TUDRP Advisory Board Meeting, Tulsa, Oklahoma, USA, 14-15 November.

Barakat, E.R., Miska, S., Yu, M. et al. 2007. The Effect of Hydraulic Vibrations on Initiation of Buckling and Axial Force Transfer for Helically Buckled Pipes at Simulated Horizontal Wellbore Conditions. Presented at the SPE/IADC Drilling Conference, Amsterdam, The Netherlands, 20-22 February. SPE-105123-MS. https://doi.org/10.2118/105123-MS.

Barton, S., Baez, F., and Alali, A. 2011. Drilling Performance Improvements in Gas Shale Plays using a Novel Drilling Agitator Device. Presented at the SPE North American Unconventional Gas Conference and Exhibition, The Woodlands, Texas, USA, 14-16 June. SPE-144416-MS. https://doi.org/10.2118/144416-MS.

Bodepudi, V., Wilson, J.M., and Patel, A. 1998. Drilling Fluid Type Affects Elastomer Selection. *Oil & Gas Journal* 96 (43).

Bu, C., Li, X., Sun, L. et al. 2016. Arithmetic Solution for the Axial Vibration of Drill String Coupling with a Down-The-Hole Hammer in Rock Drilling. *Journal of Vibration and Control* 22 (13): 3090-3101. doi:10.1177/1077546314560041.

Martinez, J., Carson, C. R., Canuel, L. A. P. et al. 2013. New Technology Enables Rigs With Limited Pump Pressure Capacity to Utilize the Latest Friction Reduction Technology. Presented at the SPE Eastern Regional Meeting, Pittsburgh, Pennsylvania, USA, 22-22 August. SPE-165700-MS.

Chopra, A.K. 2012. *Dynamics of Structures*, Fourth Edition, Prentice Hall, Upper Saddle River, New Jersey.

Clausen, J.R., Schen, A.E., Forster, I. et al. 2014. Drilling With Induced Vibrations Improves ROP and Mitigates Stick/Slip in Vertical and Directional Wells. Presented at the IADC/SPE Drilling Conference and Exhibition, Fort Worth, Texas, USA, 4-6 March. SPE-168034-MS. https://doi.org/10.2118/168034-MS.

Clayer, F., Aquitaine, E., Vandiver, J.K. et al. 1990. The Effect of Surface and Downhole Boundary Conditions on the Vibration of Drillstrings. Presented at the SPE Annual Technical Conference and Exhibition, New Orleans, Louisiana, USA, 23-26 September. SPE-20447-MS. https://doi.org/10.2118/20447-MS.

CT Energy Services. 2015. SD Ratler Series Tool Technical Data Sheet.

Dareing, D.W. and Livesay, B.J. 1968. Longitudinal and Angular Drill-String Vibrations With Damping. *Journal of Engineering for Industry* 90 (4): 671-679. doi:10.1115/1.3604707.

Duplantis, S. 2016. Slide Drilling - Farther and Faster. *Oilfield Review* 28 (2): 50-56.

Eddison, A.M. and Hardie, R. 2001. Downhole Flow Pulsing Apparatus. United States Patent 6,279,670 B1.

Forster, I. and Grant, R. 2012. Axial Excitation and Drill String Resonance as a Means of Aiding Tubular Retrieval - Small-Scale Rig Testing and Full-Scale Field Testing. Presented at the IADC/SPE Drilling Conference and Exhibition, San Diego, California, USA, 6-March. SPE-151096-MS.

Forster, I. 2015. Axial Excitation Tool String Modeling. Proceedings of the ASME 2015 34th International Conference on Ocean, Offshore and Arctic Engineering, St. John's, Newfoundland, Canada, 31 May-5 June. doi:10.1115/OMAE2015-41393.

Fu, J., Ren, Z., Bai, J. et al. 2018. The Friction-Reducing Principle and Application of The Drill String with a Hydro-Oscillator. *Journal of Petroleum Science and Engineering* 165: 453–461.

Ghasemloonia, A., Rideout, D.G., Butt, S.D. et al. 2014. Elastodynamic and Finite Element Vibration Analysis of a Drillstring with a Downhole Vibration Generator Tool and a Shock Sub. *Journal of Mechanical Engineering Science* 229 (8): 1361-1384.

Ghasemloonia, A., Rideout, D.G., Butt, S.D. et al. 2015. A Review of Drillstring Vibration Modeling And Suppression Methods. *Journal of Petroleum Science and Engineering* 131: 150-164.

Gee, R., Hanley, C., Hussain, L. et al. 2015. Axial Oscillation Tools vs Lateral Vibration Tools for Friction Reduction – What's the Best Way to Shake the Pipe?. Presented at the SPE/IADC Drilling Conference and Exhibition, London, England, UK, 1-3 March. IADC/SPE-178792-MS.

Impulse Downhole Tools. 2017. ActiPulse™ Technical Data Sheet.

Jones, S., Feddema, C., Junichi, S. et al. 2016. A New Friction Reduction Tool with Axial Oscillation Increases Drilling Performance: Field-Testing with Multiple Vibration

Sensors in One Drill String. Presented at the IADC/SPE Drilling Conference and Exhibition, Forth Worth, Texas, USA, 1-3 March. IADC/SPE-178792-MS. https://doi.org/10.2118/178792-MS.

Johancsik, C.A., Friesen, D.B, and Rapier, D. 1984. Torque and Drag in Directional Wells-Prediction and Measurement. *Journal of Petroleum Technology* 36 (6): 987-992. https://doi.org/10.2118/11380-PA.

Johnson, E. 2016. Are You Getting the Most Out of Your Agitator?. Retrieved from http://www.hxrdrillingservices.com/are-you-getting-the-most-out-of-your-agitator/, 10 March.

Khan, A., Trinh, K., Thompson, P. et al. 2019. Downhole Data Analysis for Pressure-Pulse-Generating and Axial-Oscillation Measurement Tool. SPE/ICoTA Well Intervention Conference and Exhibition, The Woodlands, Texas, USA, 26-27 March, SPE-194243. https://doi.org/10.2118/194243-MS.

Khan, K.Z. 1983. Longitudinal and Torsional Vibration of Drill Strings. Thesis Submitted to the Department of Ocean Engineering, Massachusetts Institute of Technology, USA.

Kragjcek, R.H., Al-Dossary, A.S, Koth, W.G. et al. 2011. Successful Application of New Sliding Technology for Horizontal Drilling in Saudi Arabia. *Saudi Aramco Journal Of Technology* Fall Edition: 28-33.

Larsen, L.K. 2014. Tools and Techniques to Minimize Shock and Vibration to the Bottom Hole Assembly. Thesis Submitted to the Department of Petroleum Engineering, University of Stavanger, Norway.

Lear, W.E., and Dareing, D.W. 1990. Effect of Drillstring Vibrations on MWD Pressure Pulse Signals. *ASME Journal of Energy Resources Technology* 112(2): 84-89.

Lee, H.Y. 1991. Drillstring Axial Vibration and Wave Propagation in Boreholes. Dissertation Submitted to the Department of Ocean Engineering, Massachusetts Institute of Technology, USA.

Leissa, A.W. and Qatu, M.S. 2011. *Vibrations of Continuous Systems,* second edition. McGraw-Hill.

Li, C. 1987. An Analytical Study of Drill String Vibrations. e-Library of Society of Petroleum Engineers.

Li, Z., Yanshan, U., and Guo, B. 2007. Analysis of Longitudinal Vibration of Drillstring in Air And Gas Drilling. Presented at the SPE Rocky Mountain Oil & Gas Technology Symposium, Denver, Colorado, USA, 16-18 April. SPE 107697. https://doi.org/10.2118/107697-MS.

Liu, Y., Chen, P., Ma, T. et al. 2016. Modeling Friction-Reducing Performance of an Axial Oscillation Tool Using Dynamic Friction Model. Journal of Natural Gas Science and Engineering 33: 397-404.

Liu, Y., Chen, P., Ma, T. et al. 2017. An Evaluation Method for Friction-Reducing Performance of Hydraulic Oscillator. *Journal of Petroleum Science and Engineering* 157: 107-116. 10.1016/j.petrol.2017.07.018.

McCarthy, J.P., Stanes, B.H., Clark, K.W. et al. 2009. A Step Change in Drilling Efficiency: Quantifying the Effects of Adding an Axial Oscillation Tool Within Challenging Wellbore Environments. Presented at the SPE/IADC Drilling Conference and Exhibition, Amsterdam, The Netherlands, 17-19 March. SPE/IADC 119958. https://doi.org/10.2118/119958-MS.

McIntosh, T., Baros, K.J., Gervais, J.G. et al. 2016. A Vibratory Tool Study on Extended Reach Horizontals During Coiled Tubing Drillout in the Eagle Ford Shale. Presented at the SPE/ICoTA Coiled Tubing & Well Intervention Conference and Exhibition, Houston, Texas, USA, 22-23 March. SPE-179087. https://doi.org/10.2118/179087-MS.

Mitchell, R.F. 1986. Simple Frictional Analysis of Helical Buckling of Tubing. *SPE Drilling Engineering* 01 (6): 457-465. https://doi.org/10.2118/13064-PA.

Newman, K., Burnett, T., Pursell, J. et al. 2009. Modeling the Affect of a Downhole Vibrator. Presented at the SPE/ICoTA Coiled Tubing & Well Intervention Conference and Exhibition, The Woodlands, Texas, USA, 31 March-1 April. SPE-121752-MS. https://doi.org/10.2118/121752-MS.

NOV. 2013: AgitatorTM Systems Handbook.

NOV. 2015: Agitator™ System Brochure.

NOV. 2016: Agitator™ Systems Handbook.

Paranjpe, R.S. 1990. Dynamic Analysis of a Valve Spring With a Coulomb-Friction Damper. *Journal of Mechanical Design* 112 (4): 509-513.

Patil, P. and Teodoriu, C. 2012. Effect Model Development of Torsional Drillstring and Investigating Parametrically the Stick-Slips Influencing Factors. *ASME Journal of Energy Resources Technology* 135(1): 013103.

Rao, S.S. 2007. *Vibration of Continuous Systems*, first edition. Hoboken, New Jersey: John Wiley & Sons, Inc.

Rao, S.S. 2011. *Mechanical Vibrations*, fifth edition. Upper Saddle River, New Jersey: Prentice Hall.

Rashed, G., Ghaja, R., and Hashemi, S.J. 2007. An Analytical Model for Drillstring Axial Vibration. Presented at the 14th International Congress on Sound & Vibrations, Cairns, Australia, 9-12 July.

Rasheed, W. 2001. Extending the Reach and Capability of Non Rotating BHAs by Reducing Axial Friction. Presented at the SPE/ICoTA Coiled Tubing Roundtable, Houston, Texas, USA, 7-8 March. SPE-68505-MS. https://doi.org/10.2118/68505-MS.

Robertson, L., Mason, C.J., Sherwood, A.S. et al. 2004. Dynamic Excitation Tool: Developmental Testing and CTD Field Case Histories. Presented at the SPE/ICoTA Coiled Tubing Conference and Exhibition, Houston, Texas, USA, 23-24 March. SPE-89519-MS. https://doi.org/10.2118/89519-MS.

Robertson, L. 2006. A Simple Solution Using Field Results Confirms Mathematical Modeling – Methodology for Evaluating the Effectiveness of the AG-itator. Presented at the SPE Bergen One Day Seminar, Bergen, Norway, 5 April.

Roper, W.F. and Dellinger, T.B. 1983. Reduction of Frictional Coefficient in a Borehole by the Use of Friction. United States Patent 4,384,625.

Samuel, R. 2010. Friction Factors: What are They for Torque, Drag, Vibration, Drill Ahead and Transient Surge/Swab Analyses?. Presented at the IADC/SPE Drilling Conference and Exhibition, New Orleans, Louisiana, USA, 2-4 February. SPE-128059-MS. https://doi.org/10.2118/128059-MS.

Samuel, R. and Yao, D. 2013. DrillString Vibration With Hole-Enlarging Tools: Analysis and Avoidance. *ASME Journal of Energy Resources Technology* 135(3): 032904.

Sanchez, R.A., Azar, J.J., Bassal, A.L. et al. 1997. The Effect of Drillpipe Rotation on Hole Cleaning During Directional Well Drilling. Presented at the SPE/IADC Drilling

Conference, Amsterdam, Netherlands, 4-6 March. SPE-37626-MS. https://doi.org/10.2118/37626-MS.

Schamp, J.H., Estes, B.L., and Keller, S.R. 2006. Torque Reduction Techniques in ERD Wells. Presented at the IADC/SPE Drilling Conference, Miami, Florida, USA, 21-23 February. SPE-98969-MS. https://doi.org/10.2118/98969-MS.

Schlumberger. 2015. HydraPulse™ Technical Data Sheet

Schlumberger. 2016. HydraSpeed™ Technical Data Sheet.

Schultz, R. 2013. Vibratory Downhole Tool Technologies with Application to Horizontal Drilling and Casing Installation. Retrieved from http://www.horizontal-drilling-shale-plays.com/media/downloads/31-roger-schultz-engineering-manager-tts-drilling-solutions-thrutubing-solutions.pdf, 2 February.

Shor, R.J., Dykstra, M.W., and Hoffmann, O.J. 2015. For Better or Worse: Applications of the Transfer Matrix Approach for Analyzing Axial and Torsional Vibration. Presented at the SPE/IADC Drilling Conference and Exhibition, London, England, UK, 17-19 March. SPE-173121-MS. https://doi.org/10.2118/173121-MS.

Skyles, L.P., Amiraslani, Y.A., Wilhoit, J.E. 2012. Converting Static Friction To Kinetic Friction to Drill Further And Faster in Directional Holes. Presented at the IADC/SPE Drilling Conference and Exhibition, San Diego, California, USA, 6-8 March. SPE-151221-MS. https://doi.org/10.2118/151221-MS.

Soni, M.L., Bogner, F.K. 1982. Finite Element Vibration Analysis of Damped Structures. *AIAA Journal*. 20:5, 700-707. https://doi.org/10.2514/3.51127.

Strauss, W.A. 2008. *Partial Differential Equations: An Introduction*, second edition. Hoboken, New Jersey: John Wiley & Sons, Inc.

Tian, J., Wu, C., Yang, Z. et al. 2016. Mathematical Modeling and Analysis of Drill String Longitudinal Vibration with Lateral Inertia Effect. *Hindawi Shock and Vibration*: 1-8. doi:10.1155/2016/6281264.

Tian, J., Yang, Z., Li, Y. et al. 2016. Vibration Analysis of New Drill String System with Hydro-Oscillator in Horizontal Well. *Journal of Mechanical Science and Technology* 30 (6): 2443-2451. https://doi.org/10.1007/s12206-016-0504-z.

Thorpen, P. and Sanders, I. 2015. Shedding New Light on Downhole Vibration Tools. *Oilfield Technology* August Edition.

Voghell, M., Mohanna, A., Hanley, C. et al. 2013. Downhole Vibration Analysis: Fishing Agitation Tool Efficiency in Stuck Pipe Recovery. Presented at the SPE/IADC Middle East Drilling Technology Conference & Exhibition, Dubai, UAE, 7-9 October. SPE-166745-MS. https://doi.org/10.2118/166745-MS.

Wang, P., Ni, H., Wang, X. et al. 2018. Modeling the Load Transfer and Tool Surface for Friction Reduction Drilling by Vibrating Drill-String. *Journal of Petroleum Science and Engineering* 164: 333-343.

Wang, X., Yao, X., Hu, G. et al. 2019. Drag Reduction Performance of an Axial Oscillating Tool with Different Kinds of Waveform Using a Multiscale Friction Model. *Journal of Petroleum Science and Engineering* 177: 135-153.

Wilson, J.K. and Heisig, G. 2015. Investigating the Benefits of Induced Vibrations in Unconventional Horizontals via Nonlinear Drill String Dynamics Modeling. Presented at the SPE/IADC Drilling Conference and Exhibition, London, England, UK, 17-19 March. SPE-173049-MS. https://doi.org/10.2118/173049-MS.

Wilson, J.K. and Noynaert, S.F. 2017. Inducing Axial Vibrations in Unconventional Wells: New Insights through Comprehensive Modeling. Presented at the SPE/IADC Drilling Conference and Exhibition, The Hague, The Netherlands, 14-16 March. SPE-184635-MS. https://doi.org/10.2118/184635-MS.

WWT International. 2015. WWT Non-Rotating Protectors™. Retrieved from http://wwtinternational.com/pdf/WWT_NRP_Benefits_Brochure_1_2015.pdf.

Zhang, W., Shi, H., Li, G., Song, X., Zhao, H. 2019. Mechanism Analysis of Friction Reduction in Coiled Tubing Drilling with Axial Vibratory Tool. Journal of Petroleum Science and Engineering 175: 324-337.

Nomenclature:

A	Cross-sectional area, m^2
A_n	Amplitude, m
A_p	Pump open area, m^2
B	Velocity of sound in steel, m/s
c	Viscous damping coefficient, kg/s
c_{eq}	Equivalent viscous damping, kg/s
dx	Length of differential element, m
E	Young's modulus or modulus of elasticity, N/m^2
$f(x)$	Amplitude of excitation force as a function of x
f_c	Correction factor for the buoyancy force
F_c	Coulomb frictional force, N
F_d	Damping force per length, N/m
F_N	Normal friction force or contact load, N
F_p	Hydraulic excitation force, N
g	Acceleration due to gravity, m/s^2
G	Arbitrary constant
H	Arbitrary constant
k_{f1}	Stiffness of boundary condition on uphole excitation model, N/m
k_s	AOT spring rate or stiffness, N/m
K	Stiffness per length, N
K_1	Stiffness of cylindrical bar, N/m

l	Length of drillstring section, m
M	Mass per length, kg/m
$M_n(t)$	Components of displacement excitation as a function of time
$p(t)$	Support motion
P	Axial force, N
dP	Difference in axial force, N
ΔP	Fluid pressure change, N/m^2
R_n	Fourier coefficient
sgn	Sign or signum function
t	Time, s
$T(t)$	Time dependent solution
u	Axial displacement, m
$u(x,t)$	Total axial displacement solution
$u_s(x,t)$	Support excitation
$U(x)$	Displacement dependent solution
u_x	Axial strain
u_{xx}	Gradient of axial strain
u_t	Axial velocity, m/s
u_{tt}	Axial accelerations, m/s^2
$v(x,t)$	Displacement of any point in the bar relative to the support
x	Horizontal axis
X	Maximum amplitude of response excitation, m
z	Vertical axis

$\partial P/\partial x$	Gradient of axial force, N/m
$\partial v/\partial x$	Axial strain
$\partial^2 v/\partial x^2$	Gradient of axial strain
$\partial v/\partial t$	Axial velocity, m/s
$\partial^2 v/\partial t^2$	Axial accelerations, m/s^2
δ_a	Displacement of the spring due to hydraulic excitation force
λ	Eigenvalue
μ	Friction factor
μ_c	Friction factor corrected for the buoyancy force
π	Pi = 3.14159265359
ρ	Density of drillstring material, kg/m^3
ρ_m	Mud density, kg/m^3
σ	Axial stress, N/m^2
φ_n	Phase angle, $radians$
ω	Operating frequency of AOT or frequency of pressure pulses, rad/s
ω_n	Natural frequency, rad/s

Appendix A

A.1. Contact Force in a Curved Wellbore Section

The approximate values of contact force acting on a drillstring in curved sections of a 2D wellbore can be calculated considering two different cases: (i) dropping angle and (ii) building angles. For the case of dropping angle shown in **Figure A.1**, applying summation of forces at equilibrium, $\sum Forces\ along\ normal\ force\ N = 0$. The following expression can be obtained, $W \sin I + (T + \Delta T) \sin {}^{\delta}/_{2} + T \sin {}^{\delta}/_{2} = F_N$. This equation can be expanded as: $W \sin I + T \sin {}^{\delta}/_{2} + \Delta T \sin {}^{\delta}/_{2} + T \sin {}^{\delta}/_{2} = F_N$. For small angle ${}^{\delta}/_{2}$, the normal force is determined as:

$$F_N \approx W \sin I + 2T \sin {}^{\delta}/_{2} \quad \text{(A.1)}$$

The frictional force F_c is calculated as:

$$F_c = \mu F_N \quad \text{(A.2)}$$

$$F_c = \mu\left(W \sin I + 2T \sin {}^{\delta}/_{2}\right) \quad \text{(A.3)}$$

where F_N is the normal contact load acting on the pipe, W is the weight of the pipe section, T is the tension acting on the pipe, I is the inclination angle measured from the vertical axis, δ is the dogleg or change in inclination across pipe section, F_c is the Coulomb frictional force and μ is the friction factor. W is the buoyed weight of the pipe section per unit length, which is defined as:

$$W = (\rho - \rho_m)Ag = \rho f_c Ag \quad \text{(A.4)}$$

where ρ_m is the mud density and f_c is a correction factor for the buoyancy force. Therefore, the frictional force when dropping angle F_c is expressed as:

$$F_c = \mu\left(\rho f_c A g \sin I + 2T \sin {}^{\delta}/_{2}\right) \quad \text{(A.5)}$$

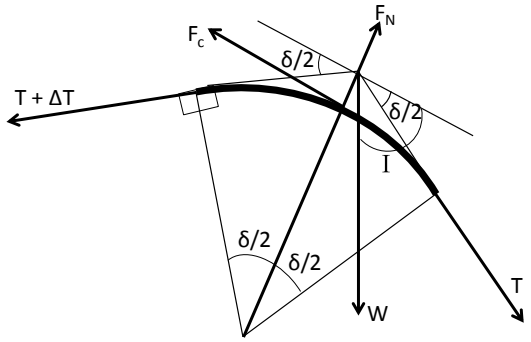

Figure A. 1: Dropping angle in a curved section

For the case of building angle shown in **Figure A.2**, applying summation of normal forces at equilibrium, $\sum Forces\ along\ normal\ force\ N = 0$, the following equation can be developed: $F_N + (T + \Delta T) \sin {}^{\delta}/_{2} + T \sin {}^{\delta}/_{2} - W \sin I = 0$. This equation can be simplified for small angle ${}^{\delta}/_{2}$ as:

$$F_N \approx W \sin I - 2T \sin {}^{\delta}/_{2} \quad \text{(A.6)}$$

Inserting Eq. A.4 into Eq. A.6, the following expression can be obtained:

$$F_N = \rho f_c A g \sin I - 2T \sin {}^{\delta}/_{2} \quad \text{(A.7)}$$

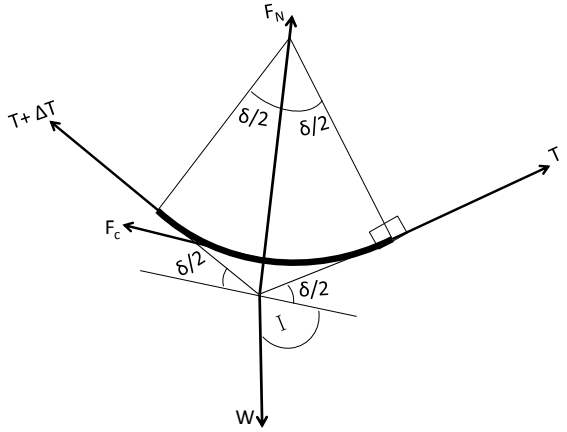

Figure A. 2: Building angle in a curved section

Therefore, the frictional force F_c when dropping angle is expressed as:

$$F_c = \mu\left(\rho f_c A g \sin I + 2T \sin {}^{\delta}/_{2}\right) \quad \text{(A.8)}$$

Appendix B

B.1 Equivalent Viscous Damping

Assuming the solution or response of a one-degree-of-freedom discrete system is of the form (Rao, 2011):

$$x(t) = Xsin(\omega t) \qquad \text{(B.1)}$$

where X is the maximum displacement (amplitude) of the system and ω is the frequency of oscillation. The energy dissipated (or energy lost per cycle) in an equivalent viscous damped harmonically forced system is: $W_d = \oint F_{eq} dx = \oint c_{eq} (\dot{x})^2 dt$, where $dx = \dot{x} dt$. Applying the change of variable method, $W_d = \oint c_{eq} \omega^2 X^2 \cos^2 \omega t \, dt$. For one cycle of oscillation, from $t = 0$ to $t = 2\pi/\omega$, $W_d = c_{eq} \omega^2 X^2 \oint_0^{2\pi/\omega} \cos^2 \omega t \, dt$. After simplification, $W_d = c_{eq} c \omega^2 X^2 \oint_0^{2\pi/\omega} \frac{1}{2} [\cos 2\omega t + 1] dt$. After evaluating the integration, the following relationship can be established:

$$W_d = \pi c_{eq} \omega X^2 \qquad \text{(B.2)}$$

The Coulomb damping force, F_c or friction damping force dissipates $W_c/4 = F_c X$ amount of energy over each quarter cycle. Hence, equating the total dissipative work per cycle of friction damping force to that of an equivalent viscous damper, as shown in Figure B1:

$W_c = 4F_c X = \pi c_c \omega X^2$.

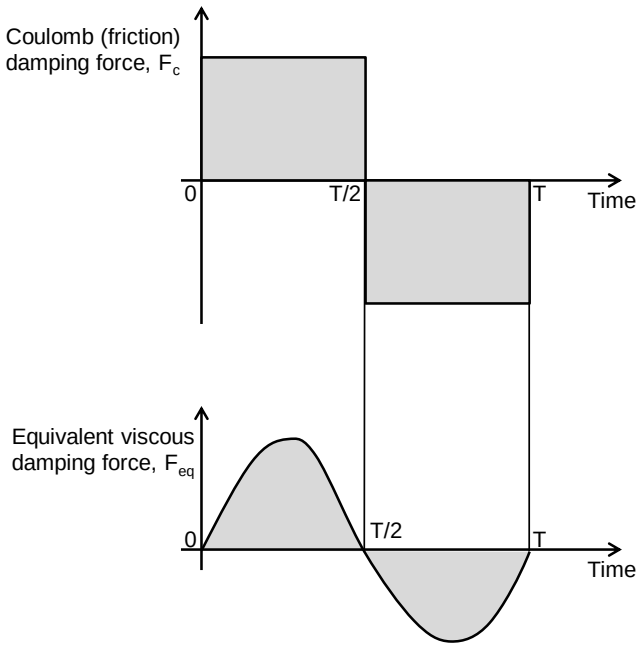

Figure B. 1: Graphical representation of Coulomb and equivalent damping force

Therefore, the equivalent viscous damping coefficient for Coulomb friction is:

$$c_{eq} = \frac{4F_c}{\pi\omega X} = \frac{4\mu F_N}{\pi\omega X} = \frac{4\mu F_N}{\pi\omega X} \qquad \text{(B.3)}$$

where μ_c is the product of μ and f_c. M is the mass of oscillating element or body and g is the acceleration of gravity. Also, the friction factor is a function of mud weight, formation friction coefficient, mud lubricity, type stiffness, cutting bed height, key seats, stabilizer contact point, differential sticking, hole tortuosity, and dogleg severity. For the 2D well described in Appendix A with no change in inclination across the pipe section, Eq. B.3 becomes:

$$c_{eq} = \frac{4\mu\rho f_c A g \sin I}{\pi\omega X} = \frac{4\mu_c \rho A g \sin I}{\pi\omega X} \qquad \text{(B.4)}$$